1-1-2016

Systems Biology of Platelet Activation

Mei Yan Lee
University of Pennsylvania, meil@seas.upenn.edu

Systems Biology of Platelet Activation

Abstract
Platelet intracellular calcium mobilization [Ca(t)]i is a measure of platelet activation and controls important events downstream that contribute to hemostasis such as granule release, cyclooxygenase-1 and integrin activation, and phosphatidylserine exposure. Accurate simulations of blood clotting events require prediction of platelet [Ca(t)]i in response to combinatorial agonists. Therefore, a data-driven human platelet calcium calculator was developed using neural network (NN) ensemble trained on pairwise agonist scanning (PAS) data. PAS deployed all single and pairwise combinations of six important agonists (ADP, convulxin, thrombin, U46619, iloprost and GSNO used at 0.1, 1, and 10xEC50 to stimulate platelet P2Y1/P2Y12, GPVI, PAR1/PAR4, TP, IP receptors, and guanylate cyclase, respectively, in Factor Xa-inhibited (250 nM apixaban), diluted platelet rich plasma. PAS of 10 healthy donors (5 male, 5 female) provided [Ca(t)]i data for training 10 neural networks (NN, 2-layer/12-nodes) per donor. Trinary stimulations were then conducted at all 0.1x and 1xEC50 doses (160 conditions) as was a sampling of 45 higher ordered combinations (four to six agonists). The NN-ensemble average accurately predicted [Ca (t)]i beyond the single and binary training set for trinary stimulations (R = 0.924). The 160 trinary synergy scores, a normalized metric of signaling crosstalk, were also well predicted (R = 0.850) as were the calcium dynamics (R = 0.871) and high-dimensional synergy scores (R = 0.695) for the 45 higher ordered conditions. The calculator even predicted sequential addition experiments (n = 54 conditions, R = 0.921). NN-ensemble is a fast calcium calculator that proved to be useful for multiscale clotting simulations that include spatiotemporal concentrations of ADP, collagen, thrombin, thromboxane, prostacyclin, and nitric oxide.

From sequential addition experiments done in PAS, it was discovered that activating platelets with thrombin in platelet-rich plasma (PRP) caused an attenuation of convulxin-induced, GPVI platelet receptor-mediated, calcium mobilization when convulxin was added to PRP approximately six minutes later. This attenuation effect was not observed when ADP and thromboxane analog, U46619 was used in place of thrombin. When PAR-1 and PAR-4 receptor agonists (AYPGKF and SFLLRN) were used instead of thrombin for the initial dispense, the subsequent convulxin-induced calcium response was also unaffected, demonstrating thrombin's unique role in causing attenuation of subsequent convulxin-induced calcium mobilization. Thrombin, unlike ADP, U46619 or the PAR-1 and PAR-4 receptor agonists, is able to polymerize fibrinogen into fibrin. When GPRP was added to prevent polymerization of fibrin, initial platelet activation by thrombin did not result in attenuation of convulxin- induced calcium mobilization. This experiment was repeated using a mixture of washed platelets and fibrinogen monomers instead of PRP and yielded similar results. The presence of polymerized fibrin also reduced platelet deposition in a microfluidic assay on a collagen surface. These results suggest that polymerized fibrin binds to and downregulates platelet GPVI, a platelet receptor that is important to thrombus growth and is central to mediating hemostasis.

Degree Type
Dissertation

Degree Name
Doctor of Philosophy (PhD)

Graduate Group
Chemical and Biomolecular Engineering

SYSTEMS BIOLOGY OF PLATELET ACTIVATION

Mei Yan Lee

A DISSERTATION

in

Chemical and Biomolecular Engineering

Presented to the Faculties of the University of Pennsylvania

in Partial Fulfillment of the Requirements for the Degree of Doctor of Philosophy

2016

Supervisor of Dissertation

_____

Scott L. Diamond

Professor, Chemical and Biomolecular Engineering

Graduate Group Chairperson

_____

Talid R. Sinno

Professor, Chemical and Biomolecular Engineering

Dissertation Committee

Talid R. Sinno, Professor, Department of Chemical and Biomolecular Engineering

Matthew J. Lazzara, Assistant Professor, Department of Chemical and Biomolecular Engineering

Lawrence F. Brass, Professor, School of Medicine

SYSTEMS BIOLOGY OF PLATELET ACTIVATION

ACKNOWLEDGMENTS

First, I would like to thank my advisor, Dr. Scott Diamond for his guidance throughout my PhD journey. He was always very patient and encouraging in his advising style.

Second, I would like to thank other Diamond Lab members who have been essential in helping me succeed. Manash Chatterjee, whose project I took over and whom I have never met in person, spoke to me on the phone on a few times to help me troubleshoot my experiments when I was starting out. Andrew Dolan was extremely helpful in training me in lab experiments as well as teaching me how to troubleshoot code, lab equipment problems, computer problems, etc. Both Andrew Dolan and Roman Voronov helped me immensely in my early years by taking an interest in my project, helping to troubleshoot my experiments, as well as indulging me in many conversations where they suggested various potential, interesting, directions my first project could take. Thanks to Shu and Brad for helping me with microfluidic experiments, and for several useful conversations in interpreting experimental results. I would also like to thank Melissa and Viraj for providing encouragement as well as invaluable advice in getting read y for a post-graduate career. Thanks to the rest of Diamond lab, Jing as well as Marvin who made the IME a great place to work in.

I want to thank my friends who have enriched my life outside of research - thanks to David, Brad, Melissa, Liana and many others who have made Philly a fun place to live in. I would also like to thank my friends at Penn Latin and Ballroom Dance, my ballroom family has made my graduate school years especially memorable. I would like to also thank Ian McMahon for standing by me and supporting me throughout this journey, being extremely patient, encouraging and helpful during challenging times.

I would finally also like to thank my family: my parents and brother. They have always been immensely supportive of my work and despite being 10,000 miles away, I am able to experience

that support. I also especially appreciate the sacrifices my parents have made for me to ensure that I had great educational opportunities, and encouraging me to take that initial leap of faith to come over to pursue an education in the United States and eventually also their support in my decision to pursue a PhD.

ABSTRACT

SYSTEMS BIOLOGY OF PLATELET ACTIVATION

Mei Yan Lee

Scott L. Diamond

Platelet intracellular calcium mobilization $[Ca(t)]_i$ is a measure of platelet activation and controls important events downstream that contribute to hemostasis such as granule release, cyclooxygenase-1 and integrin activation, and phosphatidylserine (PS) exposure. Accurate simulations of blood clotting events require prediction of platelet $[Ca(t)]_i$ in response to combinatorial agonists. Therefore, a data-driven human platelet calcium calculator was developed using neural network (NN) ensemble trained on pairwise agonist scanning (PAS) data. PAS deployed all single and pairwise combinations of six important agonists (ADP, convulxin, thrombin, U46619, iloprost and GSNO used at 0.1, 1, and 10 x EC_{50} to stimulate platelet P_2Y_1/$P2Y_{12}$, GPVI, PAR-1/PAR-4, TP, IP receptors, and guanylate cyclase, respectively, in Factor Xa-inhibited (250 nM apixaban), diluted platelet rich plasma (PRP). PAS of 10 healthy donors (5 male, 5 female) provided $[Ca(t)]_i$ data for training 10 neural networks (NN, 2-layer/12-nodes) per donor. Trinary stimulations were then conducted at all 0.1 x and 1 x EC_{50} doses (160 conditions) as was a sampling of 45 higher ordered combinations (four to six agonists). The NN-ensemble average accurately predicted $[Ca(t)]_i$ beyond the single and binary training set for trinary stimulations (R = 0.924). The 160 trinary synergy scores, a normalized metric of signaling crosstalk, were also well predicted (R = 0.850) as were the calcium dynamics (R = 0.871) and high-dimensional synergy scores (R = 0.695) for the 45 higher ordered conditions. The calculator even predicted sequential addition experiments (n = 54 conditions, R = 0.921). NN-ensemble is a fast calcium calculator that proved to be useful for multiscale clotting

simulations that include spatiotemporal concentrations of ADP, collagen, thrombin, thromboxane, prostacyclin, and nitric oxide.

From sequential addition experiments done in PAS, it was discovered that activating platelets with thrombin in platelet-rich plasma (PRP) caused an attenuation of convulxin-induced, GPVI platelet receptor-mediated, calcium mobilization when convulxin was added to PRP eight minutes later. This attenuation effect was not observed when ADP and thromboxane analog, U46619 was used in place of thrombin. When PAR-1 and PAR-4 receptor agonists (AYPGKF and SFLLRN) were used instead of thrombin for the initial dispense, the subsequent convulxin-induced calcium response was also unaffected, demonstrating thrombin's unique role in causing attenuation of subsequent convulxin-induced calcium mobilization. Thrombin, unlike ADP, U46619 or the PAR-1 and PAR-4 receptor agonists, is able to polymerize fibrinogen into fibrin. When Gly-Pro-Arg-Pro (GPRP) was added to prevent polymerization of fibrin, initial platelet activation by thrombin did not result in attenuation of convulxin- induced calcium mobilization. This experiment was repeated using a mixture of washed platelets and fibrinogen instead of PRP and yielded similar results. The presence of polymerized fibrin also reduced platelet deposition in a microfluidic assay on a collagen surface. These results suggest that polymerized fibrin binds to and downregulates platelet GPVI, a platelet receptor that is important to thrombus growth and is central to mediating hemostasis.

Table of Contents

ACKNOWLEDGEMENTS ..... **III**

ABSTRACT ..... **V**

LIST OF TABLES ..... **X**

LIST OF FIGURES ..... **XI**

1.0 INTRODUCTION **1**

1.1 PLATELET ACTIVATION *1*

1.2 ROLE OF THROMBIN *2*

1.3 ROLE OF FIBRIN *3*

1.4 ROLE OF GPVI *4*

2.0 A HUMAN PLATELET CALCIUM CALCULATOR TRAINED BY PAIRWISE AGONIST SCANNING **5**

2.1 ABSTRACT *5*

2.2 INTRODUCTION *7*

2.3 MATERIALS AND METHODS *11*

2.3.1 Pairwise Agonist Scanning (PAS) *11*

2.3.2 Trinary, Higher Order Combinations and Sequential Addition Experiments *13*

2.3.3 Calculation of Synergy Scores *14*

2.3.4 Neural Network Training and Averaging *14*

2.4 RESULTS *17*

2.4.1 Neural network prediction of platelet responses to binary agonist stimulation *17*

2.4.2 Neural network prediction of platelet responses to trinary agonist stimulation *20*

2.4.3 Neural network prediction of higher order combination experiment *26*

2.4.4 Neural network prediction of sequential addition combination experiment *26*

2.4.5 Analysis of synergy scores *29*

2.4.5 Inhibition of calcium release by iloprost *33*

2.4.6 Range of individual neural network prediction and donor responses *38*

2.5 DISCUSSION *40*

3.0 DOWNREGULATION OF PLATELET GPVI SIGNALING FOLLOWING THROMBIN STIMULATION **47**

3.1 ABSTRACT *47*

3.2 INTRODUCTION *48*

3.3 MATERIALS AND METHODS *50*

3.3.1 Platelet Calcium Assays *50*

3.3.2 Microfluidic assays *52*

3.4 RESULTS *53*

3.4.1 Thrombin uniquely attenuates subsequent platelet calcium response to convulxin *53*

3.4.2 Extent of attenuation of convulxin calcium response increases with incubation time and thrombin dose *55*

3.4.3 Activating PAR-1 and PAR-4 do not result in attenuation of subsequent platelet calcium response to convulxin *58*

3.4.4 Fibrin plays an essential role in attenuation of subsequent platelet calcium response *60*

3.4.5 Platelet convulxin response attenuation effect is reproduced in washed platelets and fibrinogen environment *62*

3.4.6 Presence of fibrin reduces platelet adhesion on collagen in microfluidic assay *63*

3.5 DISCUSSION *65*

4.0 FUTURE WORK **72**

4.1 FURTHER INVESTIGATION OF FIBRIN-GPVI INTERACTION *72*

4.2 EXTENDING HUMAN PLATELET CALCIUM CALCULATOR TO INCLUDE INDIVIDUALS WITH FAMILIAL HYPERCHOLESTEROLEMIA *74*

4.3 COMBINING PLATELET CALCIUM CALCULATOR TO BUILD AN NN-ODE MODEL *74*

4.4 HIGHER ORDER PAS *77*

4.5 BUILDING A CLASSIFICATION BASED ON PLATELET CALCIUM MOBILIZATION PHENOTYPES AS MEASURED BY PAIRWISE AGONIST SCANNING *82*

4.5.1 Gender clustering patterns *83*

4.5.2 Sources of variability in synergy scores *85*

4.5.3 SVM model building and performance *87*

4.5.6 Agonist elimination to elucidate platelet calcium signaling pathways most predictive of gender *88*

4.5.3 Implementation of SVM on reduced dimension (3D) dataset *92*

APPENDIX A: DOSE RESPONSE CURVES FOR PLATELET AGONISTS 94

APPENDIX B: INVESTIGATION OF AUTOCRINIC SIGNALING EFFECTS IN PAS .. 95

APPENDIX C: NEURAL NETWORK PREDICTION OF TRINARY COMBINATIONS 96

REFERENCES 98

LIST OF TABLES

Table 2-1 Percent inhibition of medium dose iloprost and GSNO on medium doses of various agonist. 31

Table 4-1 Platelet activation events described in ODE model 76

Table 4-2 List of Important Platelet Agonist compiled from Kauskot et al. (2012) 81

LIST OF FIGURES

Figure 2-1 Platelet signaling pathway and neural network architecture 9

Figure 2-2 Pairwise Agonist Scanning experimental method. 13

Figure 2-3 Experimental and computational workflow 16

Figure 2-4 Neural network fit of PAS experiments 19

Figure 2-5 Neural network prediction of trinary experiments. 21

Figure 2-6 Examples of NN-predicted and measured calcium time traces for the trinary combination experiment 22

Figure 2-7 Neural network prediction of higher order combination experiments. 25

Figure 2-8 Calcium time traces for the higher order combination experiment. 26

Figure 2-9 Neural network prediction of sequential addition experiments. 28

Figure 2-10 Calcium time traces for the sequential addition experiments. 29

Figure 2-11 Analysis of iloprost inhibition effects 37

Figure 2-12 Range of individual neural network responses and donor responses 39

Figure 2-13 Simulations of platelet calcium levels based on theoretical agonist distribution in vivo. 46

Figure 3-1 Different effects in attenuation of subsequent platelet convulxin calcium response by thrombin compared to ADP and thromboxane. 54

Figure 3-2 Effect of time and dose of thrombin in attenuation of subsequent platelet convulxin calcium response. 57

Figure 3-3 Platelet convulxin calcium response attenuation effect is not observed by pretreatment with PAR-1 and PAR-4 agonists 59

Figure 3-4 Fibrin plays important role in platelet convulxin response attenuation effect. 61

Figure 3-5 Platelet convulxin response attenuation effect is reproduced in washed platelets and fibrinogen mixture. 62
Figure 3-6 Presence of fibrin reduces platelet adhesion on collagen. 64
Figure 4-1 ODE-NN model of platelet 76
Figure 4-2 Clustering of synergy scores based on donor gender 84
Figure 4-3 Sources of variability in synergy scores 86
Figure 4-4 SVM model performance and impact of specific agonist elimination 91
Figure 4-5 Implementation of SVM on reduced dimension (3D) dataset 93
Figure A-4-6 Dose response curves of each agonist. 94
Figure A-2 Investigation of autocrinic signaling effects. 95
Figure A-3 Neural network prediction of the trinary combination experiment. 96

Introduction

1.1 Platelet Activation

Platelets are small anucleate blood cells that mediate thrombosis and hemostasis. In response to vessel wall injury, platelets are activated, forming a hemostatic plug to prevent further bleeding. Plate activation occurs in three overlapping phases: initiation, extension and perpetuation [1].

In the initiation phase, platelets are initially captured, activated and adhere to the site of the vessel wall injury [2]. More specifically, at the vessel wall injury site, endothelium is disrupted, exposing collagen and von Willebrand factor (vWF). Platelets bind to vWF via platelet integrins GPIbα and $\alpha_{IIb}\beta_{3.}$ Platelets then bind to collagen via platelet surface receptors (integrin $\alpha_2\beta_1$ and glycoprotein (GP) VI). This forms a platelet monolayer on the collagen surface [2]. Binding of these platelet receptors to collagen also initiates intracellular signaling pathways that result in calcium mobilization, which is a measure of platelet activation.

In the extension phase, additional platelets are recruited to the growing thrombus. In this phase, activated platelets produce soluble agonists ADP (via granule release) and thromboxane (via arachidonic acid). Furthermore, platelets accelerate local thrombin generation via its membrane surface. These locally generated ADP and thromboxane binds to platelets and activates them via G protein coupled receptors (GPCRs) causing an increase in cytosolic calcium concentration and further release of ADP and thromboxane. Thrombin also activates platelets via binding of platelet PAR-1 and PAR-4 receptors, resulting in platelet calcium mobilization. Thrombin, ADP and thromboxane all activate platelets via G protein-coupled receptors (GPCRs) [2]. This positive feedback loop amplifies the initial signals and enables rapid activation and recruitment of platelets into a growing thrombus [1]. Specifically, platelet activation via GPCRs

triggers intracellular signaling processes that convert platelet integrin $\alpha_{IIb}\beta_3$ into its active confirmation $\alpha_{IIb}\beta_3$a, resulting in fibrinogen/vWF-mediated platelet aggregation [2]. Platelets start to adhere to each other and accumulate on top of the initial platelet monolayer via fibrinogen-$\alpha_{IIb}\beta_3$a and/or via fibrinogen-vWF bridges [3].

Events in the perpetuation phase take place to stabilize and to prevent premature disaggregation of the hemostatic platelet plug [2]. Ligand binding to platelet integrin $\alpha_{IIb}\beta_3$ facilitates platelet adhesion and aggregation and triggers outside-in signaling [4]. Outside-in signaling ultimately results in platelet spreading, further granule secretion and stabilization of platelet adhesion and aggregation as well as clot retraction [4].

Thrombin is also generated via Factor Xa via the tissue factor pathway [5]. In addition to activating platelets via its receptors PAR-1 and PAR-4, thrombin cleaves fibrinopeptide A from fibrinogen Aα-chains, thus initiating and catalyzing fibrin polymerization [6]. Fibrin cross-links and stabilizes the hemostatic plug, preventing premature disaggregation. The endothelium also synthesizes prostacyclin (increases adenyl cyclase activity) and nitric oxide (prevents degradation of cAMP by intracellular phosphodiesterases). Ultimately prostacyclin and nitric oxide increase intracellular cAMP levels and downregulates platelet signaling [7].

1.2 Role of Thrombin

Thrombin is a central enzyme involved in blood coagulation and platelet aggregation [8]. Thrombin is derived from prothrombin, a glycoprotein that is synthesized from the liver and released into the blood.

During activation of the coagulation cascade, prothrombin is converted to thrombin with the help of prothrombinase, a complex that comprises serine protease FXa, cofactor Va, anionic phospholispholipids on platelet surface, as well as calcium ions [8]. Thrombin mediates

hemostasis through multiple functions. Most notably, thrombin catalyzes conversion of fibrinogen to fibrin, which helps stabilize hemostatic plugs in response to vessel wall injury. Thrombin also converts FXIII to FXIIIa, which adds structural integrity to fibrin network by covalent cross-linking of glutamine and lysine residues on fibrin molecules. Thrombin also activates platelets by binding to proteinase-activated receptors PAR-1 and PAR-4 found on platelets. Thrombin is an especially potent platelet agonist that mobilizes cytosolic calcium and results in granule release of soluble agonists, platelet aggregation, as well as surface expression of phosphatidylserine (PS, a procoagulant phospholipid) [9, 10].

Because of thrombin's multiple roles in mediating hemostasis, as well as its high potency as a platelet agonist in vivo, efficient regulation of thrombin activity is crucial to ensure proper clot formation. There are several serine protease inhibitors (serpin) that block the function of thrombin, most notably antithrombin. Antithrombin is present in blood at relatively high concentrations (2.3 μM) [8]. Many antiplatelet therapies have been developed to target thrombin function. For example, Factor Xa inhibitors such as rivaroxaban, apixaban and edoxaban have been developed to limit thrombin generation and coagulation, useful for stroke prevention and deep vein thrombosis (DVT) management. PAR-1 and PAR-4 inhibitors have also been developed. For example, PAR-1 inhibitor vorapaxar has been approved as a treatment for patients with a history of myocardial infarction and peripheral artery disease [11].

1.3 Role of Fibrin

During coagulation, thrombin catalyzes the conversion of the soluble molecule, fibrinogen, to an insoluble molecule, fibrin. At the conclusion of hemostasis, fibrinolysis occurs to aid healing at the site of injury [12]. Plasmin is the enzyme that catalyzes fibrinolysis, it converts the stable insoluble fibrin clot into soluble products that can be cleared by the liver. Plasmin is derived from the activation of its zymogen, plasminogen (abudant in circulation, 2 μM) [12]. This

activation is catalyzed by tissue-type plasminogen activator (tPA, 70 pM in plasma) that is generated by endothelial cells [12]. Its function is regulated by plasminogen activator inhibitor 1 (PA1-1). Plasmin hyperfunction results in bleeding at injury sites, whereas hypofunction has been associated with hypercoagulability and thrombosis. Many conditions such as trauma and DIC are marked by an increase in fibrin degradation products (FDP) such as D-dimers. Hyperfibrinolysis has been implicated in trauma-induced coagulopathy [13]. Several clinical assays have therefore been developed to quantify D-dimers [12].

Trauma-induced platelet dysfunction is well observed but the underlying mechanisms are poorly understood [14]. Some studies show that in trauma patients, flow cytometric markers of platelet activation were elevated, despite impaired functional aperture closure times (both collagen/ADP and collagen/epinephrine closure times) [15]. Furthermore, platelet function falls within the first six hours of hospital admission but remains suppressed even up to 120 hours after injury [14]. These studies suggest that immediate platelet activation in response to the initial tissue injury may induce a prolonged refractory state, where a fraction of activated platelets have impaired function but remain in circulation [14]. Therefore, further studying the interaction between platelet and fibrin may shed light on potential mechanisms behind joint hyperfibrinolysis and platelet dysfunction as seen in patients following trauma.

1.4 Role of GPVI

GPVI is an immunoglobulin superfamily receptor that is expressed on platelet surface in association with the Fc receptor γ chain (FcRγ chain) [16]. There are approximately 3,700 copies of GPVI per platelet.

GPVI plays an important role in thrombosis and hemostasis. It is well known that GPVI supports adhesion during the initiation phase of platelet activation via its interaction with

collagen. Collagen also activates platelets, resulting in elevated and sustained levels of cytosolic calcium that prompt important platelet procoagulant activity, such as procoagulant phosphatidylserine (PS) exposure, granule secretion and soluble platelet agonist secretion such as ADP and thromboxane that further activate platelets. In addition to these well-known GPVI functions, recently, GPVI has also been demonstrated to contribute significantly to thrombus growth and stabilization [16]. For example, in GPVI-deficient and GPVI-depleted mice with $FeCl_3$ injury, the time to occlusion was prolonged, but not the initiation of thrombus formation [17]. In another study, GPVI has been shown to mediate thrombin generation in a collagen-independent manner [18]. A common explanation in these findings is that fibrin is a ligand for GPVI, and the binding of fibrin to GPVI promotes thrombin generation.

Because of the importance of GPVI in promoting thrombus growth and stabilization, GPVI has been highlighted recently as a desirable target for antithrombotic drug development. The inhibition or downregulation of GPVI was shown to impair thrombus formation but not disrupt hemostasis (does not increase bleeding), due to existing compensatory pathways.

1.0 A human platelet calcium calculator trained by pairwise agonist scanning

2.1 Abstract

Since platelet intracellular calcium mobilization $[Ca(t)]_i$ controls granule release, cyclooxygenase-1 (COX-1) and integrin activation, and phosphatidylserine exposure, blood clotting simulations require prediction of platelet $[Ca(t)]_i$ in response to combinatorial agonists. Pairwise Agonist Scanning (PAS) deployed all single and pairwise combinations of six agonists (ADP, convulxin, thrombin, U46619, iloprost and GSNO used at 0.1, 1, and 10xEC_{50}; 154

conditions including a null condition) to stimulate platelet P_2Y_1/$P2Y_{12}$, GPVI, PAR-1/PAR-4, TP, IP receptors, and guanylate cyclase, respectively, in Factor Xa-inhibited (250 nM apixaban), diluted platelet rich plasma that had been loaded with the calcium dye Fluo-4 NW. PAS of 10 healthy donors provided $[Ca(t)]_i$ data for training 10 neural networks (NN, 2-layer/12-nodes) per donor. Trinary stimulations were then conducted at all 0.1x and 1xEC_{50} doses (160 conditions) as was a sampling of 45 higher ordered combinations (four to six agonists). The NN-ensemble average was a calcium calculator that accurately predicted $[Ca (t)]_i$ beyond the single and binary training set for trinary stimulations (R = 0.924). The 160 trinary synergy scores, a normalized metric of signaling crosstalk, were also well predicted (R = 0.850) as were the calcium dynamics (R = 0.871) and high-dimensional synergy scores (R = 0.695) for the 45 higher ordered conditions. The calculator even predicted sequential addition experiments (n = 54 conditions, R = 0.921). NN-ensemble is a fast calcium calculator, ideal for multiscale clotting simulations that include spatiotemporal concentrations of ADP, collagen, thrombin, thromboxane, prostacyclin, and nitric oxide (NO).

2.2 Introduction

Platelet activation during heart attack and stroke occurs through combined signaling pathways involving various receptors responding to collagen, thrombin, ADP, and thromboxane. Endothelial production of prostacyclin is highly protective against thrombotic platelet activation as revealed by the known cardiovascular risks of COX-2 inhibitors. Similarly, endothelial production of NO has many cardiovascular effects via vasodilation and platelet inhibition. The clinical importance of these pathways is seen in the number of drugs in clinical trials or approved that target GPVI signaling, thromboxane, ADP, or thrombin. More than 50 million U.S. adults take aspirin to inhibit platelet COX-1 production of thromboxane in order to reduce long-term risk of cardiovascular disease [19]. Clopidogrel antagonizes ADP activation of platelet $P2Y_{12}$ receptors and is widely prescribed. Numerous anticoagulants are approved to target the generation or activity of thrombin.

Platelet activation occurs through multiple signaling pathways in which agonists bind specific receptors on the platelet to trigger signaling in a dose-dependent manner. During a clotting episode, platelets respond to exposed surface collagen, released ADP, synthesized thromboxane, and the serine protease thrombin, all while being simultaneously modulated by endothelial derived nitric oxide and prostacyclin. These receptor-mediated signaling pathways are not independent and significant crosstalk can occur (*Figure 1-1*).

The Pairwise Agonist Scanning (PAS) method was first developed by Chatterjee et al.(2010) using EDTA-treated platelet rich plasma (PRP) to quantify and predict the interactions between multiple pathways (*Figure 1-2*) [20]. The PAS method measures platelet calcium responses to all individual and pairwise combinations of agonists at low, medium and high concentrations (154 conditions total for six agonists at 0.1, 1, and 10 x EC_{50}, including a null condition).

Because EDTA chelates extracellular calcium and prevents store operated calcium entry (SOCE), the measured calcium data obtained using EDTA-treated PRP is enriched in the regulatory events surrounding IP3-mediated calcium release from the dense tubular system (DTS).

With PAS data, Chatterjee et al. were able to train an artificial neural network (NN) to predict platelet calcium response to combinations of agonists beyond the training data, such as trinary combinations, sequential additions of agonists, and combinatorial responses of four to six agonists [20].

The NN model builds an estimate of higher order interactions (response to >2 agonists) by combination of the measured binary interactions. A metric called the pairwise synergy score was defined to quantify the extent of cross-talk between pairs of agonists (*Figure 1-1B*) [20]. The pairwise synergy score (S_{ij}) was defined to be the difference between the integrated area (area under the curve) for the combined response to agonists i and j relative to the integrated area for both the individual agonist responses added together, normalized to the maximum absolute S_{ij}[20]. In other words, the synergy score is a measure of deviation of the platelet response from the simple additive response of each agonist. A positive S_{ij} value indicates synergistic behavior between agonists i and j whereas a negative S_{ij} value indicates antagonistic or saturating behavior and $S_{ij} = 0$ represents a purely additive response.

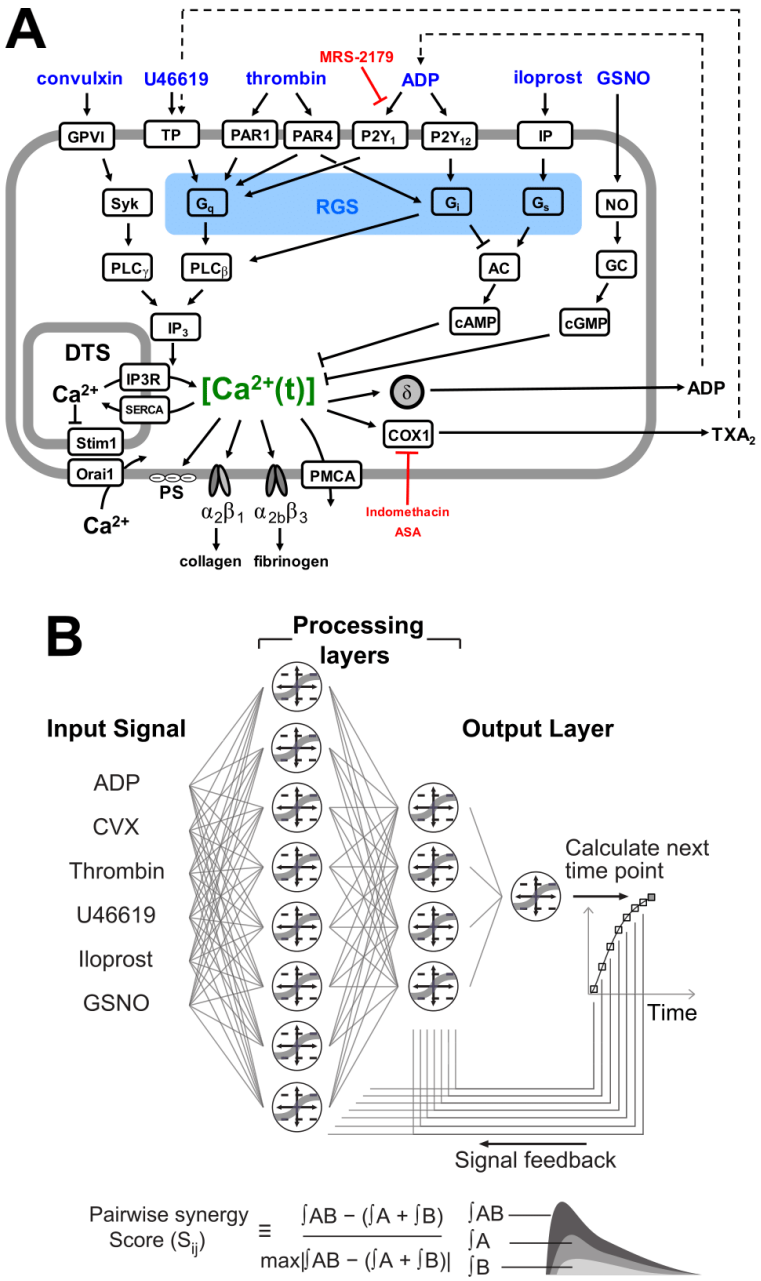

Figure 1-1 Platelet signaling pathway and neural network architecture. (A) The six agonists used in this study (ADP, convulxin, U46619, thrombin, iloprost, GSNO) and their respective platelet signaling pathways, all of which converge upon intracellular calcium mobilization. **(B)** A two-layer, 12-node neural network architecture was employed. Agonist concentrations at a given time point were fed into the processing layers; the layers then integrated the input signal with feedback at t = 1, 2, 4, 8, 16, 32, 64 and 128 seconds to calculate $[Ca^{2+}]_i$ at the next time point. The pairwise synergy score (S_{ij}) was also defined as the difference in integrated calcium response to two agonists used together and integrated response to agonists used individually, normalized by the maximum synergy score in the experiment.

Since many platelet pathways are triggered distally of IP3-released calcium and SOCE, the intracellular calcium concentrations can be used as a global metric of platelet activation. Calcium is the central "node" in platelet signaling, in that elevated calcium levels are central to downstream clotting events such as integrin activation, granule release, shape change, and phosphatidylserine exposure by platelets [21-23]. The ability to predict dynamic calcium traces for combinations of agonists enables the targeting of specific platelet pathways to increase or decrease platelet activity so as to achieve desired clinical outcome. NN trained on PAS data provides accurate calcium responses to different dose combinations of important agonists and is essential for simulating platelet function under flow. As an in silico predictor of calcium regulation, the NNs trained by PAS can be embedded in multi-scale simulations of platelet deposition under flow conditions. In the work of Flamm et al. (2011) [24], NN were trained via PAS using calcium-containing PRP and then used to predict platelet deposition rates on collagen in the absence of thrombin by accounting for platelet signaling in response to laboratory analogs of collagen, ADP, thromboxane, and prostacyclin.

A universal platelet calcium calculator provides a reference for platelet function of a healthy human. Platelet gain of function or loss of function in patients can therefore be measured in a high dimensional approach using the PAS method. Furthermore, since the specific pathways in the platelet that contribute to platelet gain or loss of function can be identified by PAS as well, PAS can be used to predict the sensitivity and resistance of drugs that target those specific agonist pathways, even loss of function mutations have been discovered with PAS [24]. Additionally, the calcium calculator can be embedded into a multiscale simulation of clotting under defined hemodynamic conditions.

In the current study, the PAS method was expanded for the use of exogenously added thrombin in the presence of normal calcium and included the potent platelet inhibitors iloprost and nitric oxide (NO). Thrombin is an extremely potent platelet activator via cleavage of platelet

PAR-1 and PAR-4 receptors. Additionally, to estimate average healthy human platelet responses, calcium data was obtained from 10 healthy donors as an ensemble-averaged predictor of platelet calcium. Distinct from the prior PAS in Chatterjee et al. (2010) where PAR-1 and PAR-4 agonist peptides were used with platelet rich plasma (PRP) treated with EDTA, the current study required a means to study exogeneously added thrombin without endogenous production of thrombin in PRP with normal calcium. In the current experimental design, blood was drawn into 250 nM apixaban (Ki = 0.08 nM) [25], a direct Factor Xa inhibitor, which does not alter extracellular calcium levels but prevents endogenous thrombin generation. This assay therefore allows the contribution of SOCE and includes the signaling distal of thrombin proteolytic activity on PAR-1 and PAR-4. Furthermore, the NN-ensemble method was employed to increase accuracy and robustness in NN predictions.

2.3 Materials and Methods

2.3.1 Pairwise Agonist Scanning (PAS)

Whole blood was drawn by venipuncture from healthy donors according to the University of Pennsylvania Institutional Review Board guidelines (protocol number: 805305), into a syringe containing apixaban (SelleckChem) with a final concentration of 250 nM. Donors self-reported to be free of any medications or alcohol use for three days prior to the blood draw. Female donors self-reported to not using oral contraceptives. Platelet rich plasma (PRP) was then obtained by subjecting the whole blood sample to centrifugation at 120g for 12 minutes. Then, 2 ml of PRP was incubated with a vial (single microplate size) of Fluo-4 NW dye mixture (Invitrogen) reconstituted with 7.8 ml of HEPES buffer and 200 μL of 77 mg/ml reconstituted probenecid (Invitrogen) for 30 minutes [20]. All single and pairwise combinations of six agonists (ADP, convulxin, thrombin, U46619, iloprost and GSNO) at low, medium and high concentrations (0.1,

1, and 10X EC_{50}), as well as a buffer condition (154 conditions total x 2 replicates) were dispensed into a 384-well plate (called the 'agonist plate') using a high throughput liquid handler (PerkinElmer Janus). The PAS agonists were: ADP ($P2Y_1$/ $P2Y_{12}$ activator, EC_{50} = 1 μM), convulxin (GPVI activator, EC_{50} = 2 nM), thrombin (PAR-1/PAR-4 activator, EC_{50} = 20 nM), U46619 (TP activator, EC_{50} = 1 μM), iloprost (IP activator, EC_{50} = 0.5 μM) and GSNO (NO donor, EC_{50} = 7 μM) (*Figure A-1*). ADP and GSNO were obtained from Sigma-Aldrich, convulxin from Pentapharm, thrombin from Haematologic Technologies Inc., U46619 and iloprost from Tocris Bioscience. After incubation with dye, the PRP was dispensed into a 384-well plate (called the 'read plate'). Both the agonist and read plate were loaded into a Molecular Devices FlexStation 3, a fluorescence reader with auto-pipetting capabilities. Agonists were dispensed to a column of wells containing the PRP, where well fluorescence F(t) was read and normalized by the pre-dispense baseline. Specifically, 20 μL of agonist was added to 30 μL of PRP in each well, giving a final volume of 50 μL. In each well, the final concentration of PRP after agonist addition was 12% PRP by vol., and the volume of calcium dye was 15 μL (30% dye by vol.). Readings were taken in intervals of 2.5 seconds. The fluorescence was read for 20 seconds before dispense, and readings were taken for 210 seconds after each dispense (EX/EM, 485 nm/525 nm). The entire plate was read, column-wise, in under 90 minutes. PAS was conducted on PRP from ten donors (50% male), each in replicate on two different days (20 PAS experiments total). In separate tests using indomethacin (Sigma-Aldrich) to block COX-1 and apyrase (Sigma-Aldrich) to degrade released ADP, there was no evidence for autocrine signaling in the dilute PRP conditions of the experiment (*Figure A-2*), as previously found with EDTA-treated PRP [20].

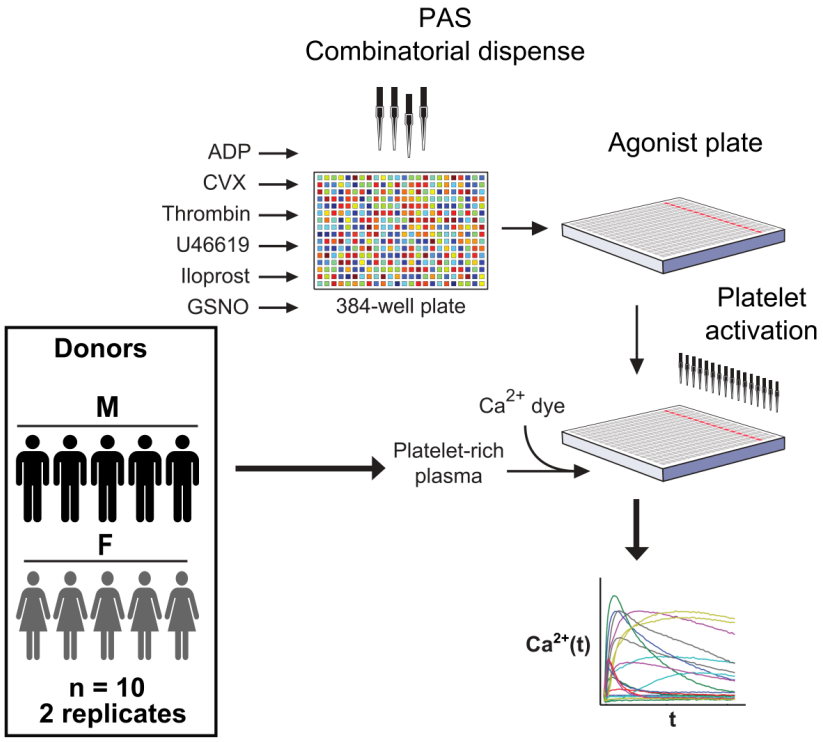

Figure 1-2 Pairwise Agonist Scanning experimental method.

2.3.2 Trinary, Higher Order Combinations and Sequential Addition Experiments

In experiments with trinary mixtures of agonists, all single and trinary combinations of the same six agonists at two different concentrations (0.1x and 1x EC_{50}), as well as a null buffer condition (173 conditions total x 2 replicates) were prepared in the agonist plate. This experiment was done once for each of the 10 PAS donors. There are 3,402 possible conditions involving four, five, or six agonists (higher order combinations of agonists) at low, medium and high concentrations. The higher order combination space was sampled in equal proportions (approximately 1.3% each of 4 to 6 agonist conditions). Thus, a total of n = 45 higher order combinations were sampled (16 four-agonist, 19 five-agonist, and 10 six-agonist conditions).

These experiments were done seven times spanning five donors (two repeat experiments for two of the donors), neither of which were present in the PAS training set. In the sequential addition experiments, all conditions involving sequential addition of three agonists (ADP, convulxin and U46619) at three different concentrations and a null buffer condition (55 conditions total x 2 replicates) were prepared in the agonist plate. The sequential addition experiment was done once on a single donor.

2.3.3 Calculation of Synergy Scores

The pairwise synergy score (S_{ij}) was defined to be the difference between the integrated calcium for the combined response to ij-agonists and the sum of the integrated calcium for both the individual agonist responses used independently, normalized by scaling to the maximum absolute synergy score observed in the experiment (*Figure 1-1B*) [20]. Synergy scores range from -1 to 1 (positive, synergistic; 0, additive; negative, antagonistic). Trinary synergy scores (S_{ijk}) were also similarly calculated as the difference of the combined response to ijk-agonists from the response for all three individual agonist responses. In general, synergy scores (S_n) are defined by Eq. 1, where the variable A_i represents the integrated calcium for the response to agonist i used independently, and $A_{1...n}$ is the area under the curve for the response to agonists 1 through n used simultaneously (n = 6 maximum for the six agonists deployed).

$$S_n = \frac{A_{1...n} - \sum_{i=1}^{n} A_i}{\max | A_{1...n} - \sum_{i=1}^{n} A_i |} \quad (1)$$

2.3.4 Neural Network Training and Averaging

The replicate wells in each PAS experiment duplicate were averaged before training. A 2-layer, 12-node dynamic neural network (NN), as employed in Chatterjee et al. (2010), was trained

on each averaged PAS experiment 10 times (n = 100), each time with a different set of initial weights and randomized division of 154 single and pairwise time course data into training and validation sets (90%/10%) (*Figure 1-1B*). All neural network model construction and training were done using the MATLAB Neural Network Toolbox (MathWorks). Training on a NN was done for a maximum of 1000 epochs, where each epoch was one pass through the training set followed by testing of the validation set. The training set vectors were used to optimize the NN weights and the validation set was used to test the weights during training so as to ensure the NN did not over fit to the training set. Early stopping was also employed, in which training would stop if the validation set error did not improve after five epochs. At the end of the training of each NN, the optimized NN weights would typically match the predicted time series to the experimental time series with a mean squared error anywhere on the order of 10^{-4} to 10^{-2}.

Each of the 100 trained NNs was then given the trinary experiment agonist concentration inputs and the resulting calcium time trace predictions were averaged to give an overall prediction for the average trinary experiment platelet response. The resulting synergy scores were also calculated and compared to the actual synergy scores for the trinary experiments. Similarly, each of the 100 trained NNs were given the higher order combination and sequential addition experimental concentration inputs, and the resulting calcium time trace predictions were compared to the measured values. A summary of the experimental and computational workflow is shown in *Figure 1-3*. In the testing of NN predictive abilities, output from all 100 NNs were averaged to give a final prediction. This approach is an ensemble method [26]. Ensemble methods are commonly used to overcome the inherent instability problem with NNs [26]. NNs (along with decision trees, multivariate adaptive regression splines etc.) are inherently unstable in that small differences in training data or conditions (e.g. initial weights) may cause variations in final predictions. Generating an ensemble of NNs and combining their outputs to produce a single

prediction has been proven by Cunningham et al. (2000) to be a robust solution to this problem [26].

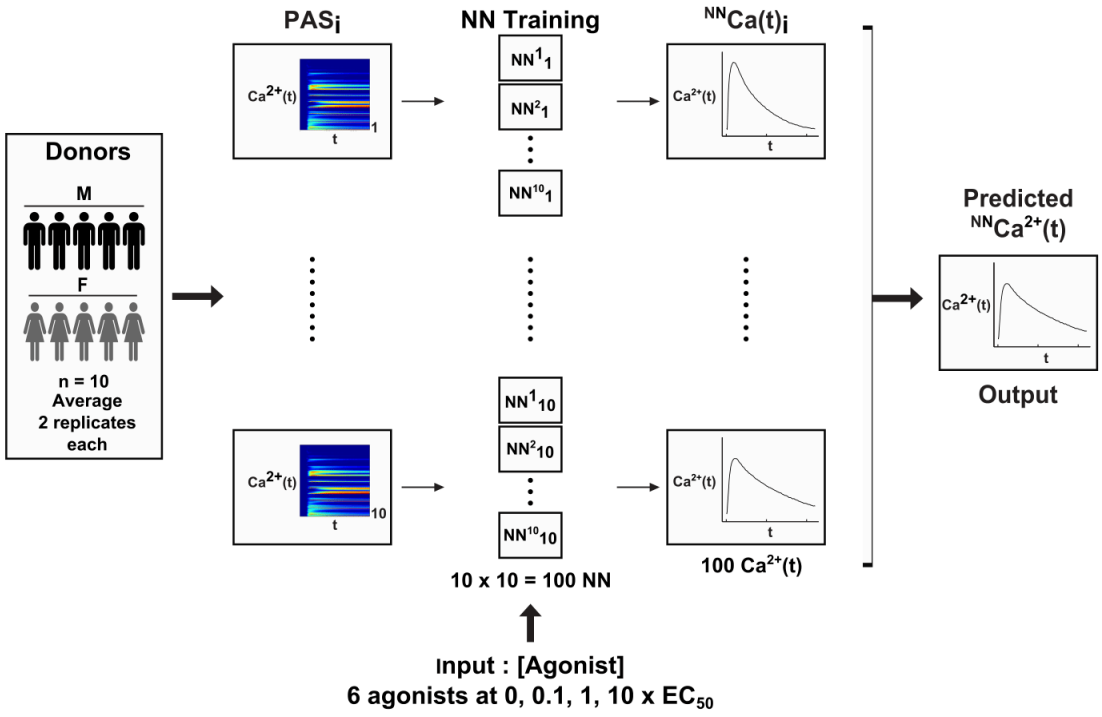

Figure 1-3 Experimental and computational workflow. The dataset consists of PAS experiments done in duplicate on PRP donated by ten donors (five male, five female). The duplicate experiments were averaged before training, i.e. n = 10. Each PAS experiment comprised a set of 154 calcium time traces, responses to all combinations of six agonists at three different concentrations and a buffer condition. A neural network was trained on each of the average PAS experiments giving a total of n = 100 trained neural networks. A different set of assay conditions (in this case, trinary combinations of the same six agonists at low and medium concentrations) are then input to each of the 100 trained neural networks (collectively called the ensemble NN) to generate predictions, which are then averaged and compared to the experimental average calcium time traces. These trinary combination experiments were done once each on the same ten donors, i.e. n = 10.

In the testing of the NN on higher order combination experiments, two additional donors (one male, one female) were used in the training set (12 donors for a total of 120 NNs). None of the 12 donors used in the training set were present in the testing donor set (five donors for a total of seven experiments). The success of the higher order combination predictions suggests that the ensemble NN was sufficiently robust to predict outcomes of donor aggregates without their

donor-specific PAS data during training, and that the NN ensemble has learned calcium mobilization patterns of an average healthy human. Furthermore, the sequential addition experiment predictions points to the ability of the ensemble NN to predict the outcome of an individual donor, not just aggregate outcomes of donors, and without having PAS data of that specific testing donor during training.

2.4 Results

2.4.1 Neural network prediction of platelet responses to binary agonist stimulation

The 10 x 10 NN-ensemble was trained on the pairwise agonist scanning (PAS) experiments of 10 donors and predicted the measured average pairwise calcium traces of those donors *(Figure 1-4A-C*) with a correlation coefficient of R = 0.975 (*Figure 1-4C*). *Figure 1-4A* indicates all 154 single and pairwise conditions used in the PAS with the corresponding calcium time traces (*Figure 1-4B*) and NN-predicted calcium time traces (*Figure 1-4C*). From *Figure 1-4A-C*, the calcium response to convulxin rose slowly, but became highly elevated and was sustained. In contrast, calcium responses to ADP or U46619 displayed rapid onset but were weaker and more transient than calcium responses to convulxin and thrombin. Interestingly, the thrombin response displayed rapid calcium mobilization, prominent elevation, and was more sustained than calcium responses observed in earlier studies with PAR-1 and PAR-4 agonist peptides [20]. A total of 135 binary synergy scores (all pairs of six agonists at three concentrations) for the PAS experiment and the NN-prediction are shown in vector form (*Figure 1-4*), representing the average human platelet phenotype. Both experimental and NN-predicted synergy values were plotted in heat map form in *Figure 1-4D*. Similar to the time series prediction, the NN ensemble was able to predict the measured average pairwise synergy scores of those ten donors (R = 0.937) (*Figure 1-4E*). Many synergy values clustered around the center of the range (S_{ij}~0, additive) with slightly more negative values extending to full antagonism (S_{ij}~ -

1). The maximum synergy score did not exceed 0.5. The most negative synergies were found with pairwise mixtures that included iloprost. The experimental and NN-predicted synergy scores were also arranged by dose and agonist pairs (*Figure 1-4F*). From *Figure 1-4F*, iloprost was inhibiting for all agonists used in combination with it. GSNO was also inhibiting for most conditions, however, low dose GSNO slightly potentiated thrombin-induced calcium response. The combination of medium or high dose thrombin with medium dose convulxin was particularly synergistic, consistent with several findings [27, 28]. Also, thrombin signaling was synergistic with thromboxane signaling which is a novel observation since both agonists signal through G_q.

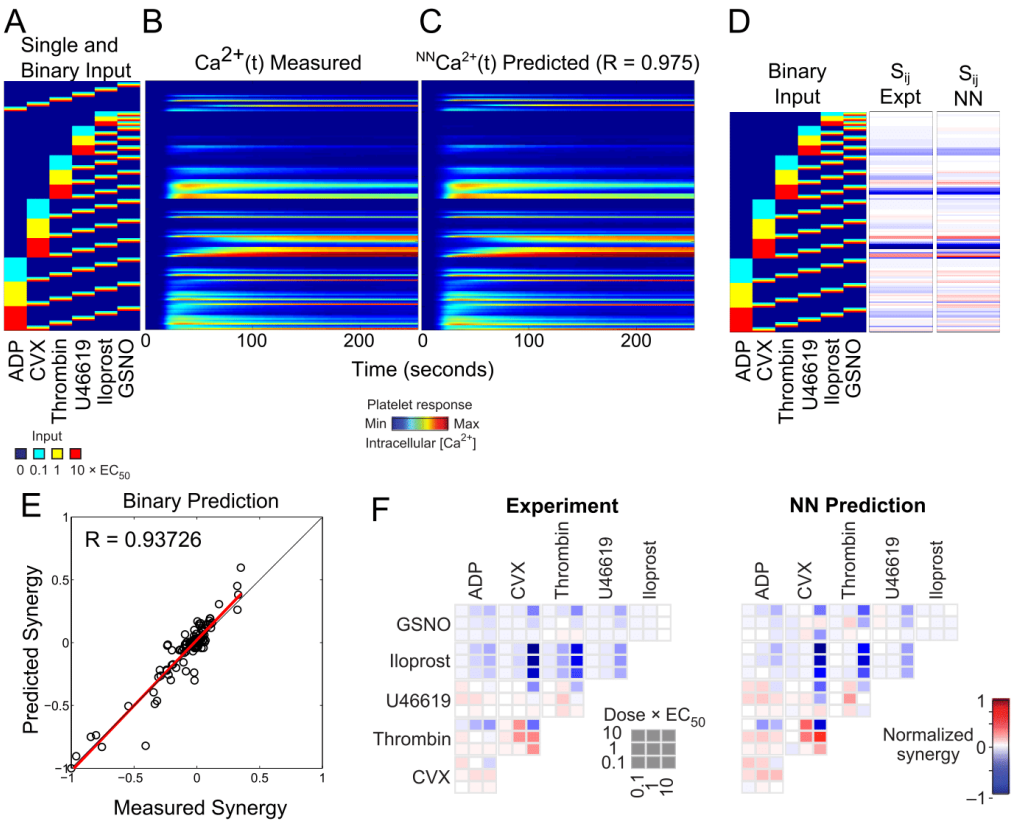

Figure 1-4 Neural network fit of PAS experiments. (A) PAS experiment input conditions: all single and pairwise combinations of six agonists at low, medium and high concentrations. **(B)** Measured average calcium time courses of ten donors in the PAS experiments. **(C)** The neural network trained on the PAS experiments of ten donors was able to fit the measured average pairwise calcium traces of those ten donors with a correlation coefficient of R = 0.975. **(D)** The experimental and NN-predicted 135 pairwise synergy scores for the PAS experiment. **(E)** The neural networks were able to fit the measured average pairwise synergy scores of those ten donors with a correlation coefficient of R = 0.937. **(F)** The experimental and NN-predicted synergy scores arranged by dose and agonist pairs.

2.4.2 Neural network prediction of platelet responses to trinary agonist stimulation

To test the predictive capability of the NN-ensemble beyond the training set, the NN-ensemble was used to predict the calcium output of trinary agonist stimulations. To avoid saturation effects of agonist induced signaling, the trinary combination experiments comprised all trinary combinations of six agonists at only the low and medium doses (*Figure 1-5*). The NN ensemble trained only on the PAS experiments of ten donors in duplicate was able to predict the measured average trinary calcium traces of those donors with high accuracy (R = 0.924) (*Figure 1-5B-C*). This demonstrated the de novo predictive capability of the neural network model. There were 160 trinary synergy scores for the trinary experiment consisting of all trinary combinations of six agonists at two different concentrations (0.1 and 1 x EC_{50}). The NN trained only on the PAS experiments of ten donors in duplicate was able to predict the measured average trinary synergy scores of those ten donors with a correlation coefficient of R = 0.850. (*Figure 1-5D*). The synergy scores plotted for the trinary experiments in *Figure 1-5D*, though also clustered around zero, extended more toward 1 (synergistic) compared to the binary synergy scores (*Figure 1-4E*), which extended toward -1 (antagonistic). This is expected, in part, because the trinary experiments were sampled across only the low and medium dose ranges, thus, there were fewer instances of saturation due to platelet activation by high doses of multiple agonists. Furthermore, only low and medium doses of the inhibitors iloprost and GSNO were used, so their strongest inhibitory/antagonistic effects at 10x EC_{50} were not present in the trinary data (but were present in the binary experiments). To illustrate the predictive power of the NN-ensemble, the full time series plots of a random sampling of the 160 trinary conditions are shown in *Figure 1-6*. Full time series plots of all 160 trinary conditions rescaled to 0.5 are also shown in *Figure A-3*. For the trinary stimulations, the predicted calcium time traces fit the experimental data over the full time domain with remarkable accuracy. The trinary agonist experiments embed information about

platelet signaling during in vivo hemostasis, thrombosis, or bleeding. For example, during the early stages of vessel wall injury, platelets are activated by collagen of the damaged vessel wall [29] which can also generate thrombin via the extrinsic pathway (distal of tissue factor). Concomitantly, endothelium-derived nitric oxide and prostacyclin modulate platelet functions. Therefore at this early stage the platelet is mainly exposed to these three agonists: exposed collagen, prevailing nitric oxide and prostacyclin, while thrombin is dynamically generated. Soluble agonists such as ADP and thromboxane become critically important during platelet mass build-up (sometimes called secondary aggregation) when activated platelets release ADP from dense granules and generate thromboxane via COX-1. Recent in vivo and in vitro studies reveal that the platelets in the "core" are exposed to high levels of thrombin, while the outer shell of platelets see little thrombin but are especially sensitive to the presence of thromboxane [30-34].

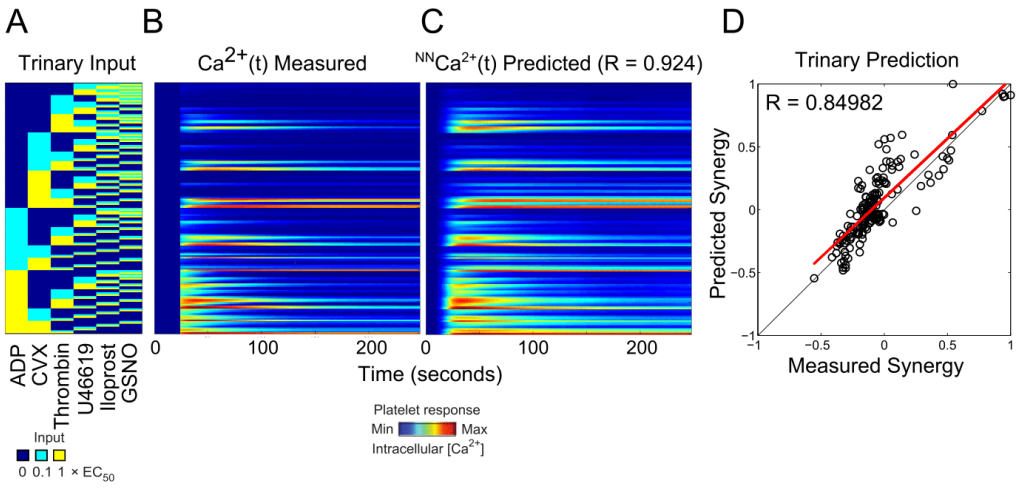

Figure 1-5 Neural network prediction of trinary experiments. (A) Trinary experiment input conditions: all trinary combinations of six agonists at low and medium concentrations. **(B)** Measured average calcium time courses of ten donors in the trinary experiments. **(C)** The neural network trained on the PAS experiments of ten donors was able to fit the measured average trinary experiment calcium traces of those ten donors with a correlation coefficient of R = 0.924. **(D)** There are 160 trinary synergy scores for the trinary combination experiment. The neural networks were able to fit the measured average trinary synergy scores of those ten donors with a correlation coefficient of R = 0.84982.

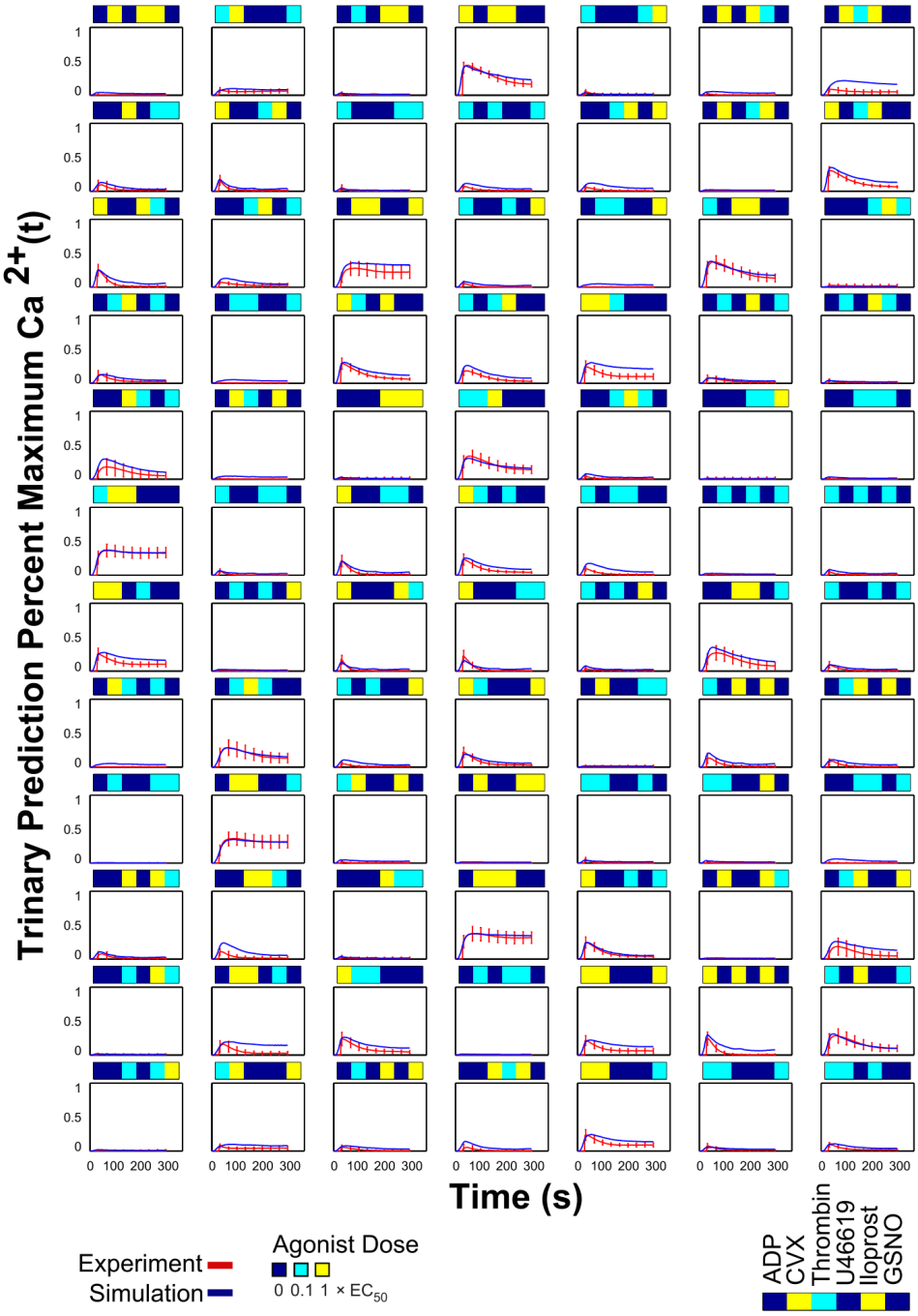

Figure 1-6 Examples of NN-predicted and measured calcium time traces for the trinary combination experiment. Plots of 84 of the 160 conditions in the trinary combination experiment (all trinary combinations of agonists at two concentrations: 0.1 x EC_{50} and 1 x EC_{50}).

2.4.3 Neural network prediction of higher order combination experiment

The higher order test of the NN-ensemble comprised a 45-condition sampling of the full experimental space in equal proportions (n = 45 total combinations: 16 four-agonist, 19 five-agonist, and 10 six-agonist conditions) (*Figure 1-7A*). In this subsequent higher order experiment, the donor pool for the generation of the PAS training dataset was expanded to 12 individuals, 10 of which were also previously used in the prediction of trinary combination outcomes. The higher order experiments were an aggregate of seven experiments spanning five donors, none of whom were utilized in the PAS training dataset. The NN-ensemble trained only on the PAS experiments of 12 donors was able to predict the calcium traces of the higher order combination experiments with sufficiently high accuracy (R = 0.871) (*Figure 1-7A-C*). This higher order experiment represented a most challenging test of the de novo predictive capability of the neural network model, more so than the trinary combination experiments of *Figure 1-5*. With up to six stimuli present, this experiment triggers an extraordinary range of signaling complexity in the platelet. The NN-ensemble trained only on the PAS experiments was able to predict the measured synergy scores with a correlation coefficient of R = 0.6953 (*Figure 1-7D*). Compared to the synergy scores of the binary (*Figure 1-4E*) and trinary experiments (*Figure 1-5D*), the synergy scores of the higher order combination experiments tended to be more antagonistic due to saturation effects. Many of the measured and predicted higher ordered synergy scores were additive (S~0) with none being highly synergistic (all S < 0.25) which occurs for saturated signaling by only a few of the agonists in the mixture. During saturation, a maximal amount of calcium is released by IP3 or conveyed by SOCE. Therefore, the actual calcium mobilization caused by high doses of ≥4 activating agonists was not expected to exceed the sum of calcium release due the individual agonists. The time series plots of all 45 conditions in the higher order combination experiment (*Figure 1-7C* and *Figure 1-8*) indicated that the NN-predicted time calcium time traces tended to

consistently under predict calcium traces involving high dose convulxin. This may be because the NN had not been trained on any data that involves calcium levels as high as that triggered by combinations of 4–6 agonists including a high dose of the potent activator convulxin. Another theory is that the NN may have over predicted the saturation effects in calcium responses that may result from combinations of multiple agonists in addition to high dose convulxin. Furthermore, the NN predictions underestimated the effect of iloprost and GSNO, in that combinations that involved those agonists tended to have calcium level predictions that were higher than the experimental values. However, the overall shape of almost all the predictions fits the experimental time traces rather well, indicating that the NN ensemble was able to capture the kinetics of these higher order combination experiments. There was no apparent trend in calcium trace prediction accuracy with increasing number of agonist (four-agonist conditions had $R = 0.82332$, five-agonist conditions had $R = 0.90699$, six-agonist conditions had $R = 0.79398$). However, this sampling of 45 conditions was only 1.3% of the complete experimental space of 3,402 possible conditions.

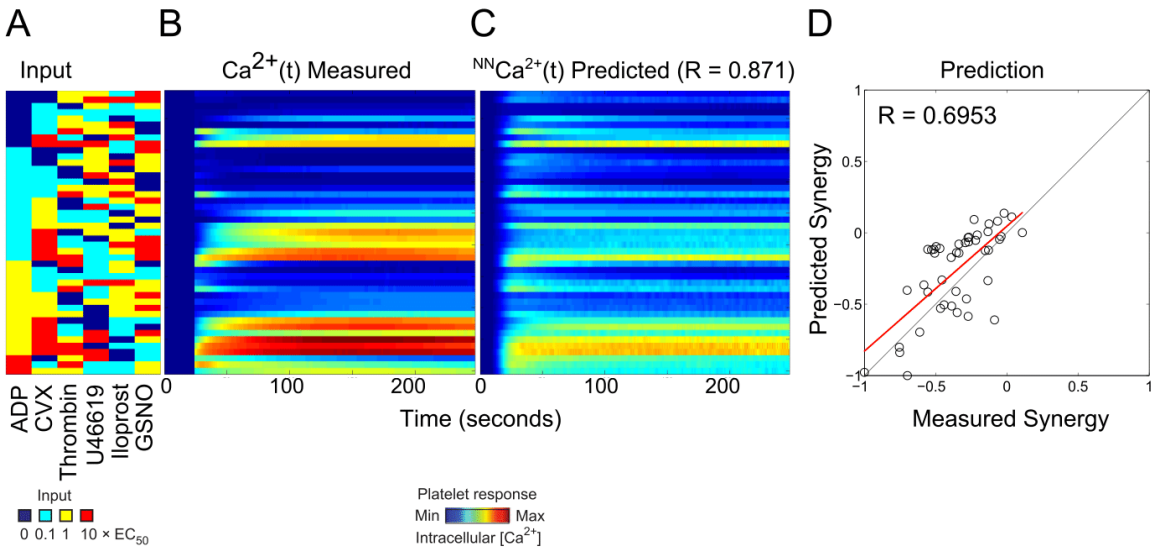

Figure 1-7 Neural network prediction of higher order combination experiments. . **(A)** Experimental input conditions that are a random sample (n = 45) of the complete experimental space involving four, five, and six agonists at low, medium and high concentrations (n = 3,402). **(B)** Average measured calcium time courses of seven experiments spanning five donors in the higher order combination experiment. **(C)** The neural network trained on the PAS experiments of 12 donors was able to fit the measured experimental calcium traces with a correlation coefficient of R = 0.871. **(D)** The neural networks were able to fit the measured average synergy scores of those ten donors with a correlation coefficient of R = 0.6953.

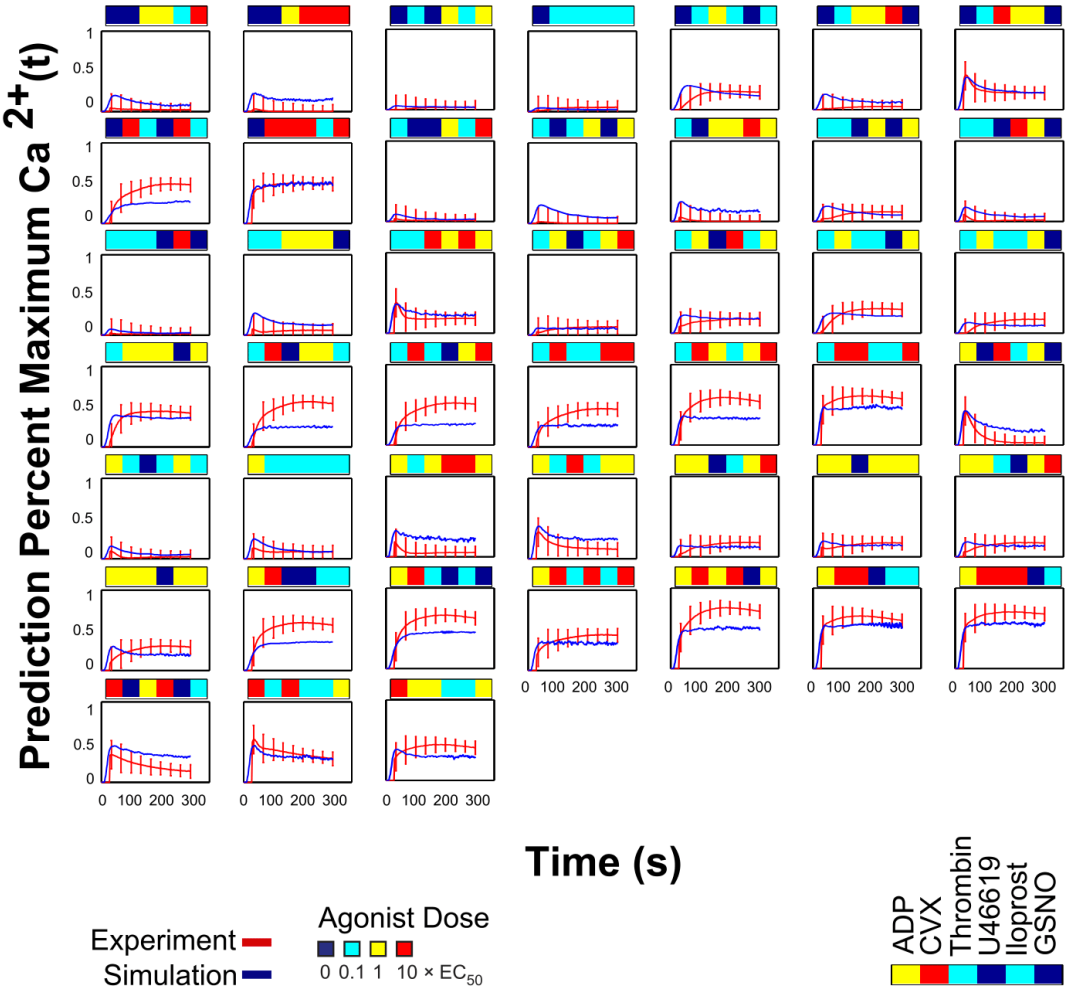

Figure 1-8 Calcium time traces for the higher order combination experiment. Plots of the 45 conditions in the higher order combination experiments.

2.4.4 Neural network prediction of sequential addition combination experiment

A sequential addition experiment was done with all permutations for a two-dispense experiment of three agonists (ADP, convulxin and U46619) in the full dose range, i.e. 54 conditions total (*Figure 1-9A*). Calcium time traces were plotted in heat map form in *Figure 1-9 B*; the arrows indicate the time at which the corresponding agonists in *Figure 1-9A* were dispensed. The NN trained on the PAS experiments, in which agonist pairs were added simultaneously, was also able to predict the calcium output of the sequential addition experiment

with a correlation coefficient of R = 0.921 (*Figure 1-9C*). The plots of both the experimental and predicted time series are shown in *Figure 1-10*. Due to limitations of working with isolated platelets in vitro (requiring use within 3 hours from venipuncture), the PAS calcium readings for sequential addition tests required a 260 second window per column for the 24 columns of the 384-well plate. The shorter 260 second training interval still provided accurate predictions for the whole 780 second window because many of the PAS calcium traces following agonist-mediated increases had decayed to resting levels within the 260 second training interval. This was true of all agonist combinations except for those involving convulxin, which generated sustained calcium levels in the 260 second window. Within this training interval, the PAS had captured the full kinetic effects of all the agonists except for convulxin. Extending the training window to 300 seconds, where the second dispense in the sequential addition experiment had happened, would not confer additional information to the NN because convulxin responses would not have started decaying at the end of 300 seconds. Therefore, the NN trained on the PAS equipped with this kinetic information, in addition to crosstalk information between these six agonists from the pairwise conditions, was able to predict calcium responses to two agonists added sequentially with sufficiently high accuracy (R = 0.921), with a tendency for mild over prediction of calcium compared to the experimental time series. Nonetheless, the shape of the NN and measured calcium traces were quite similar (*Figure 1-10*). As expected, in conditions where convulxin was added first in the sequential addition experiments, the NN predicted a sustained calcium level instead of a slight decay in calcium response toward the end of the 780 second window, since this decay had not been captured in the 260 second window of the PAS experiment used in NN training.

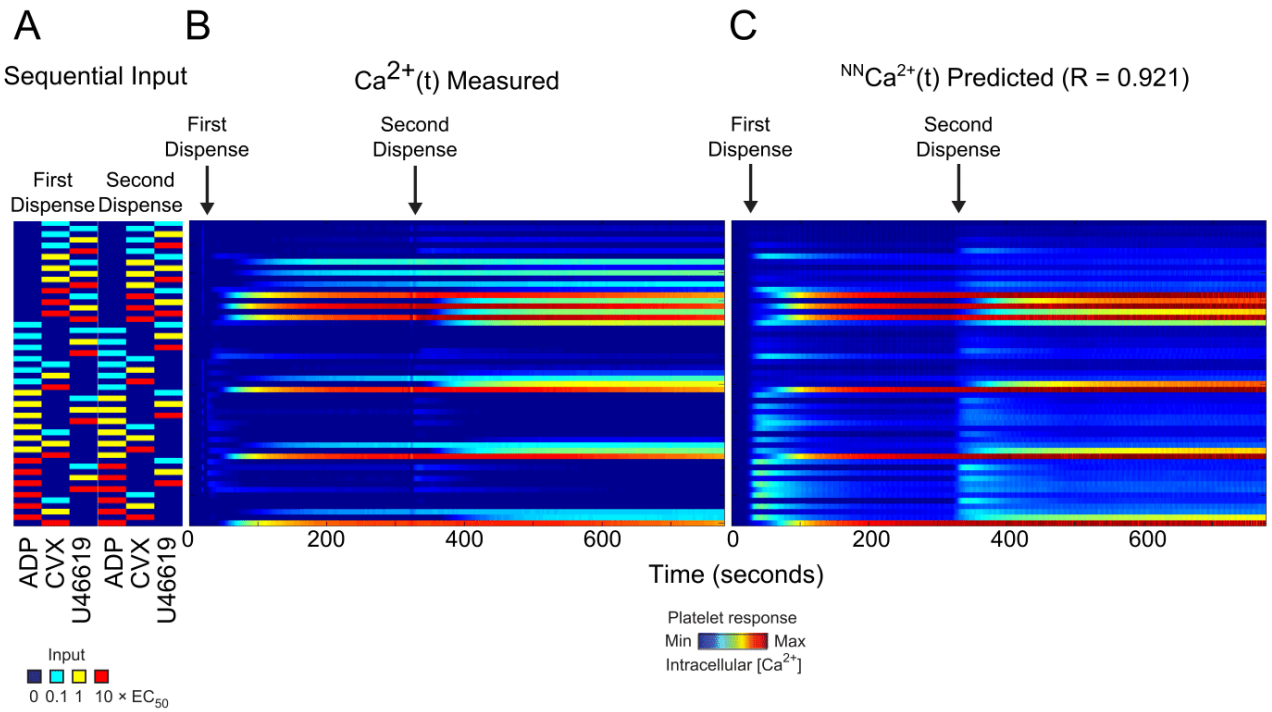

Figure 1-9 Neural network prediction of sequential addition experiments. (A) Experimental sequential input conditions (n = 54) for three agonists (ADP, convulxin and U46619). **(B)** Measured calcium time courses of Donor Y in the sequential addition experiment. **(C)** The neural network trained on the PAS experiments of ten donors was able to predict the measured sequential addition calcium traces of Donor Y with high accuracy (correlation coefficient, R = 0.921).

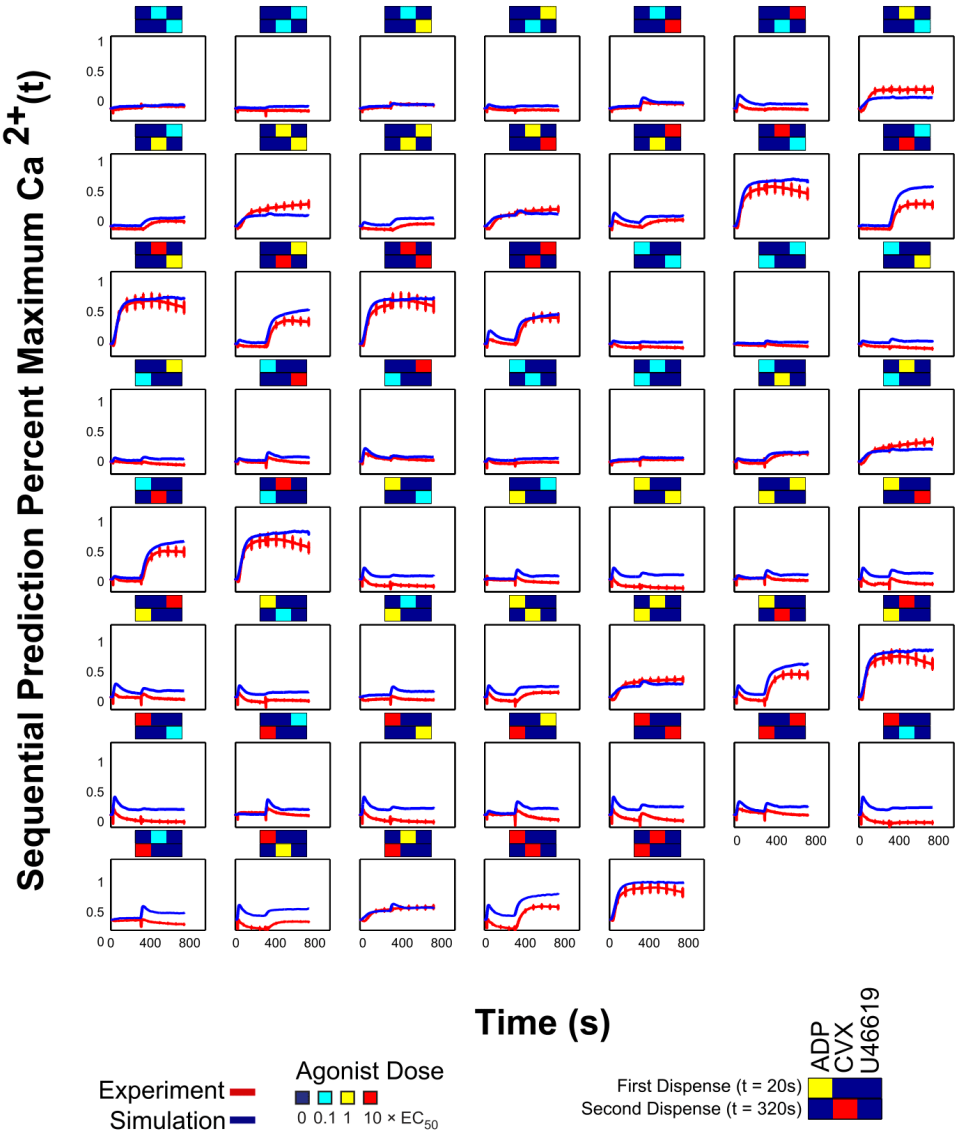

Figure 1-10 Calcium time traces for the sequential addition experiments. Plots of the 54 conditions in the sequential addition experiments.

2.4.5 Analysis of synergy scores

The synergy scores (S_{ij}) reduced more than 25,000 calcium time points from a PAS experiment to a 135-parameter vector. Each synergy score is the most succinct first order measure of crosstalk between specific pairs of agonists at specific doses. The discovery of new synergistic and antagonistic effects between specific combinations of agonists via synergy scores can

motivate efforts to study the underlying biochemical mechanisms (e.g. the thrombin-thromboxane positive synergy is unexpected since both signal through G_q). Furthermore, the synergy score may underlie a drug risk (as seen with COX-2 inhibition therapy [20]), a patient-specific drug sensitivity or resistance. Future bottom-up models that predict the 135-parameter synergy vector may require interactions and pathways not explicitly represented in the currently prevailing platelet signaling model of *Figure 1-1A*.

Synergy scores of the 10-donor, 20-experiment averaged PAS experiments were further analyzed to gain insight into platelet signaling. The same was done for the averaged trinary combination experiments and the higher order combination experiments. The mean of the standard deviation between donors for a given synergy score in the experiment is 0.0932 for binary dataset, 0.1722 for the trinary dataset, and 0.2029 for the higher order dataset. This reflects the variation in a given synergy score between donors. As the number of agonists involved increased, signaling complexity increased, resulting in larger donor variations in a given synergy score.

The mean of the pairwise S_{ij} was very close to zero (S_{ij} = - 0.0626), and the maximum synergy score was 0.3461. The mean of the trinary synergy scores was slightly less negative (S_{ijk} = -0.0401), and the maximum synergy score was 1, meaning that the maximum absolute synergy score is a synergistic one. Because trinary conditions were only sampled at the low and medium dose, calcium saturation from multiple high doses of agonists was avoided, therefore the synergy scores tended to be more synergistic. The mean of the higher order combination synergy scores was quite antagonistic (S = -0.3484), and the maximum synergy score was also very small (S = 0.1085). As more agonists are involved, platelet signaling tends to reach saturation, which shifts the mean synergy score towards antagonism, and lowers the maximum synergy score.

For the PAS and higher order combination experiments, the synergy score with the maximum magnitude was antagonistic (i.e. minimum synergy score is -1 for binary and higher

order experiment averages) because iloprost and GSNO are both strong inhibitors in this assay. For the average PAS experiment, the most antagonistic synergy score involved a high dose of iloprost; for the higher order experiment, it involved low dose iloprost and high dose GSNO. The most antagonistic synergy score for the trinary experiment is -0.5395 and it involves medium dose iloprost. Interestingly, the synergy metric indicates that IP receptor activation by iloprost, a prostacyclin mimetic, was a more potent inhibitor of calcium mobilization compared to that observed with the activation of guanylate cyclase via GSNO release of NO (*Figure 1-4F*). This was confirmed by the calculation of GSNO and iloprost percent inhibitions of various agonists used in this assay (*Table 1-1* Percent inhibition of medium dose iloprost and GSNO on medium doses of various agonist.). It is also interesting to note that low and medium dose of GSNO slightly potentiated the medium dose thrombin-induced calcium release (15.73% and 13.32% increase respectively), consistent with previous findings that low levels of the NO donor sodium nitroprusside slightly potentiated thrombin-induced calcium release via store-operated calcium entry (SOCE), whereas higher levels inhibited thrombin-induced increases in calcium [35]. Similarly, in our assay, high dose GSNO inhibited the calcium release of medium dose thrombin (39.11% inhibition). The maximum synergy score for the PAS experiment involved a high dose of convulxin and medium dose of thrombin (S_{ij} = 0.3461); the maximum of the trinary experiment involved medium dose convulxin, thrombin and GSNO (S_{ijk} = 1); the maximum of the higher order combination experiment involved high dose ADP, medium dose thrombin, high dose U46619 and low dose GSNO (S = 0.1085).

	% inhibition by Iloprost	**% inhibition by GSNO**
ADP	71.74%	34.08%
CVX	99.71%	18.58%
Thrombin	76.37%	-13.32%
U46619	91.55%	67.09%

Table 1-1 Percent inhibition of medium dose iloprost and GSNO on medium doses of various agonist.

In fact, four of the five strongest positive pairwise synergies involved convulxin and thrombin (the fifth was medium dose thrombin and U46619). Of the five strongest positive synergies in the trinary experiments, medium dose convulxin and thrombin were involved in all of them, low and medium dose GSNO was involved in two of them. Of the five strongest positive synergies in the higher order experiments, thrombin and U46619 were present in four of them; low and medium dose GSNO is involved in four of them, convulxin and thrombin were present in two of them. It is apparent that convulxin and thrombin used together gave the strongest synergistic effects, thrombin and U46619 used together also accounted for some of the strongest synergistic effects. For the trinary and higher order experiments, the presence of low and medium dose GSNO was also implicated in the highest synergy scores, and only when thrombin was present, which supports the previous finding that low levels of NO potentiates thrombin-induced calcium release via SOCE [35].

The synergistic effects between convulxin and thrombin were similarly found by Keuren et al. [27] and it was thought that thrombin-mediated influx of platelet extracellular calcium (through PAR-1 but not PAR-4) enhances the collagen induced procoagulant response. This may explain why the synergistic effects between convulxin and the PAR-1 agonist were not as prominent in previous PAS work that was done in the absence of extracellular calcium [19]. Another study that found similar synergistic effects between sub threshold concentrations of thrombin and GPVI showed that the synergism was independent of Src kinases and Syk [28]. As previously observed with EDTA-treated PRP activated by PAR-1 agonist peptide and U46619 [20], thrombin activation of PAR-1/PAR-4 and the thromboxane mimetic U46619 were synergistic (S_{ij} = 0.1127 at medium dose of thrombin and low dose U46619), and especially at medium doses of thrombin and U46619 (S_{ij} = 0.1766).

2.4.5 Inhibition of calcium release by iloprost

Iloprost and GSNO when used alone or together with each other had no effect on platelet calcium (top 9 binary conditions of *Figure 1-4A-C*), as expected. However, these compounds elevate cAMP and cGMP to attenuate calcium mobilization [36-38] and this inhibition was clearly seen in the calcium traces (*Figure 1-6, Figure 1-8*).

Iloprost was a potent, rapid, and sustained inhibitor of convulxin activity (99.6–99.7% inhibition overall) (*Figure 1-11B, H*), indicating that IP signaling was more rapid than GPVI signaling. Furthermore, iloprost was more potent than GSNO in inhibiting activity of all agonists this assay, for example, medium dose GSNO caused only 18.6% inhibition of convulxin activity (*Table 1-1*). Convulxin caused slow platelet activation since it must multimerize GPVI to induce signaling [39]. During thrombin activation of PAR-1/4, the inhibition by iloprost was also rapid (as seen by the offset in peak calcium levels), but was incomplete initially and became more pronounced after approximately 25 seconds post-stimulation (*Figure 1-11D, J.*). Low and medium levels of iloprost (0.1 and 1 x EC_{50}) resulted in similar inhibition of thrombin calcium release (~76.3 to 78.9% inhibition (*Figure 1-11D, J*). In the experiments with thrombin, iloprost may have a diffusive and kinetic advantage over thrombin which must cleave PAR-1/4 whereas iloprost simply must the bind IP receptor. A similar pattern was observed for ADP (*Figure 1-11*M, N.). However, there was no offset in peak calcium levels, potentially due to similar diffusive and binding kinetics of these two small molecules for their respective receptors. The inhibition by iloprost of ADP signaling only began after ADP-induced calcium level peaked around 20 seconds post-stimulation (41.5% to 71.7% inhibition at 0.1 and 1 x EC_{50}, respectively). During U46619 stimulation of TP receptor, the inhibition by iloprost was apparent immediately after dispense and increased after calcium levels peaked (~20 sec post-stimulation). Iloprost was slightly more potent against U46619 compared to ADP, causing 87.4% to 91.6% inhibition at 0.1

and 1 x EC_{50}, respectively (*Figure 1-11F, L*.). Overall, iloprost was more fast-acting and potent against the slower signaling agonists such as convulxin (99.6–99.7% inhibition) or thrombin (~76–79% inhibition) that required receptor multimerization or enzymatic cleavage, compared to small molecules that rapidly equilibrated with their receptors such as U46619 (87–92% inhibition) or ADP (41–72% inhibition). Iloprost may be less active against ADP compared to U46619 since ADP also binds the $P2Y_{12}$ receptor which antagonizes cAMP pathways (*Figure 1-1A*).

When ADP and convulxin were used simultaneously, ADP signaling dominated early calcium mobilization while convulxin signaling maintained sustained calcium levels. (*Figure 1-11A, G*) With combined ADP/convulxin stimulation, medium dose iloprost resulted in only 71.1% inhibition (*Figure 1-11G*) since it was not a complete blocker of the early signaling (at $t < 30$ sec) induced by ADP. A similar trend occurred with thrombin/convulxin co-stimulation (*Figure 1-11C, I*), however, iloprost was more effective in this case (83.5% inhibition with medium dose iloprost, *Figure 1-11I*) since thrombin/convulxin co-stimulation elevated calcium relatively slowly. When the weaker agonist U46619 (compared to ADP) was used with convulxin, iloprost remained a very potent inhibitor (98.9% inhibition with medium dose iloprost, *Figure 1-11E, K*).

Iloprost 0.1 x EC_{50}

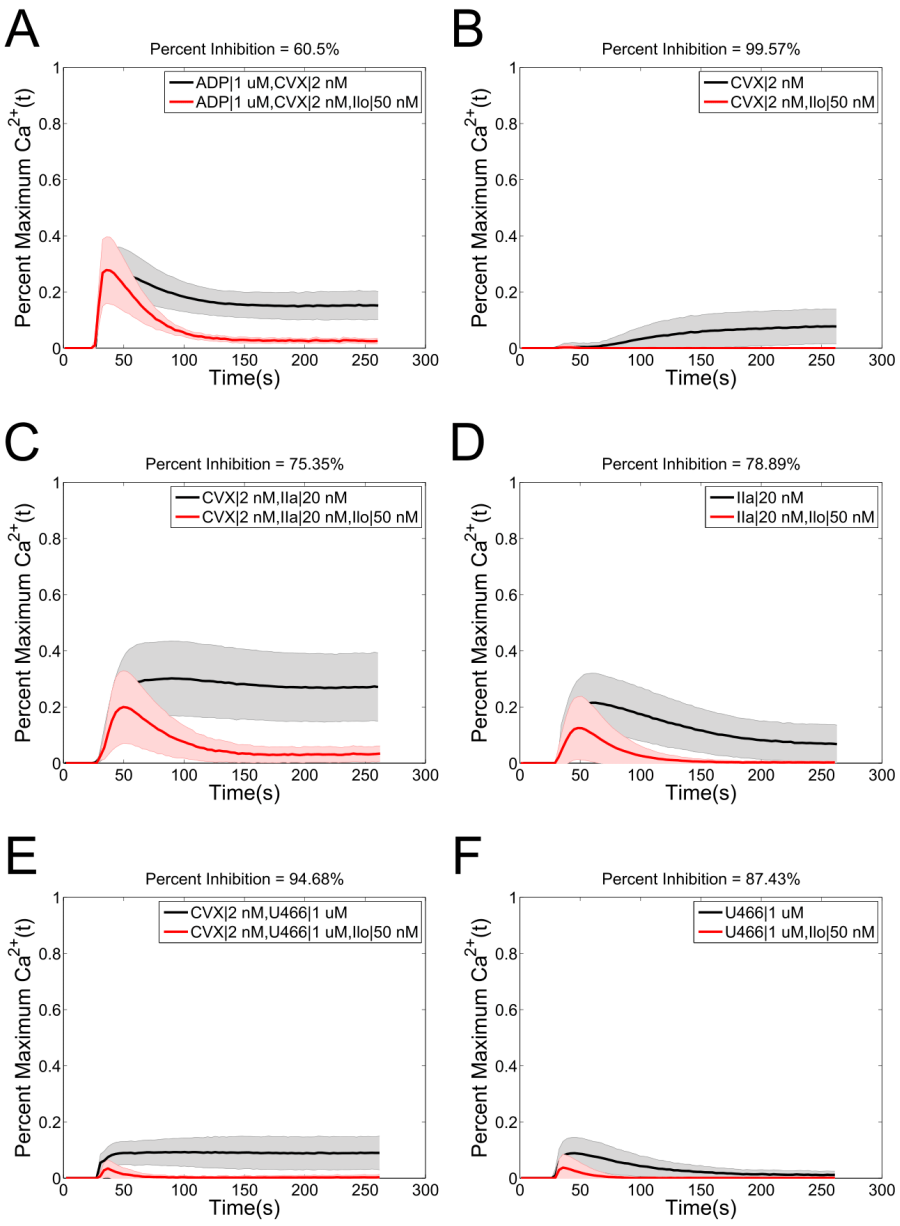

Iloprost 1 x EC_{50}

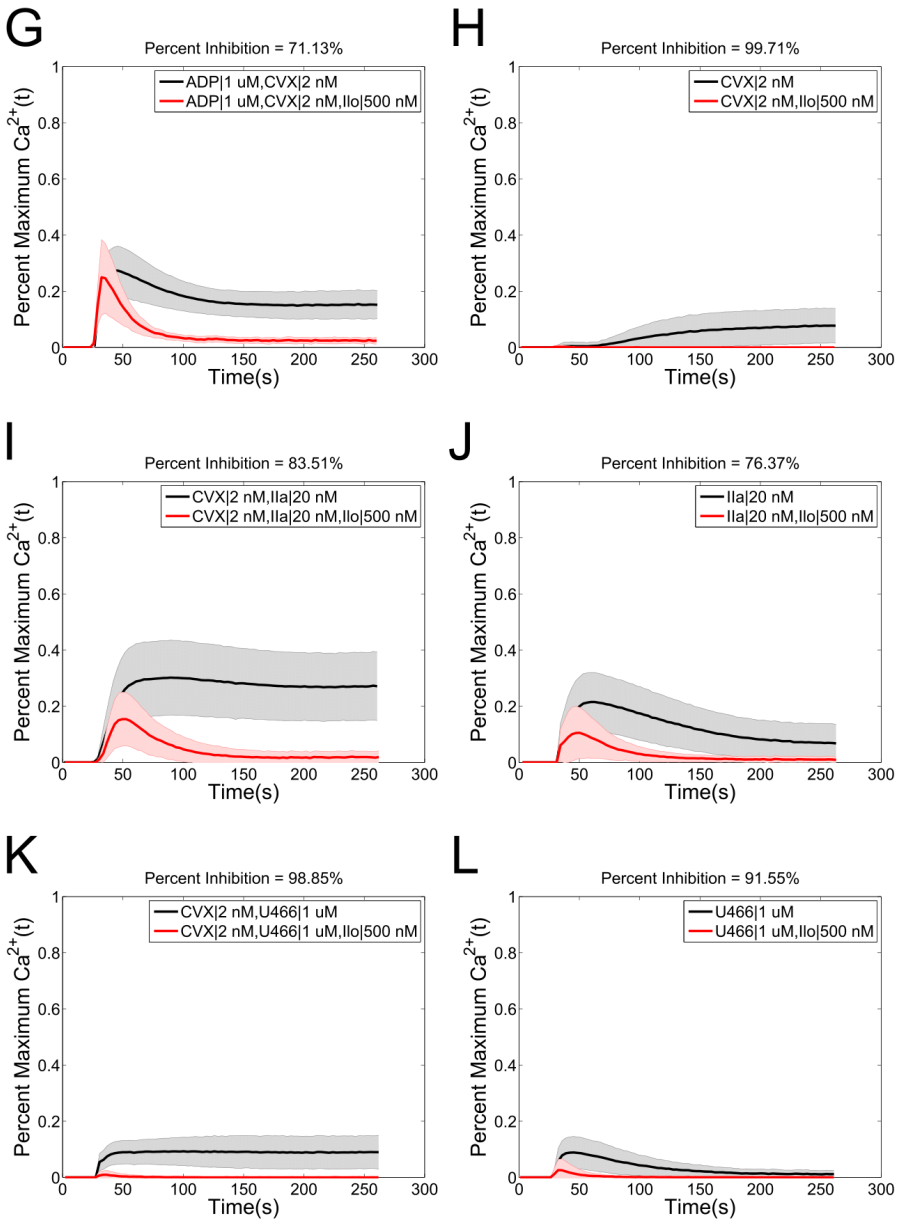

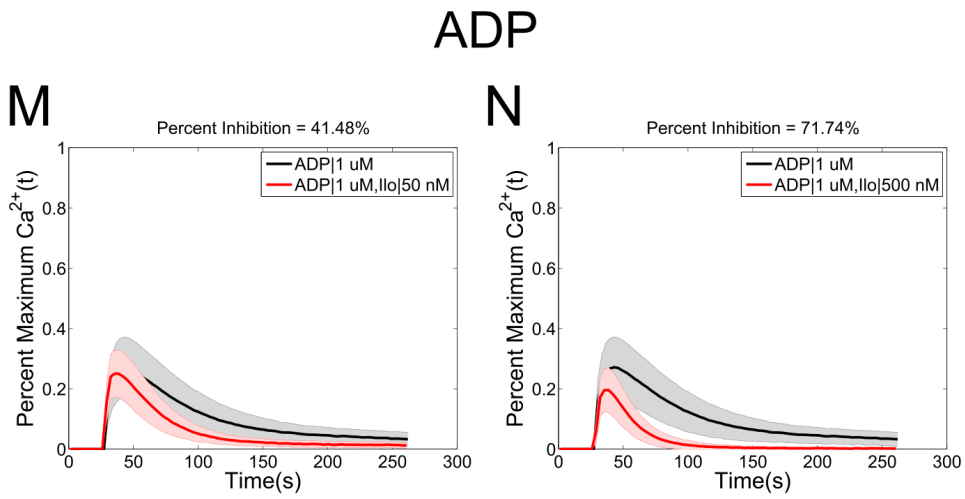

Figure 1-11 Analysis of iloprost inhibition effects

2.4.6 Range of individual neural network prediction and donor responses

The range (i.e. intradonor variation) of individual NN predictions over 10 to 12 donors for single and pairwise agonist conditions (*Figure 1-12*) was comparable to the experimental observations, as expected for NNs trained exactly on those conditions (*Figure 1-12A, B*). Similarly, the range of NN predictions for trinary agonist conditions matched the range for the experimental values as well (*Figure 1-12C*). The range of the higher order NN predictions (≥ 4 agonists) was somewhat larger than the range observed in the corresponding individual experiments (*Figure 1-12D–F*). Clearly for ≥ 4 agonists, the signaling pathways span a very complex platelet biology beyond the dimensionality of the pairwise training data. Nonetheless, the range of the NN predictions reflected to a large degree the range of the experiment itself. For example, the range of the NN predictions in *Figure 1-12E* was smaller than the range in *Figure 1-12D*; the same trend was reflected in the range of the actual experiments. Furthermore, for ≥ 4 agonists, the experimental data comprises seven experiments spanning five donors, whereas the NN used in training spanned 12 donors, which in part explains why simulation ranges were larger than ranges of experimental observations. The NN range over all 120 NNs in *Figure 1-12D* was larger than the experimental ranges, potentially reflecting donor variation but more importantly reflecting the difficulty of predicting higher dimensional responses. Despite the substantial range of individual NN predictions for the four-agonist condition depicted in *Figure 1-12D*, the mean of the NN predictions predicted the mean response of the actual experiments, a benefit of the NN-ensemble approach for predicting a pooled population dynamic.

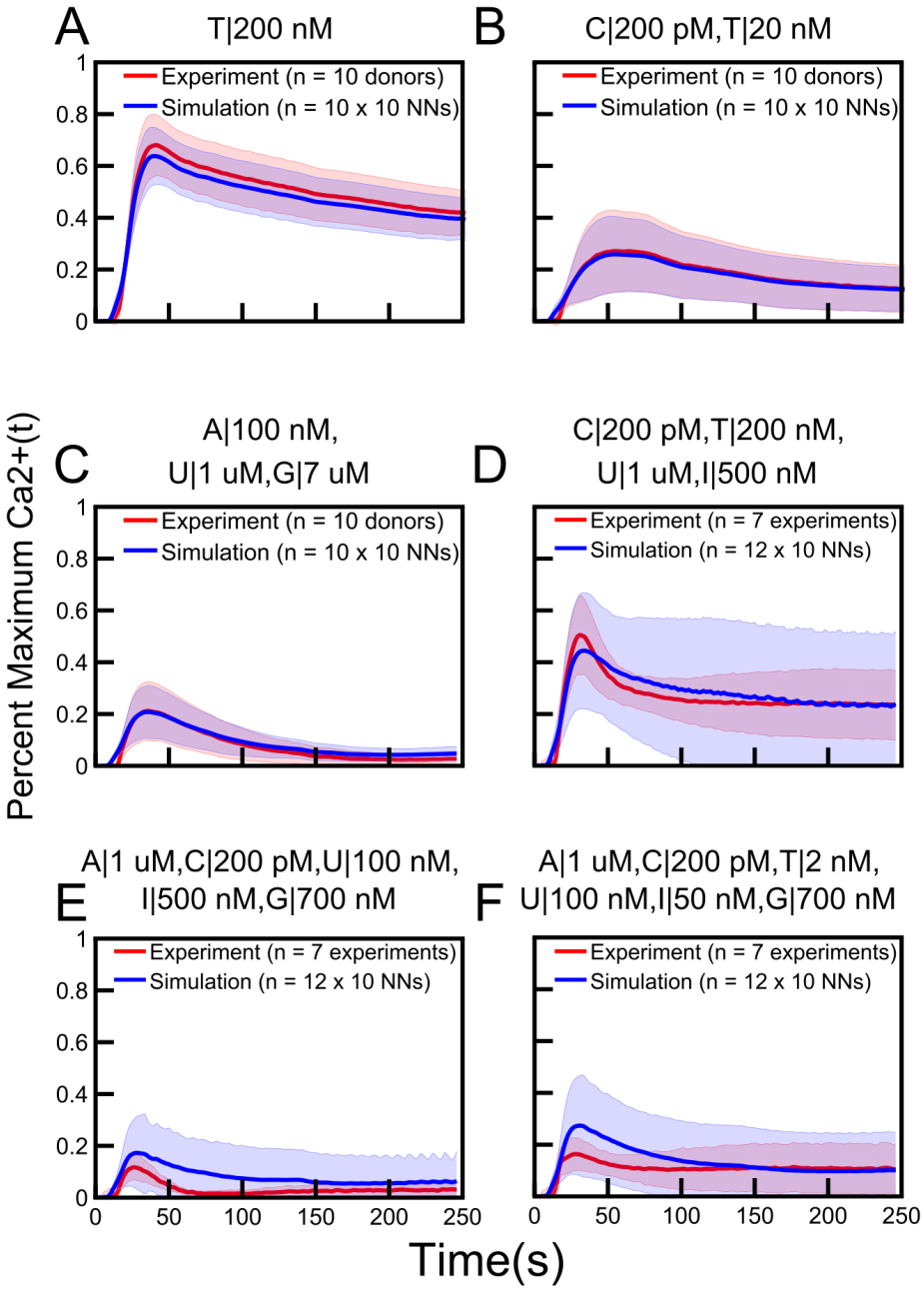

Figure 1-12 Range of individual neural network responses and donor responses

2.5 Discussion

While the full complexity of receptor mediated signaling in platelets extends well beyond the known pathways indicated in *Figure 1-1A*, a top-down approach using pairwise agonist scanning (PAS) provides an efficient data-driven method to predict platelet function. By using data obtained from multiple donors and training multiple NNs for each donor, a NN-ensemble (*Figure 1-3*) allowed accurate prediction of 135 binary stimulations and 135 synergy parameters (*Figure 1-4*). The synergy vector composed of the 135 synergy parameters is an experimentally measured human platelet phenotype (healthy adult male and female) that is fully predicted by the NN-ensemble. Furthermore, the NN-ensemble provided suitable prediction beyond the binary training set to predict trinary responses (*Figure 1-5, Figure 1-6*), higher ordered responses *(Figure 1-7, Figure 1-8),* and response to sequential stimuli (*Figure 1-9, Figure 1-10*). The major components of hemostasis and thrombosis that regulate platelet activation state are now quantitatively captured in the NN-ensemble. For large scale simulation of blood function, a user may specify or calculate any combination of the six agonists at different concentrations to produce a dynamic platelet calcium response representative of a healthy human donor.
The NN is able to do this mainly because individual and pairwise interactions dominate platelet calcium signaling crosstalk in this assay, and because all single agonists are sampled across each of their full dose ranges [20]. An ordinary differential equation (ODE) model describing the calcium mobilization mediated by all six PAS agonists would likely require an estimated >500 kinetic parameters, many of which are unavailable [20].

From the perspective of a data-driven and top-down approach, NNs have proven quite robust and well matched to PAS data sets. Also NNs are ideal for multiscale simulations that involve crosstalk between receptors. However, NNs are not mechanistic models for identification or quantification of basic biochemical mechanisms. The full calcium dataset generated in this

work can also facilitate future mechanistic model building. For example, future mechanistic models of receptor signaling and crosstalk should be testable against the 135-parameter synergy map we measured. Such mechanistic models should account for RGS proteins, PKC, cAMP/PKA, cGMP/PKG, and phosphodiesterase pathways, as well as receptor desensitization pathways including ITIM/Shp2 phosphatase, receptor internalization, and receptor shedding pathways, along with regulation of store operated calcium entry. Improved predictive capability is not necessarily an outcome of constraining of NN nodes and linkages to a preconceived reaction topology as in *Figure 1-1*.

The calcium experiments that the NN was trained on included the contributions of SOCE because Apixaban was used in place of a calcium chelator as an anticoagulant. The effect of autocrinic effects by ADP and thromboxane secretion, however, were not significant in the PAS assay due to the dilute conditions of the assay (*Figure A-2*). Such autocrinic effects however are naturally captured in multiscale simulations that include convection-diffusion of soluble agonists [24]. Other important inside-out signaling downstream of calcium mobilization, such as integrin engagement, granule release, shape change, and phosphatidylserine exposure can be simulated by incorporating the calcium model into a larger fine or coarse-grain model. For example, in Flamm et al. (2011), NN were trained via PAS using calcium-containing PRP and then used to predict platelet deposition rates on collagen in the absence of thrombin by accounting for platelet signaling in response to laboratory analogs of collagen, ADP, thromboxane, and prostacyclin [24]. Alternatively, the PAS methodology has also been adapted by Jaeger et al. [40] for flow cytometry instead of calcium measurements, so as to quantify inside-out signaling events such as: integrin $\alpha_{IIb}\beta_3$ activation, P-selectin exposure, and PS exposure using PAC-1, anti-P-selectin antibody, and annexin V, respectively.

The NN ensemble trained only on pairwise data was able to predict the calcium output of higher order agonist combination experiments with reasonably high accuracy. This was

potentially due to a sparsity-of-effects principle: a system is largely dictated by main effects and lower order interaction [41]. Adding trinary conditions to the training data might theoretically improve prediction accuracy when it comes to higher order combinations. The improvement in accuracy should be a measure of the information content of trinary data. In separate studies, we tested the utility of adding trinary stimulation data to the PAS training set in order to enhance the predictive capability of the NN-ensemble. Trinary data were incorporated into the NN ensemble in 3 different ways, each time controlling for the number of NNs in the ensemble. The first set of trinary data collected comprised 160 trinary combinations of all six agonists at only low and medium concentrations, repeated on 10 donors. Adding this trinary data reduced the higher-order combination prediction accuracy from R = 0.824 to R = 0.784, and synergy score accuracy decreased from 0.66936 to 0.66145. The second set of trinary data collected comprised 27 combinations of only three agonists (ADP, convulxin, U46619) in the full dose range, repeated on eight donors. Adding this trinary data did not substantially affect the prediction accuracy (calcium trace accuracy from R = 0.810 to R = 0.806, and synergy correlation from R = 0.66367 to R = 0.68387). The third set of trinary data collected was an unbiased, random sampling (n = 54) of the complete trinary space done on a single donor, who was not part of the original PAS dataset. Adding this trinary data increased prediction accuracy of the time courses (from R = 0.871 to R = 0.906), but reduced the accuracy of synergy scores prediction from R = 0.6953 to R = 0.53925. We conclude that incorporating a randomly sampled trinary dataset can moderately increase prediction accuracy, whereas adding a biased sample of the trinary space does not increase accuracy. In fact, adding a sample of the trinary space that does not span the full dose range may reduce accuracy. However, even in the best of the three scenarios tested, adding trinary data to the PAS training dataset did not substantially improve accuracy.

The 120-NN ensemble (R = 0.87134, mean-squared error, MSE = 0.0129) was more accurate than the average individual NN within the ensemble (R average = 0.6566, MSE average

= 0.0501) in predicting the calcium traces of higher order combination experiments. Even though the most accurate individual NN in the 120-NN ensemble (R = 0.91391, MSE = 0.0092) was more accurate than the ensemble itself, its prediction output was significantly noisier, and its synergy score prediction accuracy was much lower (R = 0.6953 to R = 0.4609). The ensemble approach reduced variances in prediction output, increased accuracy above the average NN in the 120-NN ensemble, consistent with previous findings [42], and is generally thought to be more robust [43-46]. Ensemble pruning is often used to eliminate individual models from the ensemble based on certain criteria so as to improve the new ensembles predictive ability[46]. Using the interquartile range (IQR) outlier detection method, eight high outliers spanning seven different donors were identified in the mean-squared error (MSE) measurements of each of the 120 individual NNs. Removing the eight most inaccurate individual NNs from the ensemble did not improve the ensemble accuracy (R-value improved slightly from 0.87134 to 0.87768, but MSE increased slightly from 0.0129 to 0.0148, synergy score R decreased slightly from 0.6953 to 0.68632, and noise in ensemble predictions increased). Diversity of the models (in this case originating from the different random initial weights generated at the beginning of each NN training) comprising an ensemble is important for accuracy and robustness [47-49]. To increase diversity, heterogeneous ensembles may be used instead; for example, changing the training parameters of select individual NNs or incorporating into the NN-ensemble regression models other than NNs [46].

We found that the NN-ensemble was able to account for the dynamics and magnitude of one pathway relative to that of another. Iloprost was a very potent antagonist in this assay. In vivo, prostacyclin activates IP to increase cAMP and cGMP-dependent protein kinases pKA and pKG. Both pKA and pKG phosphorylate RGS18 (a G-protein regulator), which eventually turns off G_q-signaling, the main activation pathway for U46619 and thrombin (via PAR-1) [50]. ADP signaling through $P2Y_1$ also goes through G_q-signaling. However, ADP also signals through the

$P2Y_{12}$ receptor, which involves the G_i protein (*Figure 1-1A*).Thrombin signaling through PAR-4 can go through either G_q or G_i. The existence of alternate signaling routes (through G_i) explain why iloprost inhibition is markedly less potent for ADP, and slightly less effective for thrombin as well. Furthermore, signaling through the G_i protein inhibits the rise in adenylate cyclase (precursor of cAMP which decreases intracellular calcium levels). As expected from studies of "coated" platelets [51] and studies with similar findings [27, 28], convulxin and thrombin were quite synergistic in the PAS assay. Additionally, thrombin and TP receptor signaling were somewhat synergistic, consistent with previous findings [20, 24]. In future work, the NN-ensemble can be incorporated in multi-scale and hierarchical simulations of bleeding or clotting with linkages to vascular pathophysiology. While exogenously added thrombin was used in PAS, not all of this thrombin may reach the platelet due to antithrombin. This may right shift the thrombin potency [52]. Iloprost and GSNO were also included in this assay to recapitulate endothelial-derived prostacyclin and nitric oxide effects on platelet function. The development of a healthy human platelet calcium calculator can enable various applications such as predicting thrombosis or hemostasis under flow condition or extracting information from in vitro diagnostics, potentially using platelets from patients with cardiovascular disease risks.

Furthermore, the generalizability of the neural network may be quickly improved, by training the ensemble NN on more donors. On the other hand, the human platelet calcium calculator may also be easily and quickly tailored for a specific individual by using NN trained on PAS data of only that donor. It would not be easy for the equivalent to be done for a mechanistic ODE model, as each of the many kinetic parameters has to be re-optimized for the new data. One of the potential applications for this calculator is for use in a multiscale simulation of thrombus formation. Since calcium is the central node of platelet signaling, the healthy human platelet calcium calculator can enable simulation of physiologic scenarios where agonist concentrations vary continuously, which is difficult to obtain experimentally. For example, *Figure 1-13* depicts

three theoretical phases that occur in succession for platelet activation during injury, the theoretical agonist concentration experienced by platelets at each phase, as well as corresponding simulation of calcium levels for each phase. The first phase represents the early phase of the coagulation pathway: a monolayer of platelets is exposed continuously to collagen surface on the injured endothelium. This can be represented in the PAS assay as a steady level of convulxin. The resulting simulation captures the effects of iloprost and GSNO, analogs of PGI_2 and nitric oxide, which are also released by the endothelium during clotting. The NN predicts a sustained intracellular mobilization in the studied time frame of 0 - 4 minutes. The second phase represents the autocrinic signaling phase: Calcium mobilization from phase 1 prompts dense granule secretion, releasing ADP, which further prompts thromboxane generation. Calcium mobilization also causes phosphatidylserine exposure and thus thrombin production. This is illustrated in the agonist concentration profiles. As a result the calcium levels peak slightly after ADP release, but are in general lower and less sustained than before. Phase three represents the late phase of clotting. ADP levels (released from platelet dense granules previously) decline; thromboxane levels increase slightly from phase but eventually declines. Thrombin levels continue to rise from phase 2 to a higher level than thromboxane because of contribution from both the intrinsic and extrinsic pathway, but declines eventually. The resulting calcium prediction has two peaks: one when both thrombin and thromboxane levels are rising and then a later, smaller peak when thrombin peaks but platelet-derived thromboxane and ADP have been depleted. In general, while both PGI_2 and NO act to inhibit calcium mobilization, the effect of PGI_2 is more pronounced and sustained. This agrees with Radomski et al., who found that the IC_{50} of NO was about two orders of magnitude higher than that of PGI_2 for platelet aggregation when stimulated by ADP, collagen, thrombin and U46619 [36].

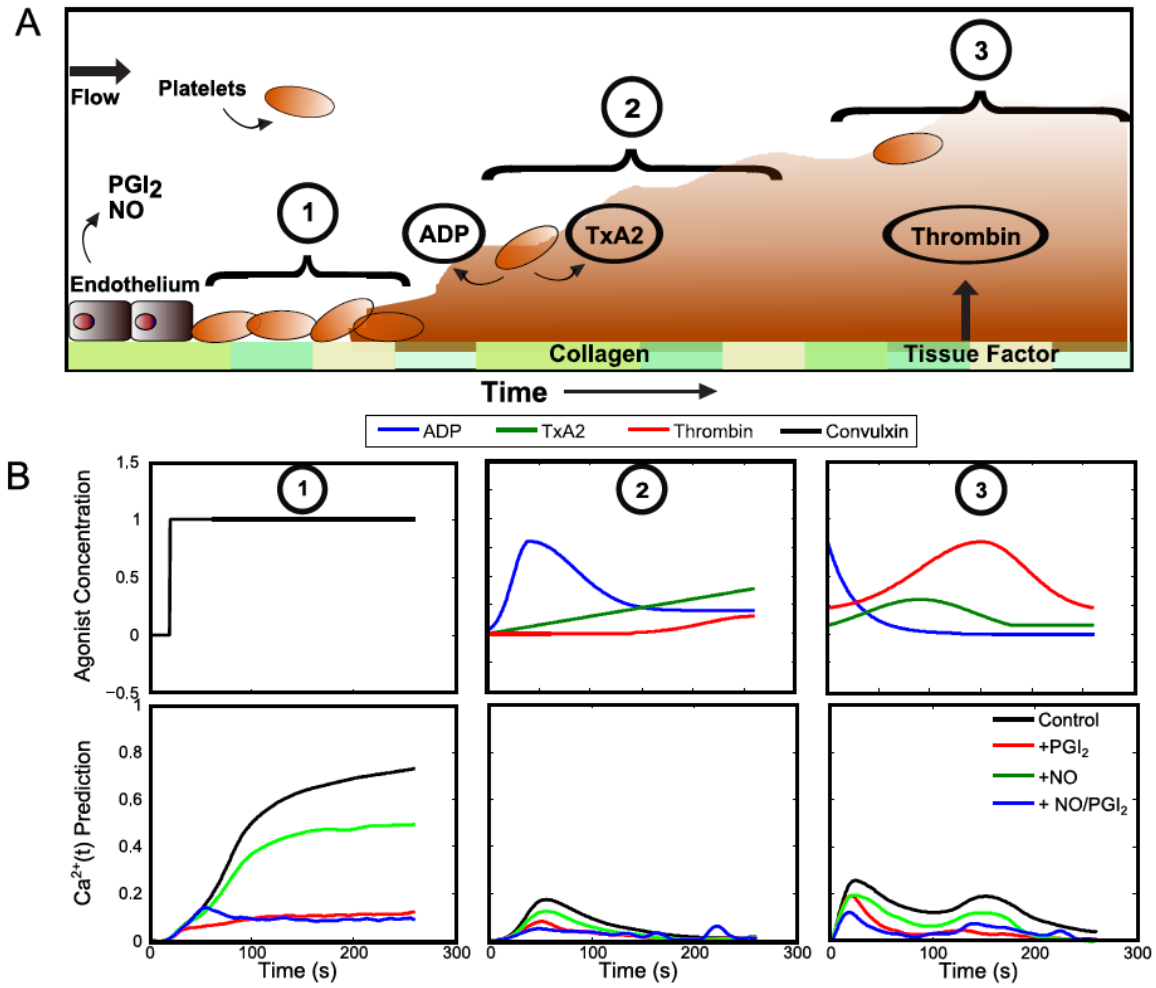

Figure 1-13 Simulations of platelet calcium levels based on theoretical agonist distribution in vivo. (A) Progression of platelet activation in vivo upon endothelial injury, defined in three phases. **(B)** The top row represents agonist concentrations in the three defined phases. Concentrations are mapped between 0 and 1 (0 being not present and 1 being $10xEC_{50}$). The bottom row represents the corresponding predicted calcium time traces.

All the above mentioned attributes of the calcium calculator, especially its ability to simulate physiologic scenarios where agonist concentrations vary continuously, makes it ideal for incorporation into a larger multiscale model of clotting. Such a model can have further applications such as predicting thrombosis or hemostasis under flow condition. In fact, in a paper currently in preparation by Lu et al. [53], a multiscale approach was developed with a goal of patient-specific simulation of thrombosis from single platelets to the whole clot, to account for:

platelet signaling (neural network trained by pairwise agonist scanning, PAS-NN), platelet positions (lattice kinetic Monte Carlo, LKMC), wall-generated thrombin (76-species ODE model), multicomponent convection-diffusion (PDE), and flow over a growing clot (lattice Boltzmann). At all times, intracellular calcium was calculated for each platelet by the PAS-NN (also known as human platelet calcium calculator) developed here, in response to its unique exposure to local collagen, ADP, thromboxane, and thrombin. When compared to microfluidic experiments of human blood clotting on collagen/TF under flow driven by constant pressure drop, the model accurately predicted clot morphology and growth with time. For TF at 0.1 and 10 molecule/μm2 and initial wall shear rate of 200 s^{-1}, the occlusive blockade of flow for a 60-μm channel occurred relatively abruptly at 500 and 400 seconds, respectively, in both experiment and simulation. Prior to occlusion, intrathrombus concentrations reached 50 nM thrombin, ~1 μM thromboxane, and ~10 μM ADP, while the wall shear rate on the rough clot surface peaked at ~500-1000 s^{-1} [53]. This demonstrates the utility and universality of the human platelet calcium calculator in predicting physiologic events.

2.0 Downregulation of platelet GPVI signaling following thrombin stimulation

3.1 Abstract

Activating platelets with thrombin in platelet-rich plasma (PRP) caused an attenuation of convulxin-induced calcium mobilization when convulxin was added to PRP 480 seconds later. This attenuation effect was not observed when ADP and thromboxane analog, U46619 was used in place of thrombin. The attenuation effect increased with higher doses of thrombin and longer times between initial thrombin dispense and later convulxin addition. When PAR-1 and PAR-4

receptor agonists (AYPGKF and SFLLRN) were used instead of thrombin for the initial dispense, the subsequent convulxin-induced calcium response was unaffected, supporting thrombin's unique role in causing attenuation of subsequent convulxin-induced calcium mobilization. Thrombin, unlike ADP, U46619 or the PAR-1 and PAR-4 receptor agonists, is able to polymerize fibrinogen into fibrin. When GPRP was added to prevent polymerization of fibrin, initial platelet activation by thrombin did not result in attenuation of convulxin- induced calcium mobilization as it did when GPRP was not present. This experiment was repeated using a mixture of washed platelets and fibrinogen monomers instead of PRP, resulting in similar results as before: the addition of thrombin to fibrinogen mixture caused an attenuation of convulxin-induced calcium mobilization when convulxin was added to the mixture 480 seconds later, but not when GPRP was added to inhibit fibrin polymerization. The presence of polymerized fibrin also reduced platelet deposition in a microfluidic assay on a collagen surface. These results suggest that polymerized fibrin binds to and downregulates platelet GPVI function.

3.2 Introduction

Platelet GPVI is an immunoglobulin superfamily receptor expressed on platelet surface in association with the FcRγ chain (Fc receptor γ chain) [16]. There are approximately 3,700 copies of GPVI on a platelet [54]. When GPVI is bound by collagen, GPVI receptors cluster, resulting in Src kinase-dependent tyrosine phosphorylation of the FcRγ chain immunoreceptor tyrosine-based activation motif [16]. This leads to the signaling protein recruitment (e.g. the Src kinase, the tyrosine kinase Syk, PLCγ2, phosphoinositide 3-kinase (PI3K) and MAPKS[55, 56]), all of which set of a signaling pathway, triggering calcium mobilization within platelets and initiating the inside-out activation of the integrin $\alpha_{IIb}\beta_3$ and the release of the secondary soluble mediators, such as ADP and thromboxane (TxA_2)[57]. This leads to platelet aggregation mediated by fibrinogen binding between platelet integrins $\alpha_{IIb}\beta_3$ and results in thrombus formation [57]. GPVI has many

activating ligands including collagen, collage-related peptide (CRP), convulxin [6, 7]. Recently it has also been found that GPVI interacts with fibronectin [58], vitronectin [59] and laminins [60], which, in addition to GPVI-collagen interaction might contribute to the role of GPVI in thrombus formation.

Platelet GPVI has been highlighted recently as a desirable target for antithrombotic drug development [61-65] because it's blockade and downregulation in *in vitro* experiments, as well as functional GPVI deficiency in animal models have been shown to impair thrombus formation, but not disrupt hemostasis [62, 65-67]. Compared to the current standard treatment of dual antiplatelet therapy combining aspirin with an ADP receptor antagonist (Clopidogrel, prasugel, tricagelor), which may be effective but increases bleeding risk [68, 69], anti-GPVI treatment could have the potential to be both effective yet safe. One option is to target events downstream of GPVI activation, such as GPVI-induced calcium mobilization. In the following experiments, polymerized fibrin (as a result of added thrombin), has been shown to downregulate convulxin-induced GPVI calcium mobilization. Understanding the mechanism underlying this observation could be important in developing a viable GPVI-targeted antithrombotic therapy. Furthermore, since elevated soluble fibrin levels have been implicated in trauma and disseminated intravascular coagulation (DIC) [70-73], understanding the mechanism behind the downregulation of GPVI signaling by polymerized fibrin has clinical importance.

The fact that GPVI is a receptor for polymerized fibrin was recently discovered [16, 18]. According to those recent studies, GPVI binding to fibrin increases platelet procoagulant activity [16], amplifies collagen-independent thrombin generation and platelet recruitment at clot surface [18], and eventually contributes to thrombus growth and stabilization [16, 74]. However, the mechanism of interaction of GPVI and fibrin is not clear, especially as it pertains to GPVI-mediated calcium signaling. Furthermore, the many procoagulant properties that fibrin-GPVI

binding reportedly confers depend on that interaction's ability to promote thrombin generation. The focus of the following experiments will be on the impact that GPVI-fibrin interaction has on GPVI-mediated calcium mobilization in apixaban-treated conditions (apixaban binds specifically to factor Xa to prevent endogenous thrombin production).

3.3 Materials and Methods

3.3.1 Platelet Calcium Assays

Whole blood was drawn by venipuncture from healthy donors according to the University of Pennsylvania Institutional Review Board guidelines (protocol number: 805305), into a syringe containing apixaban with a final concentration of 250 nM. Donors self-reported to be free of any medications or alcohol use for three days prior to the blood draw. Female donors self-reported to not using oral contraceptives.

Platelet rich plasma (PRP) was then obtained by subjecting the whole blood sample to centrifugation at 120g for 12 minutes. Then, 2 ml of PRP was incubated with a vial (single microplate size) of Fluo-4 NW dye mixture reconstituted with 7.8 ml of HEPES buffered saline (HBS, sterile filtered 20mM HEPES and 140mM NaCl dissolved in deionized water, adjusted to pH7.4 with NaOH) and 200 µL of 77 mg/ml reconstituted probenecid for 30 minutes. At this stage, for conditions involving GPRP and/or vorapaxar, GPRP and/or vorapaxar was added and incubated along with the dye in the PRP mixture to give a final concentration of 500 µM and 100 nM respectively. Meanwhile, a 384-well plate containing platelet agonists (called the 'agonist plate') was assembled. The agonists included thrombin, ADP, U46619 (a thromboxane analog), SFLLRN and AYPGKF (PAR-1 and PAR-4 receptor agonists), as well as convulxin (a collagen analog). After incubation with dye, the PRP was dispensed into a 384-well plate (called the 'read plate'). Both the agonist and read plate were loaded into a Molecular Devices FlexStation 3, a

fluorescence reader with auto-pipetting capabilities. Agonists were dispensed to a column of wells containing the PRP, where well fluorescence F(t) was read and normalized by the pre-dispense baseline. For conditions involving two dispenses, 10 μL of agonist was first added to 30 μL of PRP in each well, and at a later specified time, 10 μL of convulxin was first added, giving a final volume of 50 μL. For conditions involving only one dispense, 20 μL of agonist was added to 30 μL of PRP in each well, giving a final volume of 50 μL. In each well, the final concentration of PRP after agonist addition was 12% PRP by vol., and the volume of calcium dye was 15 μL (30% dye by vol.). The fluorescence was read for 20 seconds before first dispense, and readings were taken in intervals of 2.5 seconds (EX/EM, 485 nm/525 nm). For all experiments, the entire plate was read, column-wise, in under 90 minutes. In previous tests using indomethacin (Sigma-Aldrich) to block COX-1 and apyrase (Sigma-Aldrich) to degrade released ADP, there was no evidence for autocrine signaling in the dilute PRP conditions of the experiment [75].

For the calcium assay involving washed platelets (*Figure 2-5*), washed platelets were first obtained by subjecting whole blood to centrifugation at 200g for 14 minutes to obtain PRP. Then, 2 ml of PRP was incubated with a vial (single microplate size) of Fluo-4 NW dye mixture (Invitrogen) reconstituted with 5 ml of HBS and 200 μL of 77 mg/ml reconstituted probenecid (Invitrogen) for 30 minutes. After incubation, Tyrode's buffer containing PGE_1 (1 μM) and apyrase (1 U/mL) was added to the PRP mixture in a volume ratio of 1:5. The mixture was then spun at 1200g for 14 minutes to obtain a platelet pellet after removing the resulting supernatant. The platelet pellet was then resuspended in 1.1ml of HBS to obtain a washed platelet suspension. Then human research grade fibrinogen was added to the washed platelets mixture for a final concentration of 500nM. For the condition involving GPRP, GPRP was also added at this stage. After 10 minutes of incubation, the washed platelet and fibrinogen mixture was then dispensed

into the read plate. Then both read plate and prepared agonist plate were loaded onto the fluorescence reader and read in the same manner as all other calcium assays.

Apixaban was obtained from SelleckChem, Fluo-4 NW dye and probenecid from Invitrogen, ADP, GPRP, PGE_1 and apyrase from Sigma-Aldrich, convulxin from Pentapharm, thrombin and human research grade fibrinogen from Haematologic Technologies Inc., PAR-1 and PAR-4 agonists from Bachem, U46619 from Tocris Bioscience, and vorapaxar from Ryan Scientific.

3.3.2 Microfluidic assays

1 μL of GPRP (or HBS for control condition) was added to 19.7 μL of fluorescent fibrinogen from human plasma (Alexa Fluor® 647 conjugate), and allowed to incubate for 15 minutes. Then 2.3 μL of thrombin was added (final concentration 2.5 nM) was added to the mixture to induce polymerization of fibrinogen into fibrin. After 300 seconds, 2 μL of D-Phenylalanyl-prolyl-arginyl Chloromethyl Ketone (PPACK) was added (final concentration 100 μM) to stop thrombin activity. The mixture was then diluted 10 fold into whole blood that was drawn via venipuncture into PPACK (100 μM) and apixaban (1 μM). The resulting fibrinogen/fibrin solutions were diluted by a factor of 10 in PPACK/apixaban-treated whole blood with either 5 mM GPRP or HBS then perfused through an 8-channel microfluidic device at $200s^{-1}$ over a collagen surface. The resulting platelet and fibrin fluorescence were recorded once a minute for 6 minutes. The microfluidic device preparation and perfusion was performed by another Diamond lab member, Brad Herbig.

Fluorescent fibrinogen was obtained from Thermo Fisher Scientific, PPACK was obtained from Haematologic Technologies Inc.

3.4 Results

3.4.1 Thrombin uniquely attenuates subsequent platelet calcium response to convulxin

When thrombin is first added to PRP and convulxin (a collagen analog) is added 480 seconds afterward, the calcium signal in response to convulxin is significantly reduced compared to the control condition in which PRP was not first activated by thrombin (*Figure 2-1A*). This phenomenon was apparent at all low to medium doses of thrombin (1 nM to 10 nM or 0.5 to 5 x EC_{50}) (*Figure 2-1A*). However, this phenomenon was not observed when ADP or U46619 was added instead of thrombin. When ADP was added instead of thrombin, very low dose of ADP (10 nM or 0.01 x EC_{50}) did not affect subsequent calcium response to convulxin compared to the control condition (*Figure 2-1B*). Low to medium doses of ADP (100 nM to 1 μM or 0.1 to 1 x EC_{50}) very slightly increased subsequent calcium response to convulxin (*Figure 2-1B*). High dose of ADP (10 μM or 10 x EC_{50}) resulted in noticeable reduction in subsequent platelet calcium response to convulxin, but not to the extent seen in the case of thrombin (*Figure 2-1B*). When U46619 was added in place of thrombin, very low to medium doses of U46619 (10 nM to 1 μM or 0.01 to 1 x EC_{50}) did not affect subsequent calcium response to convulxin compared to the control condition (*Figure 2-1C*). Similarly, as seen in the case of ADP, high dose of U46619 (10 μM or 10 x EC_{50}) resulted in a detectable reduction in subsequent platelet calcium response to convulxin, but not to the extent caused by any dose of thrombin (*Figure 2-1C*).

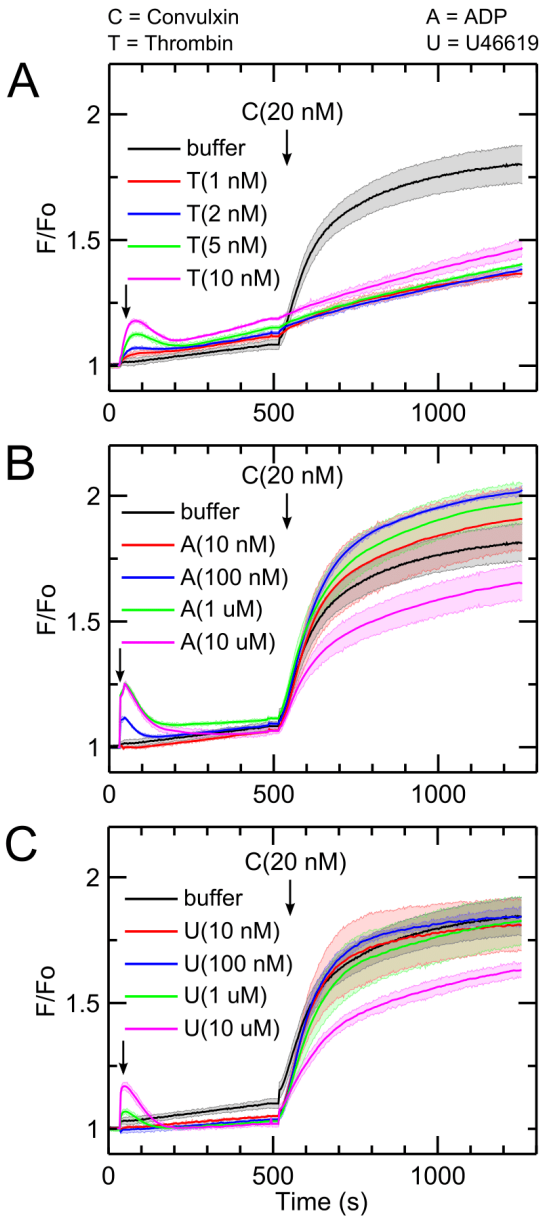

Figure 2-1 Different effects in attenuation of subsequent platelet convulxin calcium response by thrombin compared to ADP and thromboxane. (A) Platelet activation by thrombin causes a significant reduction in subsequent convulxin-induced calcium response 480 seconds later. This effect is seen for all low to relatively high doses of thrombin (1 – 10nM). **(B)** Platelet activation by ADP does not significantly attenuate subsequent convulxin-induced calcium response. Lower doses of ADP (10nM – 1uM) slightly enhance subsequent convulxin response. The high dose of ADP (10uM) slightly attenuates subsequent convulxin response. **(C)** Platelet activation by the thromboxane analog, U46619, also does not significantly attenuate subsequent convulxin-induced calcium response. Lower doses of ADP (10nM – 1uM) have no effect on subsequent convulxin response. Similarly to ADP, the high dose of U46619 (10uM) slightly attenuates subsequent convulxin response.

3.4.2 Extent of attenuation of convulxin calcium response increases with incubation time and thrombin dose

When convulxin is added after incubation time, t_{inc} = 150, 210 and 335 seconds after low dose thrombin (1 nM or 0.05 x EC_{50}) is first added to PRP, the calcium signal in response to convulxin is comparable to the control condition in which PRP was not first activated by thrombin (*Figure 2-2A*). When incubation time increases to 480 seconds, subsequent calcium response to convulxin decreases significantly, and is decreased further when incubation time increases to 600 seconds (*Figure 2-2A*). When a slightly higher dose of thrombin (2 nM or 0.15 x EC_{50}) is first added to PRP, subsequent calcium response to convulxin is not attenuated until incubation times increase to 210 seconds or higher (*Figure 2-2B*). Similarly, the extent of attenuation of convulxin calcium response generally increases with longer incubation times (*Figure 2-2B*). In general, a minimum incubation time must be met for noticeable attenuation of subsequent calcium response to convulxin, after which increasing incubation times tend to increase the extent of attenuation. This observed trend is illustrated in *Figure 2-2C*. The time needed to reach 95% of peak convulxin calcium response for the control condition is t_{95} = 86.7 seconds. Subsequent convulxin-induced calcium fluorescence intensity at t_{95} = 86.7 seconds for all conditions in *Figure 2-2A* and *Figure 2-2B* were measured and expressed as a percentage of the 95% peak convulxin response of the control condition with no thrombin pre-treatment, in *Figure 2-2C*. The resulting plot was fitted with a Hill function (*Figure 2-2C*). When platelets are pre-treated with the lower thrombin dose (1nM), reduction of convulxin response starts after only after approximately 450 seconds and drops rapidly to the maximum reduction (~80%) after approximately 500 seconds. At the higher thrombin dose (2nM), reduction of convulxin response starts much earlier (~200s) and reaches the maximum reduction (~80%) after approximately 220 seconds (*Figure 2-2C*). Perhaps because both doses of thrombin used were low (1 nM and 2 nM),

the dose of thrombin does not appear to influence the maximum extent of reduction. However, a slightly higher dose of thrombin (2 nM vs. 1 nM) reduced the incubation time needed to observe a significant reduction in subsequent convulxin response. The steep shape of the Hill function for both conditions also indicates a switch-like minimum threshold in incubation time needed for significant attenuation of subsequent convulxin response.

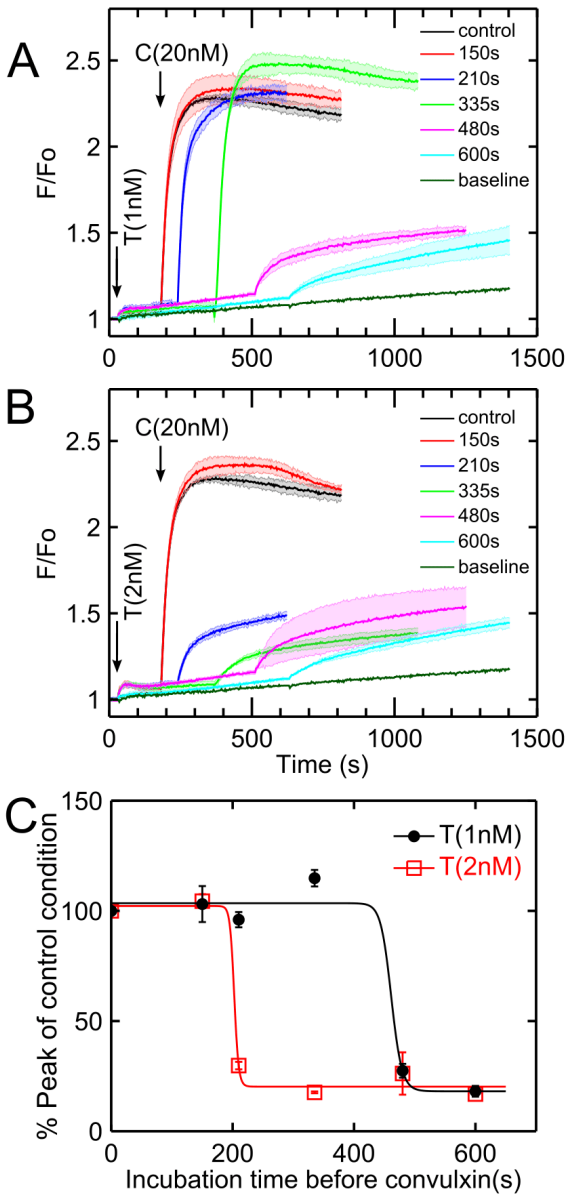

Figure 2-2 Effect of time and dose of thrombin in attenuation of subsequent platelet convulxin calcium response. **(A)** When platelets are first activated by low dose thrombin (1nM), the extent of reduction of subsequent platelet convulxin increases with time. When convulxin is introduced up to 335 seconds after thrombin, convulxin response is comparable to the control condition. When time between the two dispenses (incubation time) increases to 480 seconds and beyond, the reduction in convulxin response is significant, and increases with higher incubation times. **(B)** When platelets are first activated by a slightly higher dose (2nM), notable reduction of subsequent platelet convulxin starts at shorter incubation times (210 seconds and beyond) compared to (A). The extent of convulxin response reduction increases with increasing incubation times. **(C)** The time needed to reach 95% of peak convulxin response for the control condition is t_{95} = 86.7 seconds. Convulxin-induced calcium fluorescence intensity at t_{95} = 86.7 seconds was measured and calculated as a percentage of the 95% peak convulxin response of the control condition with no thrombin pre-treatment for all conditions in (A) and (B). The resulting plot was fitted with a Hill function.

3.4.3 Activating PAR-1 and PAR-4 do not result in attenuation of subsequent platelet calcium response to convulxin

Even though thrombin signals through PAR-1 and PAR-4 receptors, when PAR-1 and PAR-4 agonists (SFLLRN and AYPGKF) are first added instead of thrombin, subsequent platelet calcium response to convulxin is unaffected compared to the control condition (*Figure 2-3A*). This suggests that thrombin plays a unique role. When vorapaxar, a PAR-1 specific inhibitor is added, calcium signaling in response to thrombin is blocked (*Figure 2-3B*). This indicates that in these platelet calcium assays, thrombin-induced calcium mobilization is dependent on PAR-1 and cannot solely happen through PAR-4 signaling. Interestingly, when thrombin is first added to PRP incubated with vorapaxar, subsequent calcium response to convulxin is also attenuated to the same extent as the condition without vorapaxar (*Figure 2-3C*). This indicates that the convulxin response attenuation effect can happen solely through PAR-4 signaling.

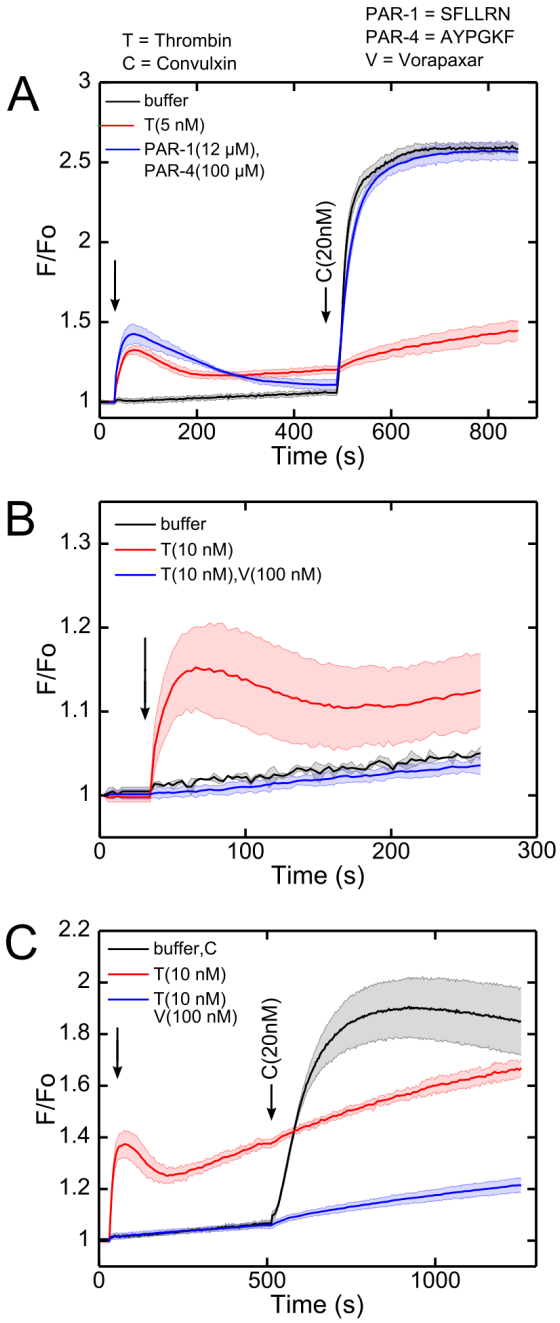

Figure 2-3 Platelet convulxin calcium response attenuation effect is not observed by pretreatment with PAR-1 and PAR-4 agonists(A) Despite thrombin signaling through PAR-1 and PAR-4, platelet activation by PAR-1 and PAR-4 specific agonists (SFLLRN and AYPGKF) does not reduce subsequent convulxin response as thrombin does, and results in convulxin response levels similar to the control condition. **(B)** Vorapaxar, a PAR-1 specific antagonist, blocks thrombin-induced calcium signaling. **(C)** The convulxin calcium response attenuation after thrombin pre-treatment effect is still apparent when Vorapaxar, a PAR-1 specific antagonist is present.

3.4.4 Fibrin plays an essential role in attenuation of subsequent platelet calcium response

When thrombin is first added to PRP incubated with GPRP, which blocks polymerization of fibrinogen into fibrin, subsequent calcium response to convulxin is unaffected compared to the control condition where thrombin was not first added (*Figure 2-4A*). This indicates that fibrin is essential for the thrombin-induced attenuation of subsequent convulxin response. Unlike thrombin, ADP does not induce polymerization of fibrinogen into fibrin. Therefore, as expected, when the experiment in *Figure 2-4A* is repeated with ADP instead of thrombin, GPRP does not affect subsequent calcium response to convulxin (*Figure 2-4B*). This indicates that thrombin-induced fibrin generation may be responsible for attenuation of subsequent calcium response to convulxin. It is also interesting to note that in all calcium responses to thrombin, the calcium signal trends upward. However, in cases with GPRP present, thrombin induced calcium mobilization is transient and eventually returns to baseline (*Figure 2-4C*).

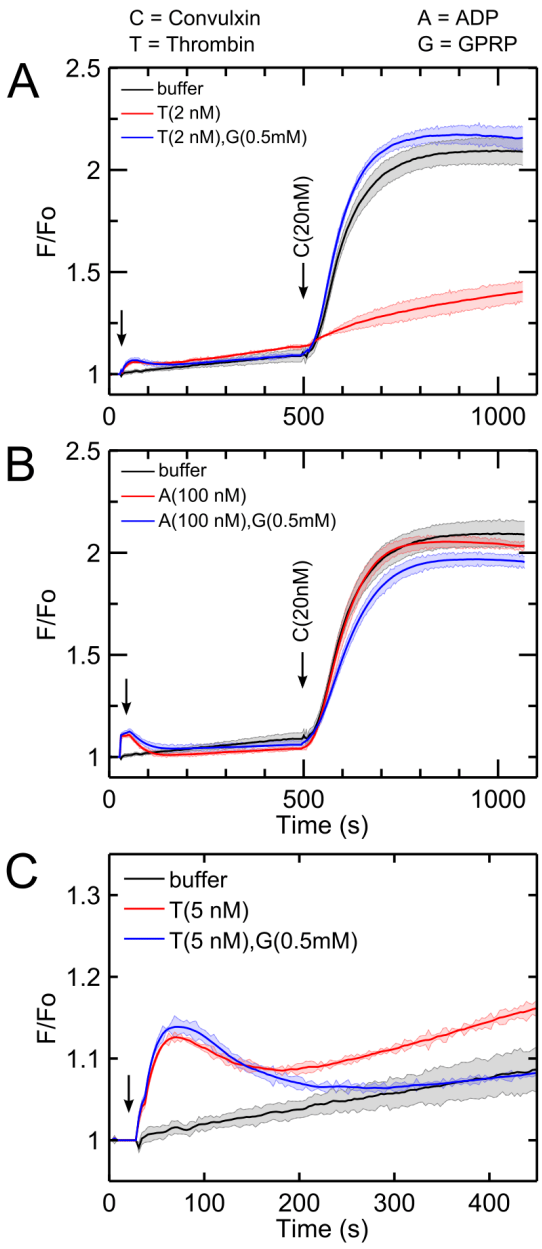

Figure 2-4 Fibrin plays important role in platelet convulxin response attenuation effect (A) GPRP inhibits fibrinogen polymerization by directly binding the fibrinogen polymerization sites. The downregulation of platelet calcium GPVI signaling by thrombin was not observed when GPRP was present. **(B)** Because platelet activation by ADP does not cause fibrinogen to polymerize into fibrin, GPRP has no effect on subsequent convulxin response. **(C)** In thrombin-induced platelet calcium signaling, calcium levels trend upward after peak. However, in the presence of GPRP, thrombin-induced calcium signaling is transient and returns to baseline levels after the peak.

3.4.5 Platelet convulxin response attenuation effect is reproduced in washed platelets and fibrinogen environment

Washed platelets were incubated with human research-grade fibrinogen (500 nM) with and without GPRP for 10 minutes before the calcium fluorescence reading *(Figure 2-5)*. Unlike the experiments in *Figure 2-1* to *Figure 2-4* that were done in PRP, in this experiment involving only washed platelets and fibrinogen, antithrombin is not present. Nonetheless, a low dose of thrombin (1nM) similarly attenuated subsequent convulxin response after 480 seconds *(Figure 2-5)*. Also, similar to experiments involving PRP, the condition involving GPRP had subsequent convulxin response levels similar to the control condition where no thrombin was added *(Figure 2-5)*. This indicates that fibrin, rather than antithrombin or other components of plasma, is responsible for the attenuation of subsequent calcium response to convulxin after platelet pre-treatment with thrombin.

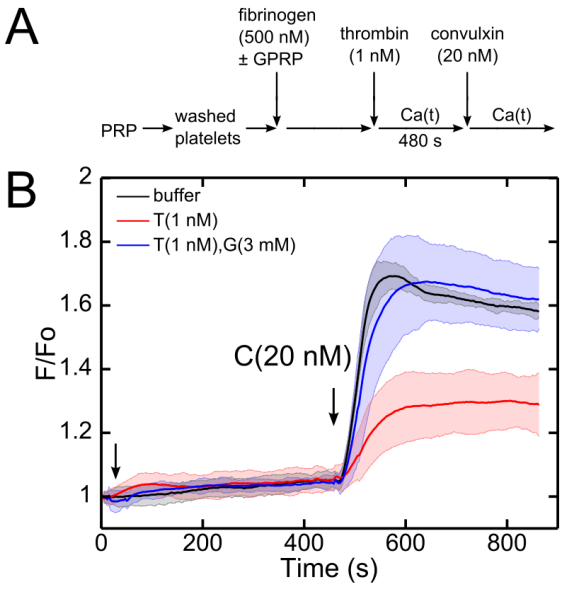

Figure 2-5 Platelet convulxin response attenuation effect is reproduced in washed platelets and fibrinogen mixture. (A) Schematic of work flow. **(B)** In a washed platelet and fibrinogen (500 nM) mixture, low dose of thrombin (1 nM) at 480 seconds incubation time significantly attenuated subsequent convulxin response, as seen in Figures 3-1 to 3-4 in PRP.

3.4.6 Presence of fibrin reduces platelet adhesion on collagen in microfluidic assay

Fluorescent fibrinogen was incubated in either 5mM GPRP (to inhibit fibrin formation) or HBS (control condition) for 10 minutes. Following incubation, 2.5nM thrombin was added to both conditions. After 300s, thrombin was quenched with 100μM PPACK in order to stop thrombin-induced fibrin polymerization. The resulting fibrinogen/fibrin solutions were diluted by a factor of 10 in PPACK/apixaban-treated whole blood (PPACK quenches thrombin and apixaban prevents endogenous thrombin production by binding to factor Xa) with either 5 mM GPRP or HBS then perfused through an 8-channel microfluidic device at $200s^{-1}$ over a collagen surface. As seen in *Figure 2-6*, as expected, 5mM GPRP (which inhibits polymerization of fibrinogen into fibrin) decreased fibrin deposition compared to the HBS control. Interestingly, in *Figure 2-6B*, GPRP increased platelet deposition on the collagen surface after 60s. This suggests that the fibrin in the control condition resulted in reduced platelet adhesion to collagen surface. In this experimental setup, thrombin is absent (due to quenching by PPACK at two different stages as well apixaban-prevention of thrombin production), which indicates that the reduction in platelet deposition is due to interaction between fibrin and GPVI, rather than an interaction between thrombin and GPVI. This result also lends strength to the argument that the attenuation effects seen in the previous calcium experiments is due to interaction between fibrin and GPVI rather than an interaction between fibrin and the collagen analog, convulxin. At 120s, low levels of fibrin resulted in more platelet deposition (+GPRP), while high levels of fibrin resulted in less platelet deposition on the collagen surface (*Figure 2-6D*). GPRP had the same effect on platelet and fibrin deposition after 240s (*Figure 2-6E*).

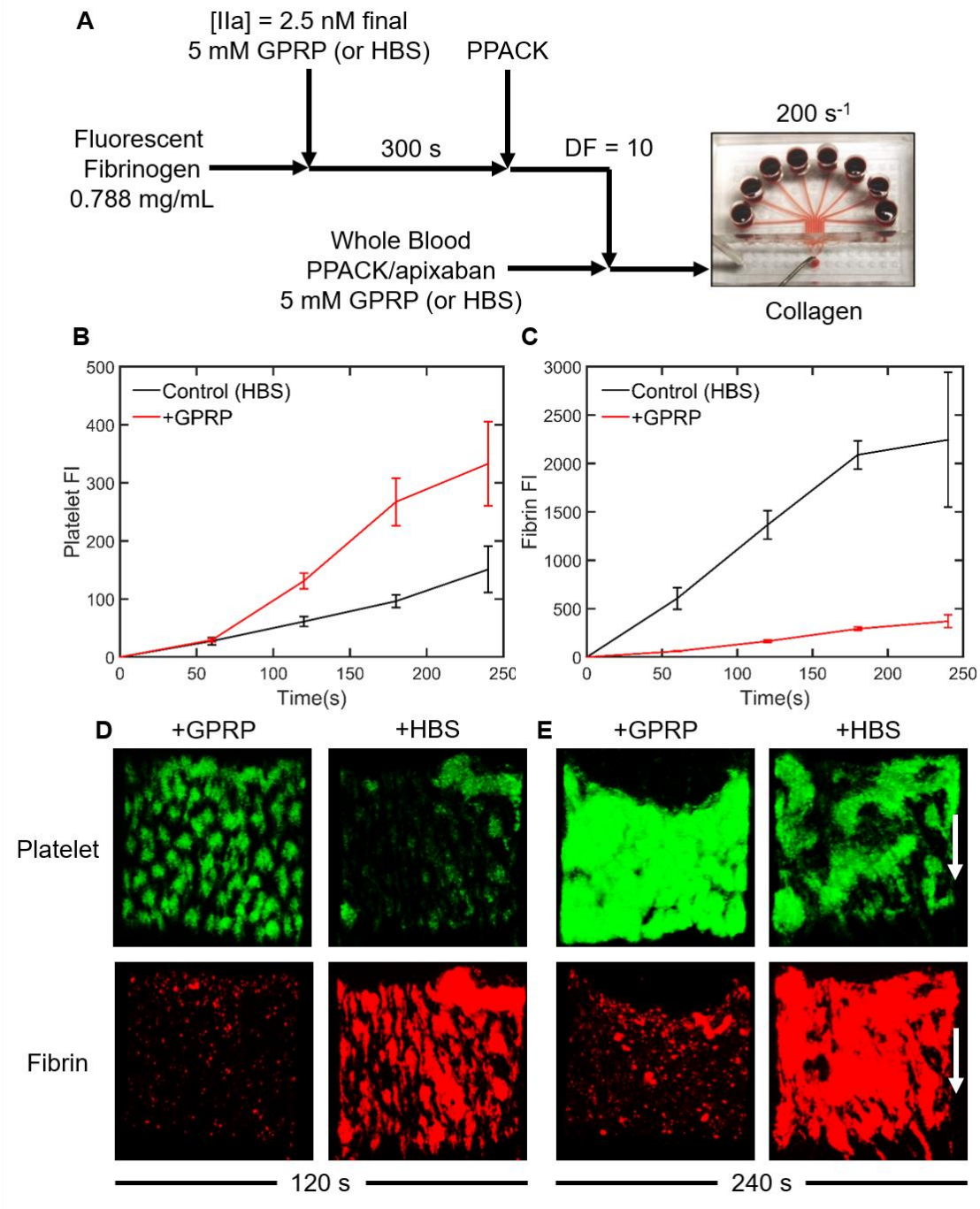

Figure 2-6 Presence of fibrin reduces platelet adhesion on collagen (A) Experimental design. Fluorescent fibrinogen is exposed to 2.5 nM thrombin with either 5 mM GPRP (inhibit fibrin formation) or HBS (control). After 300 s, the thrombin is quenched with 100 μM PPACK to stop the fibrin polymerization reaction. This reacted fibrinogen/fibrin solution is diluted by a factor of 10 in PPACK/apixaban-inhibited whole blood with either 5 mM GPRP or HBS and then perfused through the 8-channel microfluidic device at 200 s^{-1} over a collagen surface. **(B)** GPRP increases platelet deposition on the collagen surface after 60 s. **(C)** Fibrin deposition is significantly decreased when with 5 mM GPRP from the HBS control. **(D)** At 120 s, low levels of fibrin resulted in more platelet deposition (+GPRP), while high levels of fibrin resulted in less platelet adhesion. **(E)** The same effects on platelet and fibrin deposition were observed after 240 s.

3.5 Discussion

The fact that the addition of thrombin to PRP, but not ADP or the thromboxane mimetic, U46619, results in attenuation of convulxin-induced calcium mobilization when convulxin is added to PRP 480 seconds later indicates that the underlying mechanism for the downregulation of GPVI-induced calcium signaling is related to the unique function of thrombin in this assay. One of the functions of thrombin that is distinct from ADP and thromboxane in this assay is its ability to polymerize fibrinogen monomers into fibrin. The production of fibrin could play a role in the observed downregulation of GPVI-induced calcium signaling. Thrombin, with the help of metalloproteinases, has also been shown to induce low levels of GPVI-shedding [76, 77], albeit not to the extent that FXa and collagen or convulxin induces GPVI shedding. Another theory could be that thrombin induces SphK1 expression which increases formation of sphingosine 1-phosphate (Sph-1-P) in platelets through PAR-1 signaling [78], and Sph-1-P has been shown to moderately but specifically abolish convulxin-induced intracellular calcium mobilization [78], although this is not quite likely given that the effect seen in *Figure 2-1* was strong, not moderate.

The results in *Figure 2-2* indicate that the extent of the attenuation effect increases with thrombin dose as well as incubation time (time between initial thrombin dispense and subsequent convulxin dispense). The time scale in *Figure 2-2C* indicates that a maximum GPVI-signal attenuation effect was achieved at around 250 to 500 seconds (under 10 minutes), whereas thrombin-induced GPVI-shedding reached its maximum effect quite a bit later, around 30 to 40 minutes [76]. In several experiments measuring thrombin-induced fibrin polymerization, fibrin levels were measured for a maximum of 15 minutes [79, 80], as the maximum value was usually reached before then. This time scale is more compatible with the timescale of the attenuation effect of convulxin-induced GPVI calcium signaling seen in *Figure 2-2C*. This indicates that

polymerized fibrin binding to GPVI may better explain the observed GPVI-induced calcium response attenuation effect rather than thrombin (or fibrin) -induced GPVI shedding.

Unlike thrombin, PAR-1 and PAR-4 receptor agonists cannot catalyze the polymerization of fibrinogen monomers into fibrin. The inability of PAR-1 and PAR-4 receptor agonists to reproduce the attenuation effect of convulxin-induced calcium response as created by thrombin (*Figure 2-3*) supports the hypothesis that fibrin plays an essential role in the subsequent convulxin-induced calcium attenuation effect. Thrombin activates PAR-1 with approximately 30 times greater sensitivity than PAR-4, and PAR-1 activation induces a rapid increase in intracellular calcium that quickly returns to baseline, whereas the PAR-4 signaling provides a slower but more prolonged calcium increase [81]. Vorapaxar, a PAR-1 specific inhibitor, was able to completely abolish 10 nM thrombin-induced calcium signal (*Figure 2-3B*). This may be because at 10 nM, which is a low to medium concentration of thrombin (5 x EC_{50}), the thrombin-induced calcium signaling might be dominated by signaling through PAR-1 rather than PAR-4, which is likely since thrombin activates PAR-1 with about 30 times greater sensitivity than PAR-4 [81]. It has also been shown that PAR-4 receptor agonist (but not PAR-1) induced full platelet spreading on a fibrinogen matrix [82], which can be attributed to sustained calcium mobilization required for platelet spreading. The platelet spreading is thought to be mediated by activated integrin $\alpha_{IIb}\beta_3$, but the relatively new finding that fibrin binds to GPVI [16], may suggest another mechanism (through GPVI) by which platelets also spread on the fibrinogen matrix. This, along with the results in *Figure 2-3C*, may indicate that the interaction between platelet and fibrin that causes attenuation in GPVI-induced calcium signaling is largely dictated by PAR-4 rather than PAR-1.

In *Figure 2-4*, GPRP (which inhibits the polymerization of fibrinogen into fibrin) abolishes the thrombin-induced attenuation effect on subsequent convulxin calcium response.

This strongly suggests that fibrin, not thrombin, is responsible for the attenuation effect. Furthermore, as seen in *Figure 2-4C*, GPRP also abolishes the upward calcium trend following thrombin peak (after thrombin addition to PRP), suggesting that the mechanism by which this phenomenon happens involves increasing calcium mobilization. This leaves four possible explanations: polymerized fibrin binding to GPVI, fibrin binding to convulxin/collagen, fibrin binding to another platelet integrin that mediates convulxin/collagen activation of platelets (such as integrin $\alpha_2\beta_1$) or fibrin inducing GPVI-shedding.

It has been discovered recently that platelet GPVI binds to polymerized fibrin (rather than fibrinogen monomers) [16, 18], which activates platelets (as shown by increased PS exposure) and promotes thrombin generation as well as thrombus growth [17]. In the platelet calcium assays done in this study, apixaban, a direct factor Xa inhibitor is used, which prevents endogenous thrombin generation. These results may shed light on the effect and nature of the fibrin-GPVI binding independent of thrombin generation.

Regarding the possibility that fibrin induces GPVI-shedding, Factor Xa, collagen and convulxin, and to a much lesser extent, thrombin, have been shown to cause GPVI shedding [76, 77]. To our knowledge, fibrin has not been studied as a potential cause of GPVI shedding. It could be that during the duration of thrombin-induced calcium mobilization, thrombin polymerizes fibrinogen into fibrin, which binds to and activates GPVI [16, 18], causing fibrin to cleave GPVI during the process, such that by the time convulxin is added, not enough GPVI is left on platelet membrane to be activated so as to lead to a GPVI-induced calcium influx. This may also explain the upward trend of thrombin-induced calcium mobilization in *Figure 2-4A* and *Figure 2-4C*; after an initial decrease after peak thrombin response, newly polymerized fibrin may activate platelets via binding to GPVI and induce calcium mobilization while cleaving GPVI, such that when convulxin is added a 480 seconds, very little GPVI is left intact to be

activated. In the condition involving GPRP (*Figure 2-4C*), thrombin-induced calcium mobilization is transient and returns to baseline because fibrin is not formed and therefore not continuously activating GPVI. Similarly, when PAR-1 and PAR-4 receptor agonists were used to induce calcium mobilization, even though the peak calcium response was slightly higher than that of the thrombin-induced calcium response, calcium response was transient and returned to baseline because PAR-1 and PAR-4 cannot induce fibrin polymerization. The upward trend of thrombin-induced calcium mobilization may be also by aided by PAR-4 which has been shown to provide later but more sustained calcium mobilization than PAR-1 [83, 84]. GPVI shedding is regulated primarily by a-disintegrin-and-metalloproteinase 10 (ADAM10) [85]. Some other sources have also found that other members of the a-disintegrin-and-metalloproteinase family (such as ADAM17) also facilitate GPVI shedding [86]. These metalloproteinases (MMPs) are present in platelet rich plasma but is not present in washed platelets. In this washed platelet environment, we still see an attenuation of GPVI-induced calcium mobilization following thrombin addition in the control environment where fibrinogen is able to polymerize into fibrinogen, but not in the GPRP fibrin-inhibited environment. This makes it less likely that the attenuation effect seen here is due to polymerized fibrin cleavage of GPVI into sGPVI. Furthermore, as mentioned previously, the time scale in *Figure 2-2C* indicates that a maximum GPVI-signal attenuation effect was achieved at around 250 to 500 seconds (under 10 minutes), whereas thrombin-induced GPVI-shedding reached its maximum effect quite a bit later, around 30 to 40 minutes [76]. Taken together, this weakens the argument that the attenuation effect is due to polymerized fibrin cleavage of GPVI into sGPVI. This can be further confirmed by repeating the experiments in *Figure 2-4* in the presence of a broad spectrum metalloproteinase inhibitor such as GM6001 (since MMPs are essential for GPVI shedding). If the attenuation effect is still observable with successful GM6001 blocking of MMPs, then it is very unlikely that polymerized fibrin is causing GPVI shedding.

There is also the possibility that fibrin binds to convulxin, reducing its availability to bind to and activate platelet GPVI, resulting in the observed attenuation of convulxin-induced calcium mobilization. It is difficult to tell whether or not this is the case in the experiments done so far. To test this hypothesis, ligand binding assays can be done to examine the specific interaction between fibrin and convulxin or fibrin and collagen.

The procoagulant collagen surface in this microchannel causes platelet activation via GPVI and mediates adhesion through activated platelet integrin $\alpha_2\beta_1$ [87-89]. Platelets tend to bind directly to the exposed collagen through two major receptors, integrin $\alpha_2\beta_1$ and GPVI, only at high shear conditions are GPIb-V-IX receptor complex and its main ligand von Willebrand Factor additionally needed for firm platelet adhesion to the vessel wall [90]. Therefore, in this specific microfluidic assay, where shear rates are low ($200s^{-1}$, corresponding to venous shear rates), the two possible mechanisms by which platelet deposition on collagen is reduced is via reduced platelet GPVI binding to collagen and/or reduced platelet integrin $\alpha_2\beta_1$ binding to collagen. According to Niewswandt et al., GPVI but not $\alpha_2\beta_1$ plays the central role in platelet-collagen interactions under flow. GPVI facilitates platelet-collagen interactions by activating different adhesive receptors, including $\alpha_2\beta_1$integrin; however, unlike GPVI, $\alpha_2\beta_1$ integrin was found to strengthen adhesion without being essential to adhesion [91]. Therefore it is more likely that the reduction in platelet deposition on collagen observed here is due to reduction in GPVI binding to collagen rather than reduced $\alpha_2\beta_1$ binding to collagen. Furthermore, it has been demonstrated that anti-GPVI antibody, but not anti-$\alpha_2\beta_1$ antibody, inhibits convulxin-induced $[Ca^{2+}]_i$ increase [92]. This also indicates that in convulxin-induced $[Ca^{2+}]_i$ assays prior, attenuation effects seen were due to disrupted GPVI rather than $\alpha_2\beta_1$ signaling. This leads to the most likely explanation of this observation: polymerized fibrin binds to GPVI.

In similar microfluidic assays, platelets tend to adhere to localized collagen surface within the first minute. Between approximately 1 minute and about 105 seconds, platelet coverage on the collagen surface grows in two dimensions. After 105 seconds, thrombus tends to grow in height (the third dimension) due to secondary platelet-platelet aggregation, mediated by soluble agonists such as ADP (around 105 seconds) and thromboxane (around 150 seconds) [93]. Therefore, in this experimental setup, to examine platelet GPVI interaction with collagen, the focus needs to be on the time window before 105 seconds. As seen in *Figure 2-6B*, around 60-105 seconds, the GPRP platelet fluorescence intensity (FI) continuously increases over the control, indicating that platelet GPVI binding to collagen is reduced in the presence of fibrin. Pre-60 seconds, there tends not to be a big difference, probably because fibrin is just being introduced into the system and the fibrin levels for the GPRP and control condition have not diverged enough yet (*Figure 2-6C*). To more closely examine this effect, the time resolution could be increased in the primary deposition phase (< 105 seconds). In the secondary platelet aggregation phase > 105 seconds, the platelet FI for the GPRP conditions continues to increase and diverge over the control condition, but appears to converge very slightly after 180 seconds. This could mean that polymerized fibrin disrupting the GPVI binding to collagen also has an initial effect on secondary aggregation that is corrected eventually, but this would require a repeat of the same experiment with higher time resolution to verify. There has been recent evidence that GPVI plays a critical role in thrombus growth and stability [16, 18] in addition to initiation; the fact that secondary aggregation as indicated by platelet FI > 105s continues to be reduced in the presence of fibrin suggests that fibrin binding to important sites on GPVI may be weakening its ability to grow and stabilize the thrombus > 105s.

In *Figure 2-6D*, at both 120 and 240 seconds, fibrin, even in the control condition, does not show up in the spaces between the platelets (which is indicative of fibrin formed under flow),

which means that PPACK and apixaban have effectively prevented endogenous thrombin production as well as fibrin polymerization under flow. Further, the areas of fibrin fluorescence seem to overlay quite well onto areas of platelet fluorescence, indicating that platelets are where the fibrin is, which adds strength to the argument that platelets are binding to fibrin, possibly via GPVI. In previous work by Colace et al., whole blood (CTI-treated to inhibit coagulation by contact pathway) was perfused over tissue-factor treated collagen surface under pressure relief mode (which is a more physiologically relevant then the constant flow mode in *Figure 2-6*, because flow is diverted from thrombotic occluding channels to open channels which allows thrombus to grow to full occlusion) at a venous inlet flow ($200s^{-1}$) [94]. The resulting average platelet mass formed in the presence of GPRP showed 20% more platelets than that formed without GPRP, suggesting a modest role for fibrin in slowing platelet deposition and clot growth, which supports our observation [94]. The effect of GPRP in our experimental setup, however, indicates a stronger role (platelet deposition seemed to decrease by slightly more than 50% in *Figure 2-6B*).

In conclusion, the most likely explanation for reduced platelet deposition on collagen, reduced secondary aggregation, as well as attenuated calcium response to convulxin in the presence of polymerized fibrin is that polymerized fibrin binds platelet GPVI and therefore reduces GPVI-mediated platelet activation. However, the mechanism by which fibrin reduces GPVI-mediated platelet activation is not so clear. Fibrin could act as an antagonist or agonist (or both) when it binds to platelet GPVI. One way fibrin could act as an antagonist is by blocking or competing for GPVI-collagen and GPVI-convulxin binding sites when it binds to GPVI. However, recent findings show that fibrin binds to GPVI and promotes thrombin generation and thrombus growth [16, 18], effectively acting as a platelet agonist. This is not necessarily in contradiction to our findings; our experiments have examined this interaction in experimental

conditions where endogenous thrombin production is not possible due to use of Apixaban as the anticoagulant. Furthermore, in all calcium assays, thrombin-induced calcium signaling trends upward after the peak, but when GPRP is present to block fibrin polymerization, thrombin-induced calcium signaling returns to baseline after the peak *Figure 2-4C*. This points to the possibility that fibrin produced by thrombin addition continuously activates platelets such that when convulxin is added 480 seconds later, platelets are already desensitized, resulting in the observed attenuated calcium signal. The mechanism for platelet desensitization still unknown but is important to further study. Patients with trauma-induced coagulopathy tend to have elevated markers of platelet activation but reduced responsivity to platelet agonists [15]. Trauma-induced coagulopathy is also marked by an increase in thrombin and fibrin generation [95]. The central observation in this work is a recapitulation of these trauma conditions in vitro: addition of thrombin initially activates platelets and initiates fibrin formation, resulting in platelet desensitization (manifested as an attenuated calcium response) to a strong platelet agonist, convulxin, when it was added 480 seconds later. Therefore, further investigating the underlying mechanism behind this central observation could be useful in understanding the mechanism behind platelet desensitization during trauma-induced coagulopathy.

3.0 Future Work

4.1 Further Investigation of Fibrin-GPVI Interaction

The nature and effect of fibrin-GPVI interaction on platelet function, as highlighted in Chapter 3, requires further investigation.

First, platelet GPVI also facilitates platelet aggregation indirectly by activating platelets and exposing phosphatidylserine (PS). An experiment could be conducted to study collagen-

induced platelet aggregation in the presence of fibrin and without, in order to shed light on the effect of fibrin-GPVI interaction on platelet aggregation behavior, which is a platelet function not previously studied in Chapter 3. The experiment would entail drawing blood into 10% v/v sodium citrate and 250nM apixaban (to prevent endogenous production of thrombin). Sodium citrate is required to prevent instant platelet aggregation upon agitation (from stir bars in cuvette), and does not affect the ability of thrombin to form polymerized fibrin from fibrinogen. The whole blood sample would be spun into PRP for light transmission aggregometry (LTA) to be performed. Vorapaxar , a PAR-1 inhibitor, would be added to prevent full aggregation upon first dispense of thrombin but still allow thrombin to polymerize fibrinogen into fibrin. At the start of aggregometry reading, low dose thrombin (2 nM) would be added to PRP with or without GPRP (5mM) to inhibit fibrin polymerization. At 10 minutes after the first dispense, collagen would be added to induce platelet aggregation, the rate and final aggregation % would be read and compared between the conditions with and without GPRP to determine whether or not the fibrin-GPVI interaction reduces platelet aggregation.

As mentioned briefly in Chapter 3, it is unlikely that polymerized fibrin downregulates GPVI by inducing GPVI-shedding, as the attenuation effect is observable in washed platelets where the metalloproteinases (MMPs) needed for GPVI-shedding is theoretically absent. This statement can be verified by repeating the PRP calcium assay with GM6001, a broad spectrum inhibitor of metalloproteinases. It is expected that the results would be similar compared to that highlighted in Chapter 3 even in the presence of GM6001.

Finally, the microfluidic assays performed in Chapter 3 may be improved with higher time scale resolution (higher than once per minute), especially since the important primary deposition phase occurs < 105. This allows us to better determine the timescale of the effect of fibrin-GPVI interaction on platelet deposition on collagen.

4.2 Extending human platelet calcium calculator to include individuals with familial hypercholesterolemia

The neural network-based calcium calculator (NN) built in Chapter 2 can be extended to include patient populations. This study would involve individuals with familial hypercholesterolemia (FH) and individuals without known coronary heart diseases who visit the doctor's office to get a computed tomography coronary angiography (CTCA) scan. Pairwise agonist scanning (PAS) as described in Chapter 2 can be done on study participants and a NN trained exclusively on FH patients can be built. This FH-NN output can be compared to the healthy NN output [75] to shed light on the effect of FH on calcium signaling phenotypes. Furthermore, this NN can be combined with microfluidic experiments to build and validate a multiscale model to simulate thrombus growth and vessel occlusion triggered by collagen/tissue factor. This model may also be compared to the multiscale model built on healthy donors [53] to study how FH affects normal thrombus growth. Furthermore, with enough FH/healthy donors and PAS experiments, a classification model can potentially be built to identify and diagnose patients with FH based on their calcium signaling phenotype (for example using pairwise synergy scores).

4.3 Combining platelet calcium calculator to build an NN-ODE model

The neural network-based calcium calculator (NN) built in Chapter 2 can be coupled to an ODE model to predict important platelet activation phenomena in real time. Specifically, the NN built in Chapter 2 (which describes platelet receptor mediated calcium mobilization) can be coupled to a coarse-grained ODE model that further describes the effects of platelet activation events downstream of calcium mobilization such as: granule release, thromboxane and thrombin production, inside-out signaling and cell contraction. The production of secondary soluble mediators due to these events (such as ADP, thromboxane and thrombin) can be fed back into the

NN as inputs (in the form of agonist concentrations), resulting in a more comprehensive and accurate model of platelet activation and autocrinic signaling. It is important to note that the NN does not account for endogenous thrombin production and therefore does not capture the effects of autocrinic signaling [75]. Since the NN training incorporates feedback at 8 previous time points, history is important in the training of the NN. To enable the NN to more accurately give dynamic predictions in this ODE-NN coupling, the NN should additionally be trained on PAS experiments where agonists are added sequentially to improve the predictive power of the NN and avoid stability issues.

The ODE model can be built to describe five important platelet activation events downstream of calcium mobilization, as shown in *Figure 3-1*. First, inputs (agonist concentrations) are to be specified. The NN can then predict intracellular calcium levels based on the inputs. All five events described in the ODE model are a triggered, at least in part, by intracellular calcium. Three of these events lead to production of soluble secondary mediators (ADP, thromboxane and thrombin). The ODE model will calculate the concentration of these secondary mediators based on intracellular calcium levels. The agonists concentrations will be fed back into the NN and the NN would predict the resulting intracellular calcium levels. This cycle continues until steady state is reached. The signaling pathways triggered by elevated intracellular calcium levels in platelets are still largely unknown [64]. Many of the kinetic parameters in the reactions that are involved in the known pathways events are unavailable/ difficult to determine experimentally [64]. Therefore a coarse-grained ODE approach can be used. Specifically, steady state experimental data that gives the concentrations of intermediates as a function of intracellular calcium levels can be found in literature, or if the literature is not available, it may be done experimentally (*Table 1-1*). With this coarse-grained ODE approach it is estimated that about 30 ODEs would be required to describe these five events.

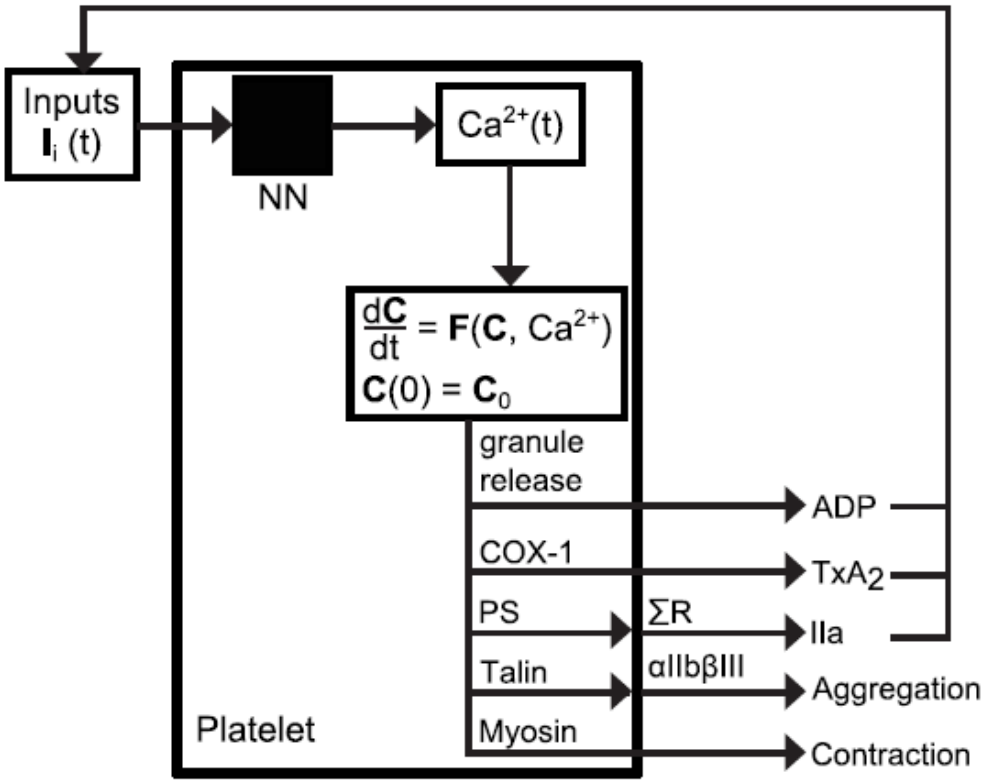

Figure 3-1 ODE-NN model of platelet

	Event	Intermediates Studied/Coarse Grained	Source
1	ADP release	Ca^{2+} → Dense-granule release (coarse grained)	Lenoci et al. (2011) [96] Jonnalagadda et al. (2012) [97]
2	Thromboxane release	Ca^{2+} → COX-1 activation	*(Experiment)*
		COX-1 activation → TxA_2 production	*(Experiment)*
3	Thrombin release	Ca^{2+} → PS exposure	*(Experiment)*
		PS exposure → Thrombin production	Chatterjee et al. (2010) [98]
4	Aggregation	Ca^{2+} → $\alpha_{2b}\beta_3$activation (PAC-1)	Lenoci et al. (2011) [96]
		$\alpha_{2b}\beta_3$activation → aggregation (KMC)	Tandon et al. (1997) [99] Laurenzi (1997) [100]
5	Contraction	Ca^{2+}→myosin activation	*(Experiment)*
		myosin activation → contraction	

Table 3-1 Platelet activation events described in ODE model

Some of the coarse-graining experiments that can be done to measure those platelet activation events as a function of calcium, so as to obtain an effective rate, K_{eff}, [96] include: for PS exposure as a function of $[Ca^{2+}]_i$, using Annexin V to measure PS exposure over time [101], concurrently measure $[Ca^{2+}]_i$ using the same PRP sample and obtain a [PS-positive] vs. $[Ca^{2+}]_i$ dataset. For TxA_2 production as a function of $[Ca^{2+}]_i$, measure TxB_2 (TxA_2 converts to TxB_2 rapidly) using ELISA [102], concurrently measure $[Ca^{2+}]_i$ using the same PRP sample, obtain a $[TxA_2]$ vs. $[Ca^{2+}]_i$ dataset. Similarly, for phosphorylated myosin as a function of $[Ca^{2+}]_i$, measure myosin-P using [32P] – phosphorylated MLC12, concurrently measure $[Ca^{2+}]_i$ using the same PRP sample, and obtain a [myosin-P] vs. $[Ca^{2+}]_i$ dataset.

Once the model ODE-NN model is built, experiments can be conducted to measure model performance. Inputs can be specified as agonist concentrations at t = 0, and a reliably measurable output would be thrombin concentration at $t = t_{end}$. Simulation can be run for ~10 minutes (typical time for aggregation to plateau). Thrombin generation in response to agonists can then be measured in experiments using a thrombin-specific substrate, such as Boc-VPR-MCA, in the well plate. The experimental thrombin generation result can then be compared to the simulation result in order to calculate accuracy and evaluate ODE-NN model performance.

4.4 Higher order PAS

The NN model that was trained on PAS (pairwise agonist scanning) in Chapter 2 can be improved by training the model on high-dimensional agonist scanning. The high-dimensional agonist scanning would include the effects of more than six agonists and improve accuracy of calcium level predictions.

The complete experimental space for six agonists at null, low, medium and high concentrations (such as in PAS) is $4^6 = 4096$ conditions. There are approximately 20 more agonists not studied by PAS in Chapter 2 that are important in calcium signaling and platelet

activation as well (*Table 3-2*). The full experimental space grows exponentially with increasing number of agonists, the full experimental space for 20 agonists is 4^{20}, or approximately 1 trillion combinations. Furthermore, we are limited to approximately conditions per experiment, mostly due to the lifetime of PRP in 250nM apixaban. Therefore it is important to establish a systematic, "smart", efficient sampling method to sufficiently inform the neural network such that is able to make reasonably accurate predictions about the complete experimental space.

In Pairwise Agonist Scanning (PAS), platelets are activated with all single and pairwise combinations of six agonists at three different conditions (154 conditions total including a null condition). Each agonist activates different receptors on the platelet. Significant crosstalk occurs between these different receptor-mediated signaling, but they all converge on calcium mobilization. As explained previously in Chapter 2, NN trained only on the resultant calcium time traces of single and pairwise interactions in the full agonist dose range was able to predict trinary, higher order (4-6 agonists) and sequential interactions with reasonably high accuracy [75]. The trinary, higher order and sequential experiments were done separately and was not part of the training set. The fact that just single and binary conditions were enough to inform the NN about conditions involving 3-6 agonists points to the possibility that there are redundancies in the information provided by some of the combinations. In other words, certain agonist combinations may not be so informative or important in describing the full experimental space. The search method may be guided by the synergy score metric previously developed by Chatterjee et al. (2010) [20]. Synergy scores are a measure of the direction and extent of cross-talk between agonist combinations [20]. Synergy scores (S_{ij}) range from -1 to 1. A positive S_{ij} value indicates synergistic behavior between agonists i and j whereas a negative S_{ij} value points to antagonistic behavior; a S_{ij} value of 0 represents a purely additive response. Combinations with high synergy

scores contain information about cross talk between signaling pathways beyond the additive response of the single agonists that the combination comprises.

In other words, the complete experimental space for six agonists at null, low, medium and high concentrations is $4^6 = 4096$ conditions. A method can be developed to probe the important directions (i.e. perform "smart" sparse sampling of combinations) such that the NN is sufficiently informed and able to predict calcium time traces of the full combinatorial space (specifically higher-order interactions). This is a fractional factorial design problem: the full combinatorial experimental space is strategically sampled by utilizing the sparsity-of-effects principle so as to reduce screening effort. The sparsity-of-effects principle states that a system is usually dominated by main effects and low-order interactions. That method can then be utilized to determine specific combinations of agonist (not limited to the six mentioned in Chapter 2) that would be most informative, so that experiments can be done to obtain corresponding calcium time traces and a neural network can be trained on just those calcium traces but still be able to predict calcium response to > 6 agonists.

One possible method to develop the "smart" sparse sampling method is to use synergy scores (S_{ij}) to point toward combinations that are most informative. For a given combination, high absolute S_{ij} values of synergy scores indicate that significant cross-talk takes place between the signaling pathways mediated by agonists involved in that given combination. In other words, that combination is information-dense. On the other hand, combinations for which S_{ij} values are close to zero demonstrate only the additive response of the single agonists that make up that combination – this information is already captured by the single agonist conditions. Experimentally, we are limited to approximately 190 conditions per experiment. Full main effects for the complete 4^6 (6 agonist) experimental space as well as the full n = 135 second order interactions (100% of 135 possible interactions) are already sampled. The S_{ij} for each of the 135 sampled combinations should then be examined, and combinations that satisfy a certain threshold,

e.g. $|S_{ij}| > 0.3$ can be picked. Utilizing data from Chapter 2, there are about 20 (out of a total of 160) combinations that satisfy this criteria for example. This process would then be repeated for each interaction order (third and higher). Next, n = 190 third order interactions would then be randomly sampled and the corresponding S_{ij} calculated. If the same example threshold was set, 52 (out of 160) combination satisfy this criteria. This is then repeated for each order interaction (4, 5 and 6). The sample size n for each order interaction will also have to be scaled to each order interaction combination space (i.e. sample size for the six-agonist experimental space has to be larger than the three-agonist experimental space). Other rules or methods for picking the samples may also be explored (e.g. Random Sampling-High Dimensional Model Representation, Markov Chain Monte Carlo, Non-linear PCA/ Diffusion maps, Locality-sensitive hashing).

Next, prediction R values (representing accuracy of model) will have to be plotted against sampling effort (effectively number of combinations sampled). We would stop at a point (i.e. pick the number of combinations sampled) where prediction ability plateaus with increasing sampling effort. Then the full 20-agonist experimental space 4^{20} can be sampled with approximately 20 experiments using one of the methods above to obtain a reasonable R value for prediction.

List of Important Platelet Agonists [103]

	Agonist	Receptor	Phase
1	Collagen (Convulxin)	GPVI	Recruitment, Adhesion, Aggregation
2	Fibrinogen, vWF, fibronectin, vitronectin, TSP-1	$\alpha_{2b}\beta_3$	
3	Fibronectin	$\alpha_5\beta_1$	
4	Laminin	$\alpha_6\beta_1$	
5	ADP	$P2Y_1$, $P2Y_{12}$	Amplification
6	Thrombin	PAR-1, PAR-4	
7	Thromboxane (U46619)	TP	
8	1-O-alkyl-2-acetyl-sn-glycero-3-phosphocholine	PAF receptors	
9	Lysophosphatidic acid	Lysophosphatidic acid receptor	
10	Vasopressin	V1a vasopressin receptor	
11	Adenosine	A2a adenosine receptor	
12	Epinephrine	b2 adrenergic receptor	
13	Serotonin (5-hydroxytryptamin)	Serotonin receptor	
14	Dopamine	Dopamine receptor	
15	ATP	$P2X_1$	
16	TPO	c-mpl	
17	Leptin	Leptin receptor	
18	Insulin	Insulin receptor	
19	PDGF	PDGF receptor	
20	Ephrine	Ephr	Stabilization
21	Gas-6	Axl/Tyro3/Mer	
22	PSGL-1,GP1b,TF	P-selectin	
23	TSP1, oxLDL, VLDL, oxPHL, collagen type V	CD36	
24	PACAP	VPAC1	Negative Regulation
25	PECAM-1	PECAM-1	
26	PGI_2	IP	
27	PGE_2	EP1-4	
28	PGD_2 receptor	PGD_2	

Table 3-2 **List of Important Platelet Agonist compiled from Kauskot et al. (2012)**

4.5 Building a classification based on platelet calcium mobilization phenotypes as measured by pairwise agonist scanning

The project described in section 4.2 (PAS experiments of FH patients) may be combined with large quantities of available PAS experimental data of healthy donors in past years as well as in the future to build a data-driven classification model that distinguishes patients from healthy donors based on PAS calcium phenotypes (for example synergy scores). If proven to be accurate, such a model may be able to aid in clinical diagnosis in the future. Once trained on PAS data of both healthy donors and patients, the model would be able to classify new donors as 'healthy' or 'patient' based on their PAS calcium phenotype. A plausible approach to building a classification model that exploits the wealth of platelet function information in the PAS experiments is described below.

In this example, I built a classification model that distinguishes male donors from female donors using a PAS dataset generated by a previous Diamond Lab member, Manash Chatterjee. The PAS experiments were performed by Manash Chatterjee as previously described [20]. I decided to use the 135-parameter synergy score of each PAS experiment as the calcium phenotype to build my classification model on. As mentioned previous in Chapter 2, synergy scores (S_{ij}) are a measure of the direction and extent of cross-talk between agonist combinations. The synergy score is defined as the difference between the observed and the predicted additive calcium level response, normalized by scaling to the maximum synergy score observed in the entire dataset. Synergy scores range from -1 to 1. Negative values for a particular pair of agonist conditions indicate antagonistic behavior, whereas positive values indicate synergistic behavior. A synergy score of 0 indicates a perfectly additive response. In previous work, synergy scores of replicate PAS experiments done on the same donor on different days self-clustered [20], demonstrating that synergy scores is a quantifiable platelet phenotype that describe an

individual's unique platelet function. In addition to predicting the sex of the donor based on the donor's PAS data, the classification model may also be used to point toward the key physiological differences that are the most informative, in this case, isolate the specific synergy scores (specific combinations of agonist) that are most predictive of donor sex.

4.5.1 Gender clustering patterns

To first demonstrate that the gender of donors had an effect on PAS synergy scores, hierarchical clustering was done on the 135-element synergy score vectors of 40 PAS experiments. The Euclidean distance between synergy score vectors between all pairs of synergy score vectors were calculated and was used as the measure of similarity between each vector. Experiments from the same donor self-clustered at the lowest level On a higher level, male donors (black text) tended to cluster together on the left and female donors (red text) tended to cluster together on the right (*Figure 3-2*). This indicates that both the identity and gender of individual donors can be distinguished based on their PAS synergy scores, and alludes to a potential phenotypical difference between male and female platelet reactivity.

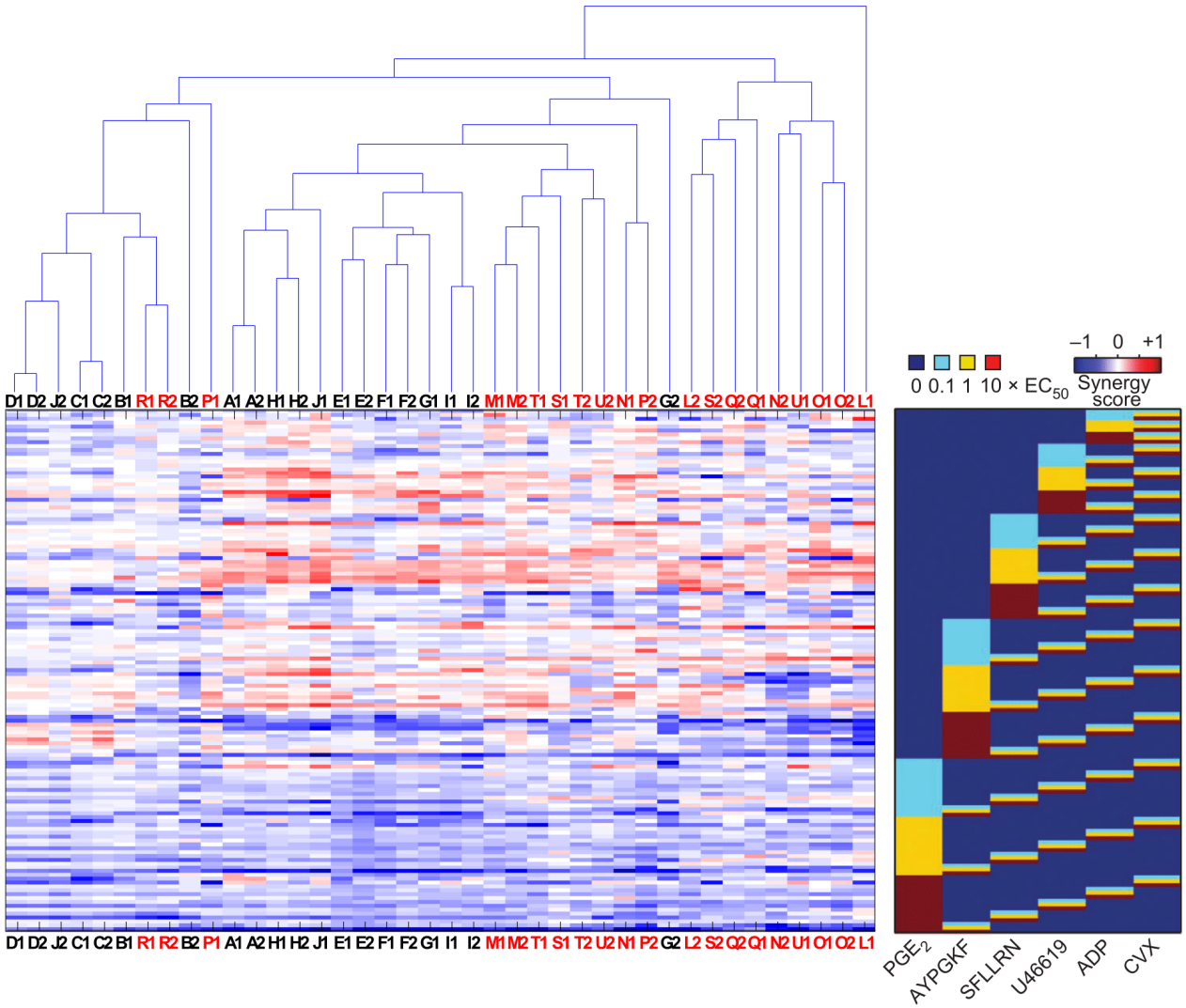

Figure 3-2 Clustering of synergy scores based on donor gender

4.5.2 Sources of variability in synergy scores

Inter-donor variability was calculated by first taking the average synergy scores of the replicate experiments of each donor, then calculating the standard deviation of average synergy scores among donors. The biggest differences in sources of variability between male and female donors come from medium and low CVX interactions (*Figure 3-3*). Among female donors (*Figure 3-3* middle panel), as opposed to among male donors (*Figure 3-3* top panel), those interactions did not contribute very much to variability. PAR-1 receptor agonist, AYPGKF pathways also contributed to variability among donors, but its contribution is significant both in men and women (*Figure 3-3*bottom panel). This indicates that GPVI signaling and crosstalk accounted most strongly for the functional differences between the male and female platelets.

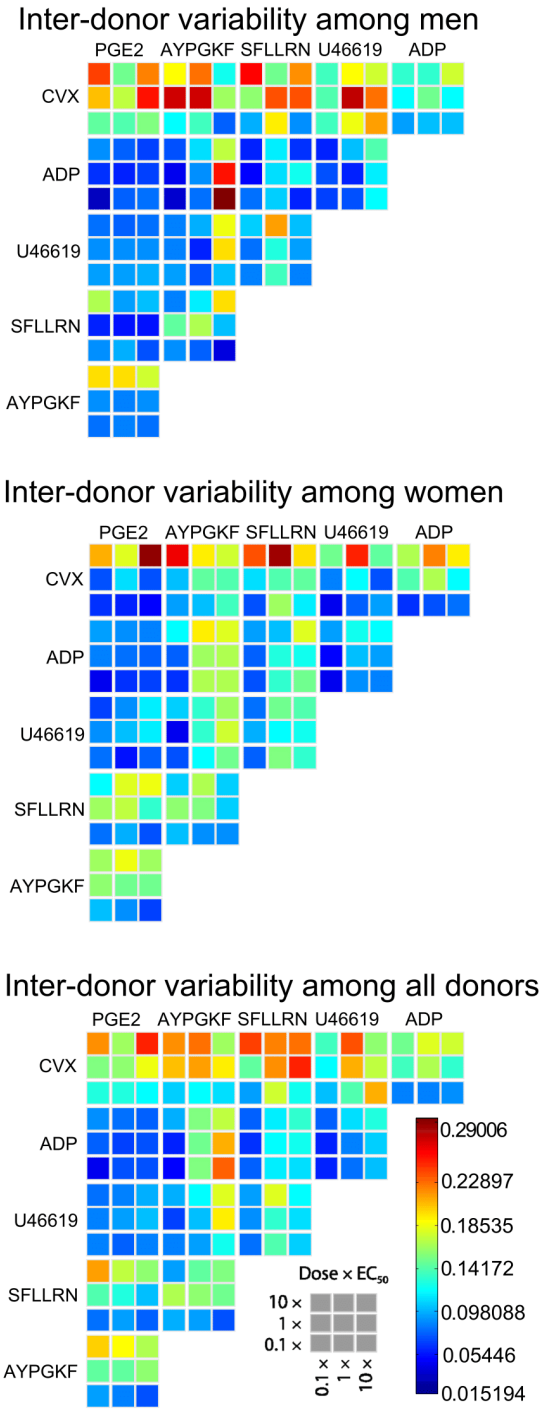

Figure 3-3 Sources of variability in synergy scores

4.5.3 SVM model building and performance

The classification model was built using support vector machines (SVM). SVM was implemented using libSVM software written for MATLAB. The dataset was first organized into a 40 x 135 matrix of synergy scores. Each row comprised of a synergy score vector of a particular PAS experiment. There were 20 total donors in this dataset, 10 of which were female and 10 others were male. Each donor had a set of two replicate experiments, giving a total of n = 40 PAS synergy score vectors. There were m = 135 pairwise conditions of the 6-agonist PAS experiment. Labels were then prepared as a binary column vector with 0 representing the male donors and 1 representing female donors. The synergy scores ranged from -1 to 1. To reduce computational time, the dataset was first preprocessed into integers that ranged from 1 to 64. All datasets were also kernelized using the intersection kernel before being trained on by the Support Vector Machine (SVM) algorithm. The new dataset was then normalized by dividing synergy scores by the maximum value of each condition. The dataset was then randomly divided in an 80/20 proportion into training and testing sets, with the constraint that there were equal numbers of male and female donors in the training and testing sets. This constraint was put in place because of the relatively small size of the dataset (n = 40); making sure that the training set had equal numbers of male and female donors would enable the SVM method trained to be more accurate despite the small size of the dataset. Leave-one-out-cross-validation (LOOCV) was then performed on the training set (consisting of 32 examples) to determine the best C-parameter to use for the actual training and testing. The C-parameter in SVM represents the extent to which the SVM algorithm allows classification errors during training. In LOOCV, one example is randomly set aside as a test sample and the rest are trained with SVM using a chosen value. This is repeated 100 times to obtain an overall error rate. This procedure is repeated with different C-parameters (100, 200, 500, 1000 and 10000), and the final C parameter chosen would be the one that produces the

lowest error rate. Then the SVM is trained on the original training set using the cross-validated C-parameter value and finally tested to obtain the test error. This entire procedure we repeated 1000 times to obtain an overall 1000-run test error.

In this SVM implementation, the dataset was split randomly into training and testing sets in an 80/20 proportion, with the constraint that there were equal number of male and female donors in each of the training and testing set. The training set further underwent LOOCV and SVM training using the cross-validated C parameter. This procedure was repeated 1000 times, each time the dataset was split randomly. As a result the average error rate over 1000-runs was 5.975%. The error matrix is a visualization of this experiment (*Figure 3-4a*); each row represents a test example, each column represents a single run of the procedure. Green represents instances that gender was correctly predicted, black represents instances where gender was incorrectly predicted (*Figure 3-4a*). The top four vectors in the figure represent male donors whereas the bottom 4 test vectors represent female donors (recall that these may not be the same donors each run because of the random split of testing and training data) (*Figure 3-4a*). Though there are $^{20}C_4$ X $^{20}C_4$ possible splits of the data (about 23 million), a 1000-run sampling is enough to get a representative error rate. The procedure was also repeated 10,000 times, and for that run the error rate was very similar: 5.7888%.

4.5.6 Agonist elimination to elucidate platelet calcium signaling pathways most predictive of gender

To determine which agonist interactions in the synergy scores were most important in determining the gender, synergy scores involving certain agonists were omitted from the training and the resulting overall 1000-run test error compared. In each of the 1000 runs, the data was first randomly divided into training and testing sets before each agonist was omitted. This was to

ensure that differences in random training/testing set divisions did not contribute to the differences obtained between 1000-run test error trained on the full dataset and that of the agonist-omitted dataset. If the 1000-run test error of a particular agonist-omitted dataset was higher than that trained on the full dataset, then that agonist is useful in predicting the gender of donors. Each agonist-omitted dataset were also compared to each other so as to rank the importance of each agonist in predicting gender of donors. This would provide insight as to which agonist pathways were most different between males and females.

The average 1000-run prediction error is plotted for each agonist omission. (*Figure 3-4* top right panel) The highest average prediction error (12.325%) occurred when synergy conditions involving the convulxin agonist were omitted from the training set. (*Figure 3-4* top right panel)This result agrees with the inter-donor variability of synergy scores (*Figure 3-3*). The most notable differences in sources of inter-donor variability of synergy scores between and male and female donors came from interactions of medium and high-dose convulxin. This difference could have contributed to the predictive power of the SVM algorithm when convulxin-related synergy scores were included in training set. Since convulxin is a GPVI receptor, this result also alludes to a possible underlying phenotypical difference in GPVI-activation pathways between male and female donors. Neeves et al. (2013) reported that women had higher platelet accumulation than men on fibrillar collagen in microfluidic flow assays [104]. However, women also had higher Von Willebrand Factor (vWF) levels than men, so these variables were not decoupled [104]. So far, there aren't any conclusive differences between male and female platelet function. The error rate dropped below the original prediction error with no omission of 5.6625% when AYPGKF, the PAR-1 agonist peptide was omitted from the training dataset (2.838%) (*Figure 3-4* top right panel). In other words, the algorithm did better (prediction error halved) when AYPGKF-related synergy conditions were removed from the training dataset. This could

mean that there are little differences in platelet activation pathways via PAR-1, and the relatively high contribution of AYPGKF to inter-donor variability of synergy scores added to the noise of the training dataset, and therefore caused SVM method trained to be less effective at predicting error. The agonist-omission error bar plots were created for male donors and female donors separately (*Figure 3-4* right middle and right bottom panel). There seemed to be differences in predictive powers of the algorithm for male donors versus female donors, which could be fixed with introducing a bias term in the SVM algorithm.

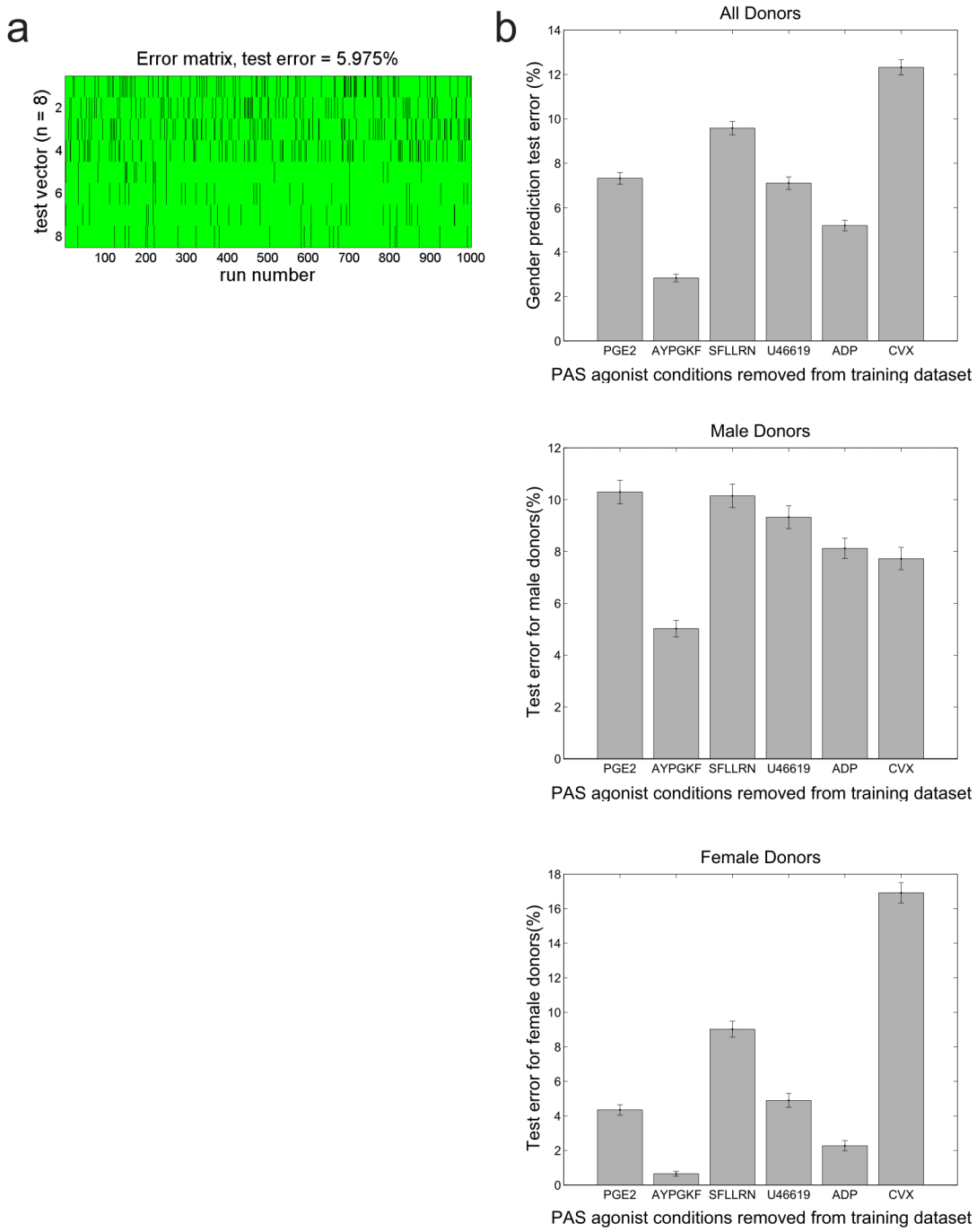

Figure 3-4 (a) SVM model performance **(b)** Impact of specific agonist elimination on SVM model performance

4.5.3 Implementation of SVM on reduced dimension (3D) dataset

This exercise was done for the purpose of visualization and understanding of the SVM method used to build this classification model. The 135-dimension PAS synergy score dataset was projected onto its top three principal components using the principal component analysis (PCA) function in MATLAB. The top three principal components are the dimensions in which the largest variability of the data is captured. The 135-dimension synergy scores are then projected onto those three principal components to produce the 40 data points as visualized in *Figure 3-5*. When SVM was implemented on the reduced dimension (3D) dataset, the resulting maximum margin hyperplane is a flat 3-D plane, with quite a few classification errors on each side (*Figure 3-5*). When SVM was done on the full 135-D dataset, the test error over 100-runs was 5.75% (*Figure 3-4*), whereas that for the 3-D dataset was 32.12%. Even when SVM was trained on the PCA-reduced 30-D dataset, the 100-run error only decreased to 22.5%. This indicates that none of the synergy scores are extraordinarily uninformative in predicting gender of the donors. In other words, the synergy score vectors data is not noisy. When the training data is 3-D, the SVM hyperplane is a 3-D plane. In this dataset, the training data is 135-D, though it is difficult to visualize the hyperplane that separates the two classes spans 135 dimensions.

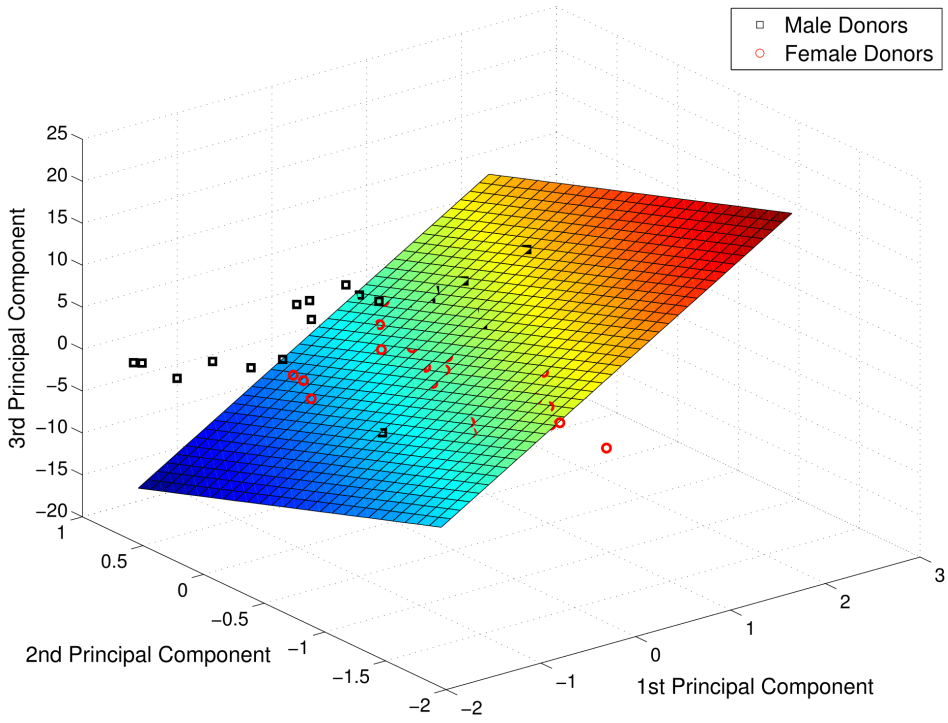

Figure 3-5 Implementation of SVM on reduced dimension (3D) dataset

Appendix A: Dose Response Curves for Platelet Agonists

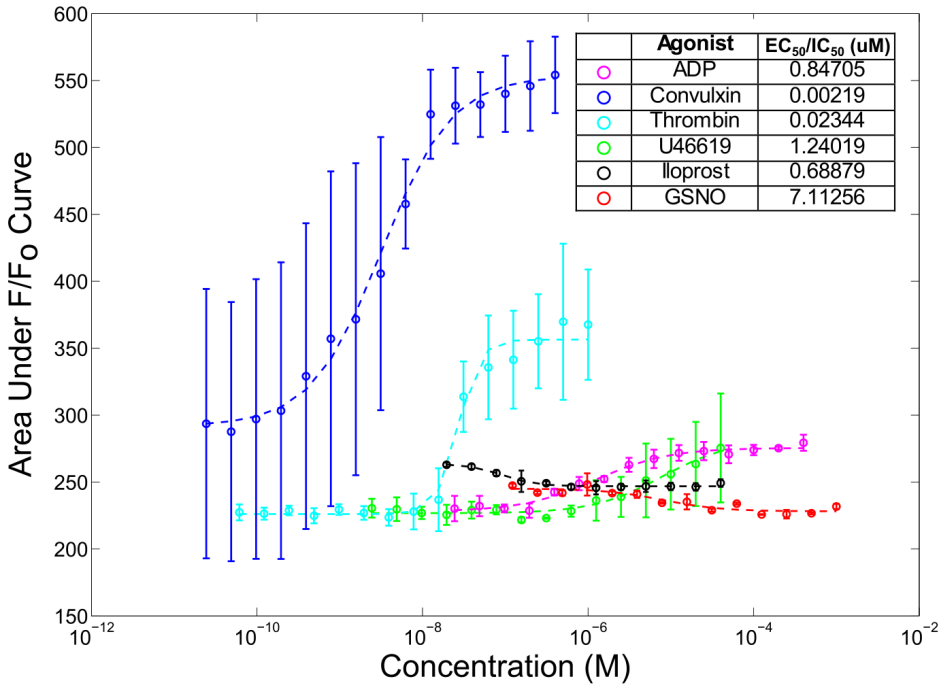

Figure A-3-6 Dose response curves of each agonist. This set of dose response curves were obtained for a single donor done in quadruplicate, and is representative of the dose response curves for the total of six donors used to calculate the average EC_{50} values shown in the table inset. EC_{50} values were calculated by fitting a four-parameter hill function curve (dashed lines) to the area under curve of the baseline-normalized fluorescence intensity (F/F_0) calcium time course. For the dose response of platelet antagonist iloprost, platelets were simultaneously stimulated with PAR-1 agonist SFLLRN (40μM). For the dose response of platelet antagonist GSNO, platelets were simultaneously stimulated with 1μM ADP

Appendix B: Investigation of Autocrinic Signaling Effects in PAS

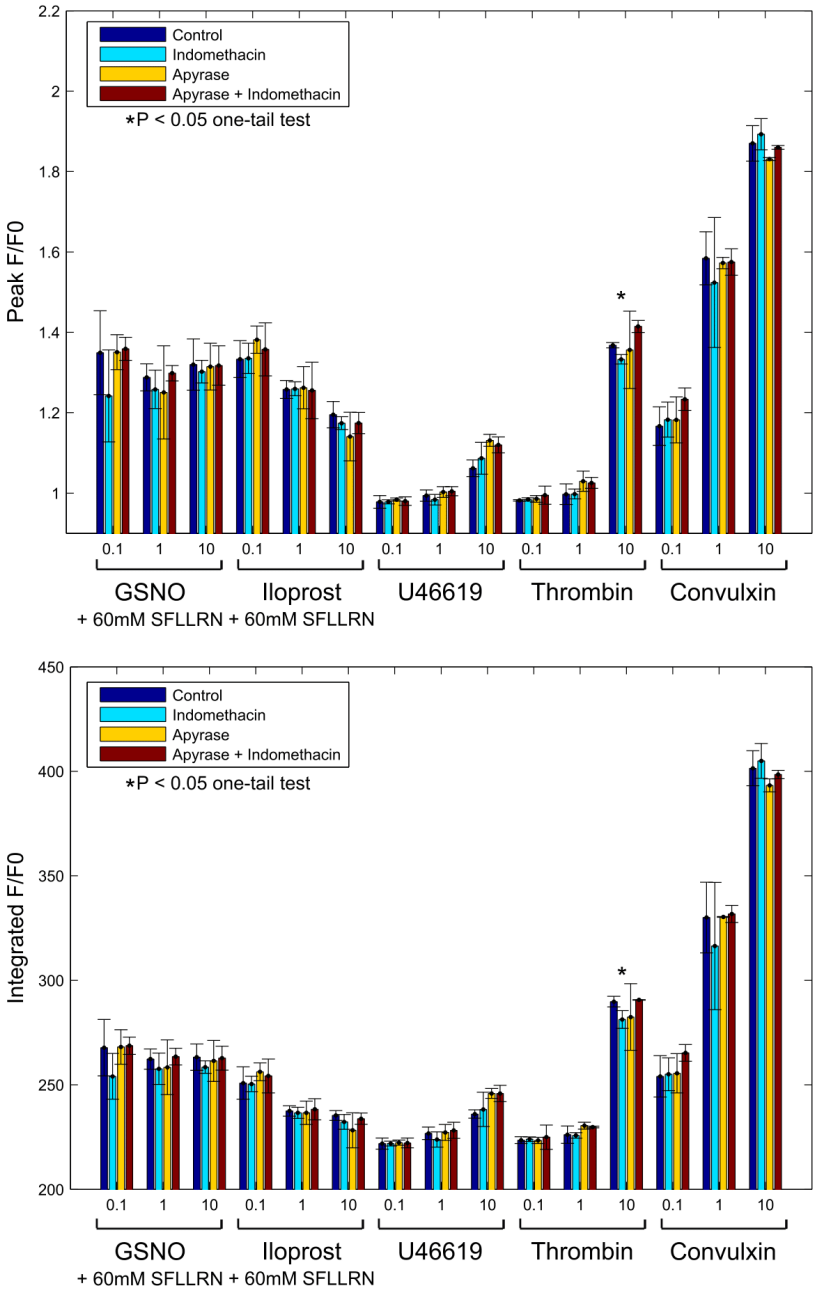

Figure A-2 Investigation of autocrinic signaling effects. To determine whether or not significant secondary autocrinic amplification effects by ADP and thromboxane secretion were present in the PAS assays, apyrase (ADP hydrolyzing enzyme, 2 Units/ml) and indomethacin (COX-inhibitor,15μM) were used. GSNO, Iloprost, U46619, thrombin and convulxin at 0.1, 1, or 10 X EC_{50} were added to platelets in similar conditions as in the PAS experiments (12% PRP, 250nM Apixaban). In the case of the inhibitors GSNO and Iloprost, platelets were co-stimulated with 60mM SFLLRN, a PAR-1 activator. Only one of the 60 conditions tested with added inhibitors produced a detectable reduction in calcium signal (one-tailed T-test $P < 0.05$).

Appendix C: Neural Network Prediction of Trinary Combinations

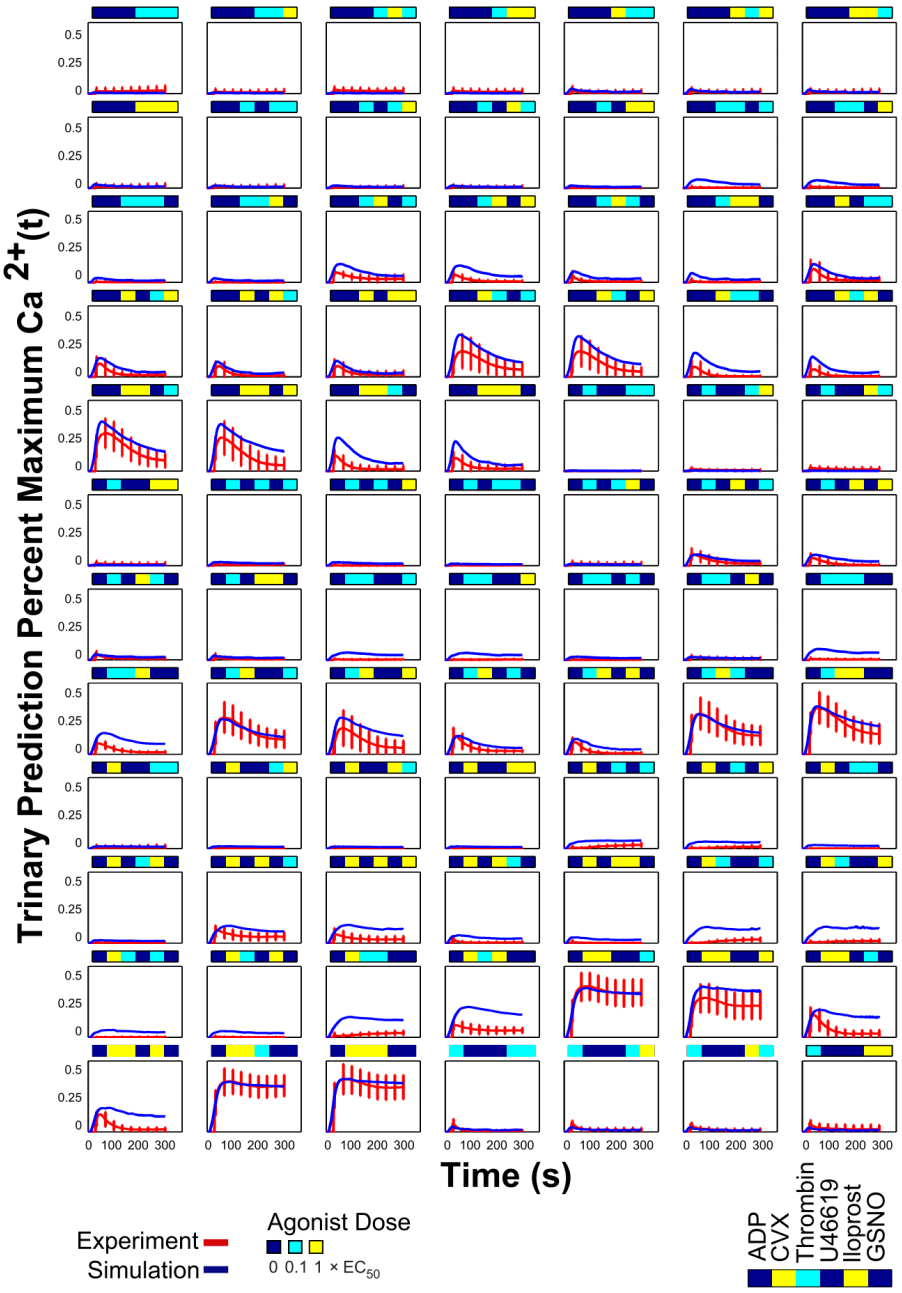

Figure A-3 Neural network prediction of the trinary combination experiment. Experimental and NN-predicted calcium traces are plotted for all 160 trinary conditions (all single and trinary combinations of agonists at two concentrations: 0.1x EC_{50} and 1x EC_{50}). Rescaled to 0.5 for easy visualization.

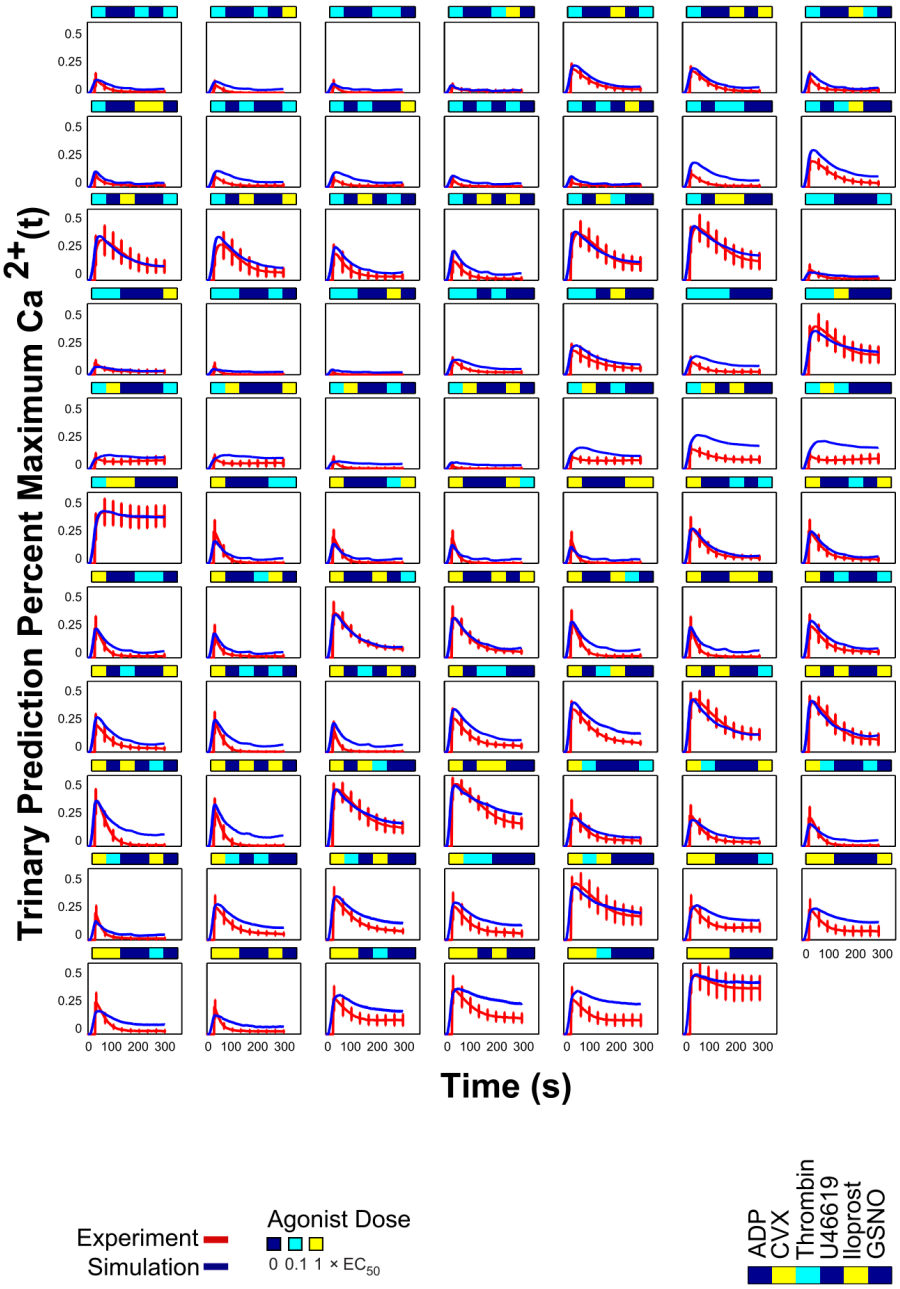

Figure A-3 Neural network prediction of the trinary combination experiment. Experimental and NN-predicted calcium traces are plotted for all 160 trinary conditions (all single and trinary combinations of agonists at two concentrations: 0.1x EC_{50} and 1x EC_{50}). Rescaled to 0.5 for easy visualization.

REFERENCES

1. Brass LF, Stalker TJ, Zhu L, Woulfe DS. Signal Transduction During Platelet Plug Formation. In: Michelson AD, editor. Platelets2007. p. 319-20.

2. Offermanns S. Activation of platelet function through G protein-coupled receptors. Circ Res. 2006;99(12):1293-304. Epub 2006/12/13. doi: 10.1161/01.res.0000251742.71301.16. PubMed PMID: 17158345.

3. Bledzka K, Smyth SS, Plow EF. Integrin alphaIIbbeta3: from discovery to efficacious therapeutic target. Circ Res. 2013;112(8):1189-200. Epub 2013/04/13. doi: 10.1161/circresaha.112.300570. PubMed PMID: 23580774; PubMed Central PMCID: PMCPMC3711133.

4. Li Z, Delaney MK, O'Brien KA, Du X. Signaling during platelet adhesion and activation. Arterioscler Thromb Vasc Biol. 2010;30(12):2341-9. Epub 2010/11/13. doi: 10.1161/atvbaha.110.207522. PubMed PMID: 21071698; PubMed Central PMCID: PMCPMC3085271.

5. Stassen JM, Arnout J, Deckmyn H. The hemostatic system. Curr Med Chem. 2004;11(17):2245-60. Epub 2004/09/24. PubMed PMID: 15379710.

6. Mosesson MW. Fibrinogen and fibrin structure and functions. J Thromb Haemost. 2005;3(8):1894-904. Epub 2005/08/17. doi: 10.1111/j.1538-7836.2005.01365.x. PubMed PMID: 16102057.

7. Haslam RJ, Dickinson NT, Jang EK. Cyclic nucleotides and phosphodiesterases in platelets. Thromb Haemost. 1999;82(2):412-23. Epub 1999/12/22. PubMed PMID: 10605732.

8. Davie EW, Kulman JD. An overview of the structure and function of thrombin. Semin Thromb Hemost. 2006;32 Suppl 1:3-15. Epub 2006/05/05. doi: 10.1055/s-2006-939550. PubMed PMID: 16673262.

9. Majerus PW, Miletich JP. Relationships between platelets and coagulation factors in hemostasis. Annu Rev Med. 1978;29:41-9. Epub 1978/01/01. doi: 10.1146/annurev.me.29.020178.000353. PubMed PMID: 348040.

10. Bevers EM, Comfurius P, van Rijn JL, Hemker HC, Zwaal RF. Generation of prothrombin-converting activity and the exposure of phosphatidylserine at the outer surface of platelets. Eur J Biochem. 1982;122(2):429-36. Epub 1982/02/01. PubMed PMID: 7060583.

11. Holinstat M, Bray PF. Protease receptor antagonism to target blood platelet therapies. Clin Pharmacol Ther. 2016;99(1):72-81. Epub 2015/10/27. doi: 10.1002/cpt.282. PubMed PMID: 26501993.

12. Olson JD. D-dimer: An Overview of Hemostasis and Fibrinolysis, Assays, and Clinical Applications. Adv Clin Chem. 2015;69:1-46. Epub 2015/05/03. doi: 10.1016/bs.acc.2014.12.001. PubMed PMID: 25934358.

13. Sorensen B, Fries D. Emerging treatment strategies for trauma-induced coagulopathy. Br J Surg. 2012;99 Suppl 1:40-50. Epub 2012/03/28. doi: 10.1002/bjs.7770. PubMed PMID: 22441854.

14. Kutcher ME, Redick BJ, McCreery RC, Crane IM, Greenberg MD, Cachola LM, et al. Characterization of platelet dysfunction after trauma. J Trauma Acute Care Surg. 2012;73(1):13-9. Epub 2012/06/30. doi: 10.1097/TA.0b013e318256deab. PubMed PMID: 22743367; PubMed Central PMCID: PMCPMC3387387.

15. Jacoby RC, Owings JT, Holmes J, Battistella FD, Gosselin RC, Paglieroni TG. Platelet activation and function after trauma. J Trauma. 2001;51(4):639-47. Epub 2001/10/05. PubMed PMID: 11586152.

16. Alshehri OM, Hughes CE, Montague S, Watson SK, Frampton J, Bender M, et al. Fibrin activates GPVI in human and mouse platelets. Blood. 2015;126(13):1601-8. Epub 2015/08/19. doi: 10.1182/blood-2015-04-641654. PubMed PMID: 26282541; PubMed Central PMCID: PMCPMC4582337.

17. Bender M, Hagedorn I, Nieswandt B. Genetic and antibody-induced glycoprotein VI deficiency equally protects mice from mechanically and FeCl(3) -induced thrombosis. J Thromb Haemost. 2011;9(7):1423-6. Epub 2011/05/04. doi: 10.1111/j.1538-7836.2011.04328.x. PubMed PMID: 21535392.

18. Mammadova-Bach E, Ollivier V, Loyau S, Schaff M, Dumont B, Favier R, et al. Platelet glycoprotein VI binds to polymerized fibrin and promotes thrombin generation. Blood. 2015;126(5):683-91. Epub 2015/05/16. doi: 10.1182/blood-2015-02-629717. PubMed PMID: 25977585.

19. Campbell CL, Smyth S, Montalescot G, Steinhubl SR. Aspirin dose for the prevention of cardiovascular disease: a systematic review. Jama. 2007;297(18):2018-24. Epub 2007/05/10. doi: 10.1001/jama.297.18.2018. PubMed PMID: 17488967.

20. Chatterjee MS, Purvis JE, Brass LF, Diamond SL. Pairwise agonist scanning predicts cellular signaling responses to combinatorial stimuli. Nat Biotechnol. 2010;28(7):727-32. Epub 2010/06/22. doi: 10.1038/nbt.1642. PubMed PMID: 20562863; PubMed Central PMCID: PMCPmc3010846.

21. Shattil SJ, Brass LF. Induction of the fibrinogen receptor on human platelets by intracellular mediators. J Biol Chem. 1987;262(3):992-1000. Epub 1987/01/25. PubMed PMID: 3100533.

22. Stefanini L, Roden RC, Bergmeier W. CalDAG-GEFI is at the nexus of calcium-dependent platelet activation. Blood. 2009;114(12):2506-14. Epub 2009/07/25. doi: 10.1182/blood-2009-04-218768. PubMed PMID: 19628710.

23. Crittenden JR, Bergmeier W, Zhang Y, Piffath CL, Liang Y, Wagner DD, et al. CalDAG-GEFI integrates signaling for platelet aggregation and thrombus formation. Nat Med. 2004;10(9):982-6. Epub 2004/08/31. doi: 10.1038/nm1098. PubMed PMID: 15334074.

24. Flamm MH, Colace TV, Chatterjee MS, Jing H, Zhou S, Jaeger D, et al. Multiscale prediction of patient-specific platelet function under flow. Blood. 2012;120(1):190-8. Epub 2012/04/21. doi: 10.1182/blood-2011-10-388140. PubMed PMID: 22517902; PubMed Central PMCID: PMCPmc3390957.

25. Pinto DJ, Orwat MJ, Koch S, Rossi KA, Alexander RS, Smallwood A, et al. Discovery of 1-(4-methoxyphenyl)-7-oxo-6-(4-(2-oxopiperidin-1-yl)phenyl)-4,5,6,7-tetrahydro-1H -pyrazolo[3,4-c]pyridine-3-carboxamide (apixaban, BMS-562247), a highly potent, selective, efficacious, and orally bioavailable inhibitor of blood coagulation factor Xa. J Med Chem. 2007;50(22):5339-56. Epub 2007/10/05. doi: 10.1021/jm070245n. PubMed PMID: 17914785.

26. Cunningham P, Carney J, Jacob S. Stability problems with artificial neural networks and the ensemble solution. Artif Intell Med. 2000;20(3):217-25. Epub 2000/09/22. PubMed PMID: 10998588.

27. Keuren JF, Wielders SJ, Ulrichts H, Hackeng T, Heemskerk JW, Deckmyn H, et al. Synergistic effect of thrombin on collagen-induced platelet procoagulant activity is mediated through protease-activated receptor-1. Arterioscler Thromb Vasc Biol. 2005;25(7):1499-505. Epub 2005/04/23. doi: 10.1161/01.ATV.0000167526.31611.f6. PubMed PMID: 15845904.

28. Hughan SC, Hughes CE, McCarty OJ, Schweighoffer E, Soultanova I, Ware J, et al. GPVI potentiation of platelet activation by thrombin and adhesion molecules independent of Src kinases and Syk. Arterioscler Thromb Vasc Biol. 2007;27(2):422-9. Epub 2006/11/18. doi: 10.1161/01.atv.0000252826.96134.21. PubMed PMID: 17110603; PubMed Central PMCID: PMCPmc2990469.

29. Brass LF, Wannemacher KM, Ma P, Stalker TJ. Regulating thrombus growth and stability to achieve an optimal response to injury. J Thromb Haemost. 2011;9 Suppl 1:66-75. Epub 2011/08/04. doi: 10.1111/j.1538-7836.2011.04364.x. PubMed PMID: 21781243; PubMed Central PMCID: PMCPmc3422128.

30. Welsh JD, Colace TV, Muthard RW, Stalker TJ, Brass LF, Diamond SL. Platelet-targeting sensor reveals thrombin gradients within blood clots forming in microfluidic assays and in mouse. J Thromb Haemost. 2012;10(11):2344-53. Epub 2012/09/18. doi: 10.1111/j.1538-7836.2012.04928.x. PubMed PMID: 22978514; PubMed Central PMCID: PMCPmc4082909.

31. Muthard RW, Diamond SL. Blood clots are rapidly assembled hemodynamic sensors: flow arrest triggers intraluminal thrombus contraction. Arterioscler Thromb Vasc Biol. 2012;32(12):2938-45. Epub 2012/10/23. doi: 10.1161/atvbaha.112.300312. PubMed PMID: 23087356; PubMed Central PMCID: PMCPmc3586804.

32. Welsh JD, Stalker TJ, Voronov R, Muthard RW, Tomaiuolo M, Diamond SL, et al. A systems approach to hemostasis: 1. The interdependence of thrombus architecture and agonist movements in the gaps between platelets. Blood. 2014;124(11):1808-15. Epub 2014/06/22. doi: 10.1182/blood-2014-01-550335. PubMed PMID: 24951424; PubMed Central PMCID: PMCPmc4162110.

33. Tomaiuolo M, Stalker TJ, Welsh JD, Diamond SL, Sinno T, Brass LF. A systems approach to hemostasis: 2. Computational analysis of molecular transport in the thrombus microenvironment. Blood. 2014;124(11):1816-23. Epub 2014/06/22. doi: 10.1182/blood-2014-01-550343. PubMed PMID: 24951425; PubMed Central PMCID: PMCPmc4162111.

34. Stalker TJ, Welsh JD, Tomaiuolo M, Wu J, Colace TV, Diamond SL, et al. A systems approach to hemostasis: 3. Thrombus consolidation regulates intrathrombus solute transport and local thrombin activity. Blood. 2014;124(11):1824-31. Epub 2014/06/22. doi: 10.1182/blood-2014-01-550319. PubMed PMID: 24951426; PubMed Central PMCID: PMCPmc4162112.

35. Blackmore PF. Biphasic effects of nitric oxide on calcium influx in human platelets. Thromb Res. 2011;127(1):e8-14. Epub 2010/11/09. doi: 10.1016/j.thromres.2010.10.002. PubMed PMID: 21056902.

36. Radomski MW, Palmer RM, Moncada S. Comparative pharmacology of endothelium-derived relaxing factor, nitric oxide and prostacyclin in platelets. Br J Pharmacol. 1987;92(1):181-7. Epub 1987/09/01. PubMed PMID: 3311265; PubMed Central PMCID: PMCPmc1853617.

37. Radomski MW, Rees DD, Dutra A, Moncada S. S-nitroso-glutathione inhibits platelet activation in vitro and in vivo. Br J Pharmacol. 1992;107(3):745-9. Epub 1992/11/01. PubMed PMID: 1335336; PubMed Central PMCID: PMCPmc1907743.

38. Moro MA, Russel RJ, Cellek S, Lizasoain I, Su Y, Darley-Usmar VM, et al. cGMP mediates the vascular and platelet actions of nitric oxide: confirmation using an inhibitor of the soluble guanylyl cyclase. Proc Natl Acad Sci U S A. 1996;93(4):1480-5. Epub 1996/02/20. PubMed PMID: 8643658; PubMed Central PMCID: PMCPmc39965.

39. Polgar J, Clemetson JM, Kehrel BE, Wiedemann M, Magnenat EM, Wells TN, et al. Platelet activation and signal transduction by convulxin, a C-type lectin from Crotalus durissus terrificus (tropical rattlesnake) venom via the p62/GPVI collagen receptor. J Biol Chem. 1997;272(21):13576-83. Epub 1997/05/23. PubMed PMID: 9153205.

40. Jaeger DT, Diamond SL. Pairwise agonist scanning-flow cytometry (PAS-FC) measures inside-out signaling and patient-specific response to combinatorial platelet agonists. Biotechniques. 2013;54(5):271-7. Epub 2013/05/15. doi: 10.2144/000114027. PubMed PMID: 23662898; PubMed Central PMCID: PMCPmc4086368.

41. Montgomery DC. Design and Analysis of Experiments. 4th ed. New York: Wiley; 1997.

42. Garcia-Pedrajas N, Hervas-Martinez C, Ortiz-Boyer D. Cooperative coevolution of artificial neural network ensembles for pattern classification. Evolutionary Computation, IEEE Transactions on. 2005;9(3):271-302. doi: 10.1109/TEVC.2005.844158.

43. Liu Y, Yao X. Ensemble learning via negative correlation. Neural Netw. 1999;12(10):1399-404. Epub 2003/03/29. PubMed PMID: 12662623.

44. Breiman L. Random Forests. Machine Learning. 2001;45(1):5-32. doi: 10.1023/A:1010933404324.

45. Rodriguez JJ, Kuncheva LI, Alonso CJ. Rotation forest: A new classifier ensemble method. IEEE Trans Pattern Anal Mach Intell. 2006;28(10):1619-30. Epub 2006/09/22. doi: 10.1109/tpami.2006.211. PubMed PMID: 16986543.

46. Jo, Mendes-Moreira o, Soares C, Al, M p, Jorge r, et al. Ensemble approaches for regression: A survey. ACM Comput Surv. 2012;45(1):1-40. doi: 10.1145/2379776.2379786.

47. Partridge D, Yates WB. Engineering multiversion neural-net systems. Neural Comput. 1996;8(4):869-93. Epub 1996/05/15. PubMed PMID: 8624963.

48. Kuncheva L, Whitaker C. Measures of Diversity in Classifier Ensembles and Their Relationship with the Ensemble Accuracy. Machine Learning. 2003;51(2):181-207. doi: 10.1023/A:1022859003006.

49. Windeatt T, Roli F, Aksela M. Comparison of Classifier Selection Methods for Improving Committee Performance. Multiple Classifier Systems. Lecture Notes in Computer Science. 2709: Springer Berlin Heidelberg; 2003. p. 84-93.

50. Louwette S, Van Geet C, Freson K. Regulators of G protein signaling: role in hematopoiesis, megakaryopoiesis and platelet function. J Thromb Haemost.

2012;10(11):2215-22. Epub 2012/08/23. doi: 10.1111/j.1538-7836.2012.04903.x. PubMed PMID: 22908964.

51. Dale GL. Coated-platelets: an emerging component of the procoagulant response. J Thromb Haemost. 2005;3(10):2185-92. Epub 2005/10/01. doi: 10.1111/j.1538-7836.2005.01274.x. PubMed PMID: 16194197.

52. Xu Z, Chen N, Shadden SC, Marsden JE, Kamocka MM, Rosen ED, et al. Study of blood flow impact on growth of thrombi using a multiscale model. Soft Matter. 2009;5(4):769-79. doi: 10.1039/B812429A.

53. Lu Y, Lee MY, Zhu S, Sinno TR, Diamond SL. Multiscale simulation of thrombus growth and vessel occlusion triggered by collagen/tissue factor using a data-driven m. PLoS Computational Biology. 2016.

54. Watson SP, Herbert JM, Pollitt AY. GPVI and CLEC-2 in hemostasis and vascular integrity. J Thromb Haemost. 2010;8(7):1456-67. Epub 2010/03/30. doi: 10.1111/j.1538-7836.2010.03875.x. PubMed PMID: 20345705.

55. Gibbins J, Asselin J, Farndale R, Barnes M, Law CL, Watson SP. Tyrosine phosphorylation of the Fc receptor gamma-chain in collagen-stimulated platelets. J Biol Chem. 1996;271(30):18095-9. Epub 1996/07/26. PubMed PMID: 8663460.

56. Poole A, Gibbins JM, Turner M, van Vugt MJ, van de Winkel JG, Saito T, et al. The Fc receptor gamma-chain and the tyrosine kinase Syk are essential for activation of mouse platelets by collagen. Embo j. 1997;16(9):2333-41. Epub 1997/05/01. doi: 10.1093/emboj/16.9.2333. PubMed PMID: 9171347; PubMed Central PMCID: PMCPMC1169834.

57. Li W, Tang X, Yi W, Li Q, Ren L, Liu X, et al. Glaucocalyxin A inhibits platelet activation and thrombus formation preferentially via GPVI signaling pathway. PLoS One. 2013;8(12):e85120. Epub 2014/01/05. doi: 10.1371/journal.pone.0085120. PubMed PMID: 24386454; PubMed Central PMCID: PMCPMC3875551.

58. Bultmann A, Li Z, Wagner S, Peluso M, Schonberger T, Weis C, et al. Impact of glycoprotein VI and platelet adhesion on atherosclerosis--a possible role of fibronectin. J Mol Cell Cardiol. 2010;49(3):532-42. Epub 2010/05/01. doi: 10.1016/j.yjmcc.2010.04.009. PubMed PMID: 20430036.

59. Schonberger T, Ziegler M, Borst O, Konrad I, Nieswandt B, Massberg S, et al. The dimeric platelet collagen receptor GPVI-Fc reduces platelet adhesion to activated endothelium and preserves myocardial function after transient ischemia in mice. Am J Physiol Cell Physiol. 2012;303(7):C757-66. Epub 2012/07/21. doi: 10.1152/ajpcell.00060.2012. PubMed PMID: 22814400.

60. Inoue O, Suzuki-Inoue K, McCarty OJ, Moroi M, Ruggeri ZM, Kunicki TJ, et al. Laminin stimulates spreading of platelets through integrin alpha6beta1-dependent activation of GPVI. Blood. 2006;107(4):1405-12. Epub 2005/10/13. doi: 10.1182/blood-2005-06-2406. PubMed PMID: 16219796; PubMed Central PMCID: PMCPMC1895394.

61. Jiang P, Jandrot-Perrus M. New advances in treating thrombotic diseases: GPVI as a platelet drug target. Drug Discov Today. 2014;19(9):1471-5. Epub 2014/06/17. doi: 10.1016/j.drudis.2014.06.005. PubMed PMID: 24931218.

62. Zahid M, Mangin P, Loyau S, Hechler B, Billiald P, Gachet C, et al. The future of glycoprotein VI as an antithrombotic target. J Thromb Haemost. 2012;10(12):2418-27. Epub 2012/10/02. doi: 10.1111/jth.12009. PubMed PMID: 23020554.

63. Kraft P, De Meyer SF, Kleinschnitz C. Next-generation antithrombotics in ischemic stroke: preclinical perspective on 'bleeding-free antithrombosis'. J Cereb Blood Flow Metab. 2012;32(10):1831-40. Epub 2012/07/19. doi: 10.1038/jcbfm.2012.108. PubMed PMID: 22805877; PubMed Central PMCID: PMCPMC3463876.

64. Stegner D, Haining EJ, Nieswandt B. Targeting glycoprotein VI and the immunoreceptor tyrosine-based activation motif signaling pathway. Arterioscler Thromb Vasc Biol. 2014;34(8):1615-20. Epub 2014/06/14. doi: 10.1161/atvbaha.114.303408. PubMed PMID: 24925975.

65. Dutting S, Bender M, Nieswandt B. Platelet GPVI: a target for antithrombotic therapy?! Trends Pharmacol Sci. 2012;33(11):583-90. Epub 2012/08/21. doi: 10.1016/j.tips.2012.07.004. PubMed PMID: 22901552.

66. Kuijpers MJ, Gilio K, Reitsma S, Nergiz-Unal R, Prinzen L, Heeneman S, et al. Complementary roles of platelets and coagulation in thrombus formation on plaques acutely ruptured by targeted ultrasound treatment: a novel intravital model. J Thromb Haemost. 2009;7(1):152-61. Epub 2008/11/06. doi: 10.1111/j.1538-7836.2008.03186.x. PubMed PMID: 18983512.

67. Hechler B, Gachet C. Comparison of two murine models of thrombosis induced by atherosclerotic plaque injury. Thromb Haemost. 2011;105 Suppl 1:S3-12. Epub 2011/04/12. doi: 10.1160/ths10-11-0730. PubMed PMID: 21479341.

68. Patrono C, Andreotti F, Arnesen H, Badimon L, Baigent C, Collet JP, et al. Antiplatelet agents for the treatment and prevention of atherothrombosis. Eur Heart J. 2011;32(23):2922-32. Epub 2011/10/25. doi: 10.1093/eurheartj/ehr373. PubMed PMID: 22019823.

69. Hankey GJ, Eikelboom JW. Antithrombotic drugs for patients with ischaemic stroke and transient ischaemic attack to prevent recurrent major vascular events. Lancet Neurol. 2010;9(3):273-84. Epub 2010/02/23. doi: 10.1016/s1474-4422(10)70038-7. PubMed PMID: 20170841.

70. Bredbacka S, Edner G. Soluble fibrin and D-dimer as detectors of hypercoagulability in patients with isolated brain trauma. J Neurosurg Anesthesiol. 1994;6(2):75-82. Epub 1994/04/01. PubMed PMID: 8012177.

71. Scherer RU, Spangenberg P. Procoagulant activity in patients with isolated severe head trauma. Crit Care Med. 1998;26(1):149-56. Epub 1998/01/15. PubMed PMID: 9428558.

72. Wada H, Sakuragawa N, Shiku H. Hemostatic molecular markers before onset of disseminated intravascular coagulation in leukemic patients. Semin Thromb Hemost. 1998;24(3):293-7. Epub 1998/08/13. doi: 10.1055/s-2007-995857. PubMed PMID: 9701463.

73. Hayakawa M, Gando S, Ono Y, Wada T, Yanagida Y, Sawamura A, et al. Noble-Collip Drum Trauma Induces Disseminated Intravascular Coagulation But Not Acute Coagulopathy of Trauma-Shock. Shock. 2015;43(3):261-7. Epub 2014/11/26. doi: 10.1097/shk.0000000000000281. PubMed PMID: 25423126.

74. Nieswandt B, Pleines I, Bender M. Platelet adhesion and activation mechanisms in arterial thrombosis and ischaemic stroke. J Thromb Haemost. 2011;9 Suppl 1:92-104. Epub 2011/08/04. doi: 10.1111/j.1538-7836.2011.04361.x. PubMed PMID: 21781245.

75. Lee MY, Diamond SL. A human platelet calcium calculator trained by pairwise agonist scanning. PLoS Comput Biol. 2015;11(2):e1004118. Epub 2015/02/28. doi: 10.1371/journal.pcbi.1004118. PubMed PMID: 25723389; PubMed Central PMCID: PMCPMC4344206.

76. Al-Tamimi M, Grigoriadis G, Tran H, Paul E, Servadei P, Berndt MC, et al. Coagulation-induced shedding of platelet glycoprotein VI mediated by factor Xa. Blood. 2011;117(14):3912-20. Epub 2011/01/22. doi: 10.1182/blood-2010-08-301523. PubMed PMID: 21252089.

77. Stephens G, Yan Y, Jandrot-Perrus M, Villeval JL, Clemetson KJ, Phillips DR. Platelet activation induces metalloproteinase-dependent GP VI cleavage to down-regulate platelet reactivity to collagen. Blood. 2005;105(1):186-91. Epub 2004/09/02. doi: 10.1182/blood-2004-07-2842. PubMed PMID: 15339851.

78. Mahajan-Thakur S, Bohm A, Jedlitschky G, Schror K, Rauch BH. Sphingosine-1-Phosphate and Its Receptors: A Mutual Link between Blood Coagulation and Inflammation. Mediators Inflamm. 2015;2015:831059. Epub 2015/11/26. doi: 10.1155/2015/831059. PubMed PMID: 26604433; PubMed Central PMCID: PMCPMC4641948.

79. Malinowska J, Nowak P, Olas B. Comparison of the effect of homocysteine in the reduced form, its thiolactone and protein homocysteinylation on hemostatic properties of

plasma. Thromb Res. 2011;127(3):214-9. Epub 2010/12/28. doi: 10.1016/j.thromres.2010.11.027. PubMed PMID: 21186049.

80. Nowak P, Zbikowska HM, Ponczek M, Kolodziejczyk J, Wachowicz B. Different vulnerability of fibrinogen subunits to oxidative/nitrative modifications induced by peroxynitrite: functional consequences. Thromb Res. 2007;121(2):163-74. Epub 2007/05/01. doi: 10.1016/j.thromres.2007.03.017. PubMed PMID: 17467041.

81. Sidhu TS, French SL, Hamilton JR. Differential signaling by protease-activated receptors: implications for therapeutic targeting. Int J Mol Sci. 2014;15(4):6169-83. Epub 2014/04/16. doi: 10.3390/ijms15046169. PubMed PMID: 24733067; PubMed Central PMCID: PMCPMC4013622.

82. Mazharian A, Roger S, Berrou E, Adam F, Kauskot A, Nurden P, et al. Protease-activating receptor-4 induces full platelet spreading on a fibrinogen matrix: involvement of ERK2 and p38 and Ca2+ mobilization. J Biol Chem. 2007;282(8):5478-87. Epub 2007/01/04. doi: 10.1074/jbc.M609881200. PubMed PMID: 17200114.

83. Covic L, Gresser AL, Kuliopulos A. Biphasic kinetics of activation and signaling for PAR1 and PAR4 thrombin receptors in platelets. Biochemistry. 2000;39(18):5458-67. Epub 2000/05/23. PubMed PMID: 10820018.

84. Shapiro MJ, Weiss EJ, Faruqi TR, Coughlin SR. Protease-activated receptors 1 and 4 are shut off with distinct kinetics after activation by thrombin. J Biol Chem. 2000;275(33):25216-21. Epub 2000/06/06. doi: 10.1074/jbc.M004589200. PubMed PMID: 10837487.

85. Facey A, Pinar I, Arthur JF, Qiao J, Jing J, Mado B, et al. A-Disintegrin-And-Metalloproteinase (ADAM) 10 Activity on Resting and Activated Platelets. Biochemistry. 2016;55(8):1187-94. Epub 2016/02/04. doi: 10.1021/acs.biochem.5b01102. PubMed PMID: 26840909.

86. Bender M, Hofmann S, Stegner D, Chalaris A, Bosl M, Braun A, et al. Differentially regulated GPVI ectodomain shedding by multiple platelet-expressed proteinases. Blood. 2010;116(17):3347-55. Epub 2010/07/21. doi: 10.1182/blood-2010-06-289108. PubMed PMID: 20644114.

87. Neeves KB, Maloney SF, Fong KP, Schmaier AA, Kahn ML, Brass LF, et al. Microfluidic focal thrombosis model for measuring murine platelet deposition and stability: PAR4 signaling enhances shear-resistance of platelet aggregates. J Thromb Haemost. 2008;6(12):2193-201. Epub 2008/11/06. doi: 10.1111/j.1538-7836.2008.03188.x. PubMed PMID: 18983510.

88. Maloney SF, Brass LF, Diamond SL. P2Y12 or P2Y1 inhibitors reduce platelet deposition in a microfluidic model of thrombosis while apyrase lacks efficacy under flow conditions. Integr Biol (Camb). 2010;2(4):183-92. Epub 2010/05/18. doi:

10.1039/b919728a. PubMed PMID: 20473398; PubMed Central PMCID: PMCPMC4441395.

89. Colace T, Falls E, Zheng XL, Diamond SL. Analysis of morphology of platelet aggregates formed on collagen under laminar blood flow. Ann Biomed Eng. 2011;39(2):922-9. Epub 2010/10/16. doi: 10.1007/s10439-010-0182-4. PubMed PMID: 20949319.

90. Nuyttens BP, Thijs T, Deckmyn H, Broos K. Platelet adhesion to collagen. Thromb Res. 2011;127 Suppl 2:S26-9. Epub 2011/01/05. doi: 10.1016/s0049-3848(10)70151-1. PubMed PMID: 21193111.

91. Nieswandt B, Brakebusch C, Bergmeier W, Schulte V, Bouvard D, Mokhtari-Nejad R, et al. Glycoprotein VI but not alpha2beta1 integrin is essential for platelet interaction with collagen. Embo j. 2001;20(9):2120-30. Epub 2001/05/02. doi: 10.1093/emboj/20.9.2120. PubMed PMID: 11331578; PubMed Central PMCID: PMCPMC125246.

92. Jandrot-Perrus M, Lagrue AH, Okuma M, Bon C. Adhesion and activation of human platelets induced by convulxin involve glycoprotein VI and integrin alpha2beta1. J Biol Chem. 1997;272(43):27035-41. Epub 1997/10/27. PubMed PMID: 9341142.

93. Li R, Fries S, Li X, Grosser T, Diamond SL. Microfluidic assay of platelet deposition on collagen by perfusion of whole blood from healthy individuals taking aspirin. Clin Chem. 2013;59(8):1195-204. Epub 2013/04/18. doi: 10.1373/clinchem.2012.198101. PubMed PMID: 23592503; PubMed Central PMCID: PMCPMC4119612.

94. Colace TV, Muthard RW, Diamond SL. Thrombus growth and embolism on tissue factor-bearing collagen surfaces under flow: role of thrombin with and without fibrin. Arterioscler Thromb Vasc Biol. 2012;32(6):1466-76. Epub 2012/04/21. doi: 10.1161/atvbaha.112.249789. PubMed PMID: 22516070; PubMed Central PMCID: PMCPMC3418805.

95. Shaz BH, Winkler AM, James AB, Hillyer CD, MacLeod JB. Pathophysiology of early trauma-induced coagulopathy: emerging evidence for hemodilution and coagulation factor depletion. J Trauma. 2011;70(6):1401-7. Epub 2011/04/05. doi: 10.1097/TA.0b013e31821266e0. PubMed PMID: 21460741; PubMed Central PMCID: PMCPMC3131448.

96. Lenoci L, Duvernay M, Satchell S, DiBenedetto E, Hamm HE. Mathematical model of PAR1-mediated activation of human platelets. Mol Biosyst. 2011;7(4):1129-37. Epub 2011/01/14. doi: 10.1039/c0mb00250j. PubMed PMID: 21229145.

97. Jonnalagadda D, Izu LT, Whiteheart SW. Platelet secretion is kinetically heterogeneous in an agonist-responsive manner. Blood. 2012;120(26):5209-16. Epub

2012/10/23. doi: 10.1182/blood-2012-07-445080. PubMed PMID: 23086755; PubMed Central PMCID: PMCPMC3537312.

98. Chatterjee MS, Denney WS, Jing H, Diamond SL. Systems biology of coagulation initiation: kinetics of thrombin generation in resting and activated human blood. PLoS Comput Biol. 2010;6(9). Epub 2010/10/14. doi: 10.1371/journal.pcbi.1000950. PubMed PMID: 20941387; PubMed Central PMCID: PMCPMC2947981.

99. Tandon P, Diamond SL. Hydrodynamic effects and receptor interactions of platelets and their aggregates in linear shear flow. Biophys J. 1997;73(5):2819-35. Epub 1997/11/25. doi: 10.1016/s0006-3495(97)78311-5. PubMed PMID: 9370476; PubMed Central PMCID: PMCPMC1181184.

100. Laurenzi IJ, Diamond SL. Kinetics of random aggregation-fragmentation processes with multiple components. Phys Rev E Stat Nonlin Soft Matter Phys. 2003;67(5 Pt 1):051103. Epub 2003/06/06. doi: 10.1103/PhysRevE.67.051103. PubMed PMID: 12786130.

101. Ramstrom S, Ranby M, Lindahl TL. Platelet phosphatidylserine exposure and procoagulant activity in clotting whole blood--different effects of collagen, TRAP and calcium ionophore A23187. Thromb Haemost. 2003;89(1):132-41. Epub 2003/01/24. doi: 10.1267/thro03010132. PubMed PMID: 12540963.

102. Jackson EC, Ortar G, McNicol A. The effects of an inhibitor of diglyceride lipase on collagen-induced platelet activation. J Pharmacol Exp Ther. 2013;347(3):582-8. Epub 2013/09/18. doi: 10.1124/jpet.113.205591. PubMed PMID: 24042163.

103. Kauskot A, Hoylaerts MF. Platelet Receptors. Antiplatelet Agents: Springer-Verlag Berlin Heidelberg. p. 23-57.

104. Neeves KB, Onasoga AA, Hansen RR, Lilly JJ, Venckunaite D, Sumner MB, et al. Sources of variability in platelet accumulation on type 1 fibrillar collagen in microfluidic flow assays. PLoS One. 2013;8(1):e54680. Epub 2013/01/29. doi: 10.1371/journal.pone.0054680. PubMed PMID: 23355889; PubMed Central PMCID: PMCPMC3552855.